The Pennsylvania State University

The Graduate School

Department of Bioengineering

MECHANISMS OF SHEAR-INDUCED ADAPTIVE RHEOLOGY IN ENDOTHELIAL CELLS

A Dissertation in

Bioengineering

by

Jhanvi Hirji Dangaria

Submitted in Partial Fulfillment
of the Requirements
for the Degree of

Doctor of Philosophy

May 2008

The thesis of Jhanvi Hirji Dangaria was reviewed and approved* by the following:

Peter J. Butler
Associate Professor of Bioengineering
Thesis Advisor
Chair of Committee

Cheng Dong
Professor of Bioengineering

William O. Hancock
Associate Professor of Bioengineering

Erin D. Sheets
Assistant Professor of Chemistry

Herbert H. Lipowsky
Professor of Bioengineering
Head of the Department of Bioengineering

*Signatures are on file in the Graduate School

ABSTRACT

Vascular endothelial cells (ECs) constitute the endothelium which lines the entire cardiovascular system and is consequently exposed to mechanical stimuli, such as fluid shear stress due to blood flow and cyclic stretch due to hydrostatic pressure fluctuations, and to chemical stimuli, such as growth factors, inflammatory cytokines, and hormones. Vascular health and pathology is tied to the adaptation of cell mechanics through the regulation of cellular structures that sense and respond to mechanical forces. While long term shear adaptation of endothelial cells has been studied extensively, little is know about the temporal changes in cell mechanics occurring on same time scale as hemodynamic forces. The interplay of force, dynamic cell mechanics, and biochemical signaling is the main focus of the studies summarized in this dissertation.

The principal tools used to determine shear-induced temporal changes in cell mechanics were particle tracking microrheology, and analysis of creep functions. To implement these methods, a custom image-correlation based algorithm was designed in LabVIEW to measure nano-scale motions of cellular features and endocytosed beads. Time-lapse images were acquired using high-resolution differential interference contrast digital microscopy of confluent endothelial cells in a flow chamber. These techniques were optimized for use on cells in flow chambers by extensive minimization of motion artifacts. In particular, photolithography was used to microfabricate fiduciary posts on glass coverslips. Position of microposts relative to thermally-induced motion of vesicles in cells was used to subtract low- and high-frequency microscope stage motion artifacts and to facilitate sub-pixel tracking from time-lapse images of adherent cells.

This study documents the first reported observations of rapid changes in cell mechanics in response to large temporal fluctuations in shear stress (i.e. step change). Endothelial cells subjected to a step change in shear stress from 0 to 10 dynes/cm^2 became significantly more compliant as early as 30 seconds after onset of shear stimulation. Viscoelastic parameters recovered within 4 minutes of shearing even though shear stress was maintained and no further rheological modulation was observed after cessation of shear stress. Using a phenomenological model of a viscoelastic liquid, overall macrorheological parameters were calculated and the time and length scales of viscoelastic deformation were found to be 3 sec and 50 nm, respectively.

Furthermore, experiments were designed to explore the role of actomyosin interactions in the dynamic control of EC mechanics. This study grew from knowledge that overall cellular mechanics is strongly dependent on actin and from recent *in vitro* (model polymer systems) and *in vivo* (dictyostelium cells and myoblasts) studies suggesting a triple role for myosin II in regulating cytoplasmic rheology through cellular prestress, actin crosslinking, and facilitated polymer diffusion. A novel observation from these studies is that actomyosin regulates macrorheology (i.e. viscoelastic deformation in response to shear stress), microrheology (i.e. constrained thermal motion of small beads) and cellular activation. In fact, the observation of a shear-induced, actin-dependent contraction, the onset time of which depended on myosin II may point the way to a new understanding of the dynamic control of cell mechanics. Together, these studies provide new insight into how early mechanotransduction events may depend on dynamic modulation of mechanical properties and suggest that dynamic adaptive rheology may be one link between hemodynamic force and vascular disease.

TABLE OF CONTENTS

LIST OF FIGURES

LIST OF TABLES

ACKNOWLEDGEMENTS

My graduate school experience has been interesting thanks to all the people I met and worked with during my stay at Penn State. First and foremost, I would like to thank my advisor Dr. Peter J. Butler for his guidance, support and encouragement through the course of my graduate studies. I would also like to extend my gratitude to my committee members Drs. Cheng Dong, William Hancock and Erin Sheets for their suggestions and critique of this dissertation.

Dr. Nadine B. Smith, thank you for being my friend, philosopher and guide. I would also like to thank the Bioengineering department faculty and staff for always willing to help.

This work is the result of constant knowledge transfer and collaborations with many people. I thank Dr. Margaret Slattery for sharing her cell culture expertise and Dr. Sung Yang for his help with photolithography and fabrication of microposts. To all the past and current members of the Butler lab, thank you for your help and all the insightful discussions through the years. To Tristan Tabouillot, Rama Gullapalli, Aparna Subbu, Gayatri Muthukrishnan, Shankar Shastry and Vijay Wadhwa, thank you for being such great friends and for all the fond memories. To Vikram Mishra, thank you for being so patient and supportive during times of trouble.

To my parents Asha and Hirji Dangaria, and my brother Nikunj, thank you for your unwavering love and support. Mom and Dad, without your encouragement I would not have reached this milestone. This dissertation is dedicated to you.

Chapter 1

BACKGROUND

1.1 Hemodynamic forces acting on the vascular endothelium

Endothelial cells make up the endothelium, the innermost lining of blood vessels, and are thus continually exposed to hemodynamic forces due to blood flow. These forces can be resolved into shear stress, the parallel component representing the frictional force exerted on the vessel wall, and tensile stress, the perpendicular component resulting from blood vessel distension from blood pressure. *In vivo*, the cardiac cycle generates pulsatile flow with varying temporal and spatial gradients as represented in Figure **1-1**. Regions in the vasculature, experiencing mean positive shear stress i.e. laminar flow patterns, appear to be devoid of atherosclerotic lesions. Thus mean positive shear stress is thought to be atheroprotective (reviewed in (Davies, 1995)). In contrast, atherosclerotic lesions are localized in areas of flow recirculation where shear stress is low and blood flow is unsteady, non-laminar, or has a reversing component (Chiu et al., 2005). Fluid shear stress also regulates many physiological processes such as inflammation (Shyy et al., 1994), wound healing (Gojova and Barakat, 2005), hemostasis (Galbusera et al., 1997), vascular tone (Butler et al., 2000) and remodeling (Gusic et al., 2005) of the endothelium

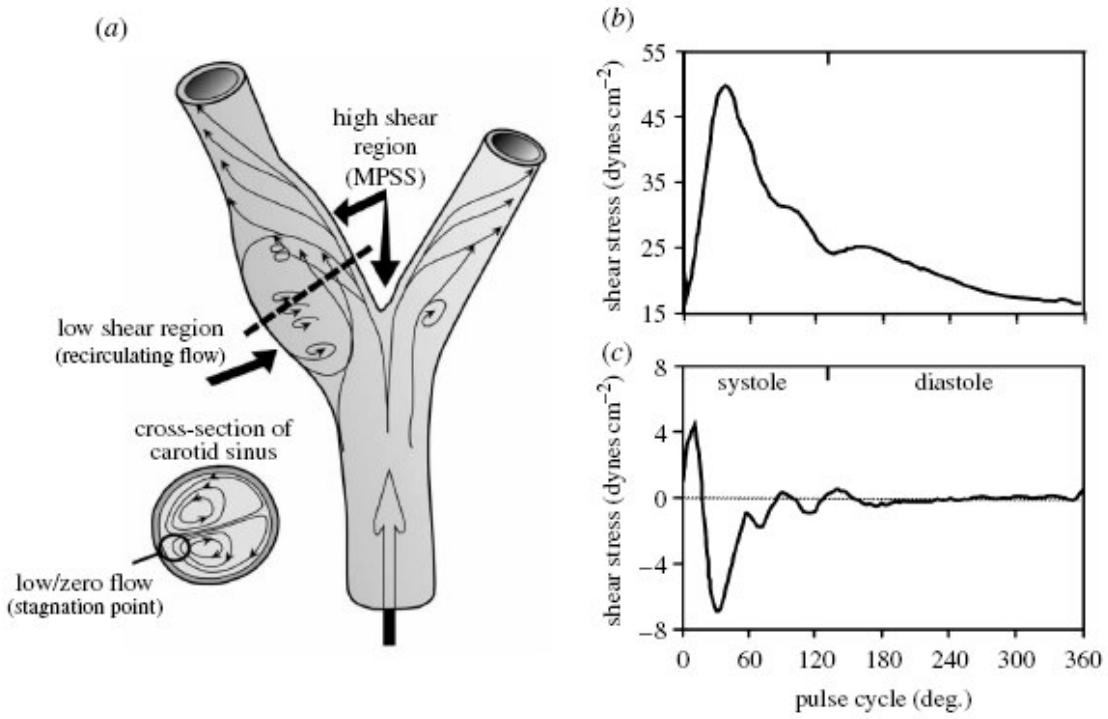

Figure **1-1**: a) Flow patterns in the carotid bifurcation. Regions of high shear stress are atheroprotective while regions experiencing low shear stress are atherogenic. b) Shear stress along the inner wall of the bifurcation. c) Shear stress in recirculation regions. Adapted from (Ku et al., 1985;Ingber, 2006)

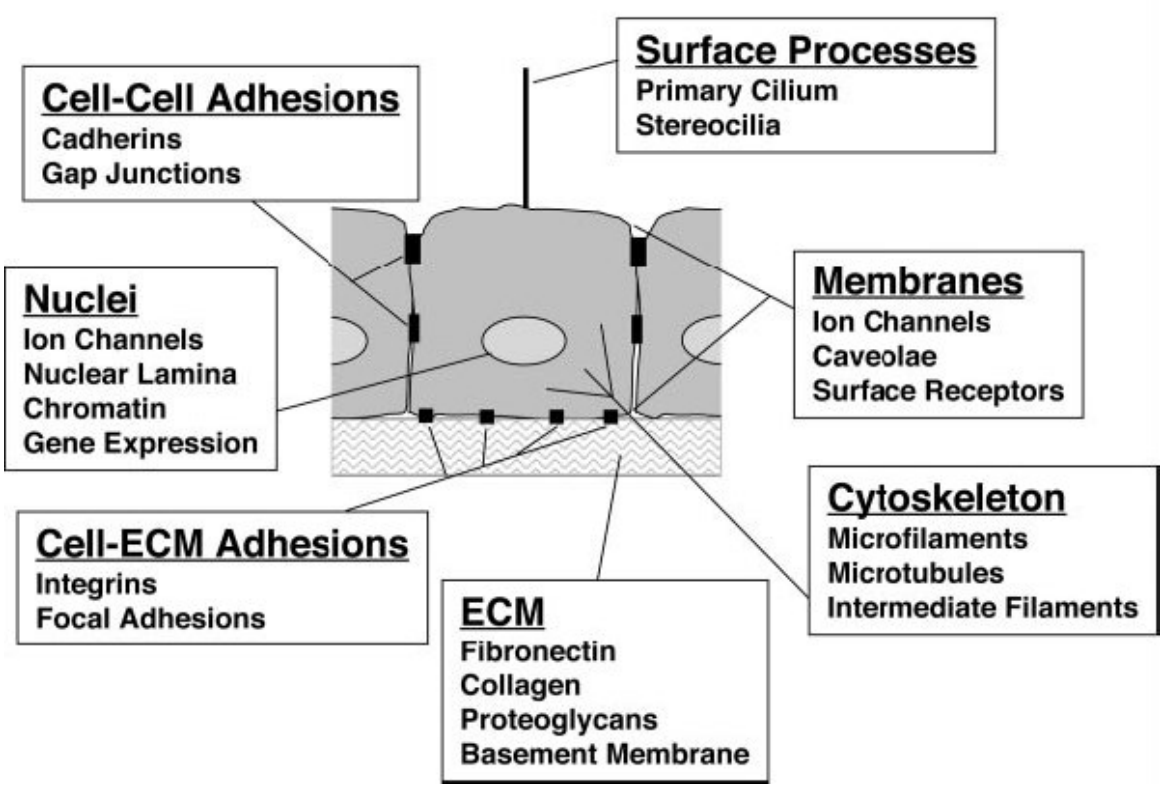

Figure **1-2**: Cells sense mechanical signals and transduce them into biochemical signals through a variety of cellular structures and molecules. Adapted from (Ingber, 2006)

Prior studies have shown that cells sense mechanical signals and transduce them into a variety of biochemical signals through multiple cellular structures such as the cell membrane (Butler et al., 2001;Haidekker et al., 2000;Gudi et al., 1998), glycocalyx (Florian et al., 2003;Pahakis et al., 2007), cytoskeleton (Helmke and Davies, 2002;Galbraith et al., 1998), G proteins (Gudi et al., 1998), integrins (Ishida et al., 1997;Li et al., 1997), Ca^{2+} channels (Naruse and Sokabe, 1993;Sigurdson et al., 1993) and cell-cell junction proteins (Fujiwara et al., 2001). It is usually presumed that the forces acting on the cell distend some part of the cell leading to changes in protein conformation or changes in the association of molecules (Kaazempur Mofrad et al.,

2005). The distension or strain is thus a function of the mechanical properties of the cell. Traditionally, cell mechanics has been studied using continuum theories and static mechanics. Recent advances in understanding force distribution through the cytoskeleton and polymer physics have highlighted the need to address cell mechanics at the molecular level. Furthermore, the studies outlined in this thesis highlight the need to consider the cell as mechanically dynamic and continuously adaptive in the face of changing forces. Such understanding provides the foundation to insight into the fundamental mechanisms of how cells convert force into biochemical signals.

1.2 Role of cell mechanics in mechanotransduction

Cells are known to have both solid-like and liquid-like properties and thus their ability to withstand external forces is best understood using traditional methods of rheology (Janmey and Weitz, 2004). Since many cell functions require cell deformation (from externally imposed forces or from forces generated internally) the rheology of the cell becomes the conceptual link between force and biology. For example, cell mechanics governs basic cellular functions such as migration (Bray D, 2001), adhesion (Sackmann and Bruinsma, 2002), differentiation (Grill et al., 2003), and maintaining cell shape (Boal D, 2002). Intracellular mechanics can depend on several factors but it is now recognized that actin filament organization, cross-linking and bundling, actin polymerization and depolymerization, and actomyosin contractility are the main factors governing cellular rheology (Lee et al., 2006).

Knowledge of the underlying origins of the mechanical properties of this network is essential in determining the role of actin cytoskeleton in modulating cell mechanics. Although molecular mechanisms of mechanotransduction remain the center of controversy, growing evidence points towards a greater role of the endothelial cell cytoskeleton in transmission and sub-cellular distribution of shear forces from the apical cell surface.

1.2.1 Cytoskeleton

The endothelial cell cytoskeleton consists of three types of cytosolic fibers: actin filaments (7 to 9 nm diameter) (Furukawa and Fechheimer, 1997), intermediate filaments (10 nm diameter) (Herrmann and Aebi, 2004), and microtubules (25 nm diameter)(Desai and Mitchison, 1997). Polymerization of globular G-actin monomers results in the formation of double-stranded, helical actin filaments. *In vivo,* actin filaments are organized into two-dimensional rigid networks (stress fibers), and three-dimensional gels, with the aid of various cross-linking and bundling proteins such as α-actinin and filamin. Of the three, actin filaments (F-actin) are the most abundant and located in close proximity to the apical and basal cell membranes. These networks provide a mechanical framework to sustain cell shape, motility and mechanosensitivity.

Various attempts have been made to characterize rheology of F-actin networks, *in vitro*, in terms of single filament elasticity and dynamics (Gardel et al., 2003). Macroscopically, rheological measurements completely describe the mechanical response of a material. Complex viscoelastic materials like semi flexible F-actin networks exhibit

the properties of solids as well as liquids and thus they are best characterized by frequency-dependent complex shear modulus. The following section describes various methodologies employed to estimate mechanics and nano-scale dynamics of the endothelial cell cytoplasm.

1.3 Experimental techniques to quantify cell rheology

The study of deformation and flow of material in response to applied stress is known as rheology. Such measurements provide an insight into structural rearrangements and mechanical properties of various materials. Conventionally, mechanical rheometers are used to apply a small oscillatory strain γ and measure the resultant shear stress σ over frequency ranges up to MHz. The complex shear modulus thus obtained is an average measurement of bulk response. Measurements of this kind are acceptable in cases where the material in question is homogenous. Intracellular F-actin networks are composed of a variety of cross-linking proteins and semi flexible polymers are extremely heterogeneous. At microscopic length scales, the mechanical response no longer scales with the bulk response. Hence, direct measurements of local viscosity and elasticity are required.

Microrheology is a new measurement technique wherein motions of nanometer to micrometer sized spherical probes are used to obtain readouts of local mechanical properties of the microenvironments in which they are embedded. If the particle size is larger than the characteristic length scale of the medium, particle motions are interpreted as a frequency-dependent, linear viscoelastic bulk response. For particle sizes smaller than or on the order of structural length scales, motions are representative not only of the

local viscoelastic spectrum but also steric effects between the probe and the cavity walls in which it is embedded (Valentine et al., 2004).

1.3.1 Active Microrheology

Active microrheology methods involve application of external stress, locally on the spherical probe and measuring strain to compute shear moduli. Stress can be applied using magnetic and optical fields as well as atomic force microscopy (AFM) techniques.

1.3.1.1 Magnetic rheometry

Magnetic bead microrheometry involves application of forces on the order of 10 nN (Bausch et al., 1998) on ~4.5μm diameter, paramagnetic beads. Beads may be coated such that they can selectively attach to integrin receptors on the cell surface. Bead motions in response to applied force pulses are measured using particle tracking. In the study performed by Bausch *et al.*, 3D shear modulus values of NIH 3T3 fibroblasts were 20 to 40 kPa and cytoplasmic viscosity was estimated to be 2000 Pa-sec. In a similar technique employed by Wang *et al*. called magnetic twisting cytometry (Wang et al., 1993), rigidity modulus values ranging from 1 to100 Pa were reported in bovine capillary endothelial cells.

1.3.1.2 Atomic force microscopy (AFM)

Atomic force microscopy has the capability of providing information pertaining to surface structure and topography by using a sharp tip at the end of a flexible cantilever to locally indent a sample. Sinusoidal forces are applied to the cantilever and varying z - positions of the AFM tip corresponding to the cell indentation depth are monitored. The AFM tip is used in such a way to apply local compressive stresses directly on the cell surface. Frequency-dependent complex viscoelastic modulus $G^*(\omega)$ is computed from applied force and indentation depth (Alcaraz et al., 2003). The elastic shear modulus has been reported to be ~400-600Pa. Since imaging and elastic or viscoelastic response of thin samples are obtained simultaneously, it is possible to correlate changes in mechanics and structure of the sample.

Active microrheology measurements have the advantage of probing small volumes of the sample locally, by applying large stresses and measuring resultant strain. However, these methods require complicated instrumentation set-up. Depending on the micromanipulation technique used, rigidity modulus values differ by several orders of magnitude (Laurent et al., 2002). Discrepancies in reported modulus values may arise due to differences in cell types and physiological conditions under which measurement was performed, magnitude of stress applied in each technique (0.1 to 10^4 pN/μm^2) and dimensions of the probes used.

1.3.2 Passive microrheology

Passive microrheology techniques involve the use of thermal fluctuations or Brownian dynamics of embedded markers to measure structure and rheology of a material. Since no external stresses are applied to the material, the measured viscoelastic response always falls in the linear regime. The thermal energy k_BT creates a random force of the order of k_BT/a on an embedded probe with radius *a*. This force on a probe with radius ~500 nm is on the order of 1 pN and can create local deformations in the medium around the probe. The motion of this probe is governed by the properties of the microenvironment surrounding it (Tseng et al., 2002). In this way, the time-dependent position autocorrelation function or mean squared displacement (MSD) (defined by equation **1.1**) of the embedded probes can completely define the frequency-dependent complex shear modulus $G^*(\omega)$ where τ indicates the time lag and MSD values are averaged over all starting times *t*. By computing time-averages, we assume that the medium is in thermal equilibrium and its properties do not change over time. The MSD of embedded probes can be related to 2- dimensional diffusion coefficient *D* as shown in equation **1.2**.

The Stokes-Einstein equation describes relation between diffusion coefficient D and viscous drag coefficient for a sphere of radius *a*.

$$\left\langle \Delta r^2(\tau) \right\rangle = \left\langle \left[x(t+\tau) - x(t) \right]^2 \right\rangle + \left\langle \left[y(t+\tau) - y(t) \right]^2 \right\rangle \qquad (\mathbf{1.1})$$

$$\left\langle \Delta r^2(\tau) \right\rangle = 4D\tau \qquad (\mathbf{1.2})$$

where k_B is the Boltzman's constant, T is temperature and η is viscosity of the medium surrounding the sphere. For pure diffusion, MSD scales linearly with τ while for subdiffusive motions, the slope of MSD versus τ plots lies between 0 and 1. A detailed analysis of the derivation of $G^*(\omega)$ from $\left\langle \Delta r^2(\tau) \right\rangle$ is described by Mason (Mason, 2000).

1.3.2.1 Effects of probe surface chemistry on rheology

Passive microrheology techniques are suitable only for sufficiently soft materials since the embedded probes exert very small forces on their surrounding medium and thus move only on the order of nanometers to microns. This technique is sensitive to the size and surface chemistry of the probe and to the resolution with which the position can be detected. Interactions between probes and the medium in which they are embedded are highly dependent on the surface chemistry of the probes. This is also true for biopolymers like F-actin networks. McGrath *et al*. studied the effect of actin-adsorption on polystyrene (PS) beads and its corresponding effect on micromechanical moduli (McGrath et al., 2000). Polystyrene beads were coated with bovine serum albumin (BSA) to prevent actin binding. Actin was polymerized in the presence of unmodified polystyrene beads, carboxylated beads, and silica beads. It was reported that with the exception of BSA coated PS beads, all others adsorbed significant amounts of actin. Moduli values also differed depending on the surface coating, with PS beads exhibiting the highest and BSA-PS beads exhibiting lowest moduli values. Thus, a variable response is observed depending on the size and surface characteristics of the probes. If the particles aggregate

within the network, they can potentially alter the macroscopic F-actin structure (McGrath et al., 2000).

In this study, microrheology measurements were obtained using endogenous vesicles as well as endocytosed carboxylated polystyrene beads. Using endogenous tracers has a distinct advantage that the local environment in the cell is not externally modified (Yamada et al., 2000), however, in bovine aortic endothelial cells very few vesicles are seen in the first place and many times these vesicles exhibit motion in the z-axis hence cannot be tracked for the entire time duration. In chapter 4, we used 0.5 μm endocytosed carboxylated polystyrene beads to obtain better tracking statistics per cell. We used 0.5 μm beads specifically in keeping with the average endogenous vesicle diameter which was found to be ~ 0.5 μm.

1.4 Modeling approaches to describe cellular rheology

A wide range of models have been used to describe mechanics in living cells such as finite element-based continuum models (Charras and Horton, 2002;Ferko et al., 2007;Karcher et al., 2003), phenomenological models using springs and dashpots (Sato et al., 1996;Schmid-Schonbein et al., 1981), tensegrity model of the cytoskeleton (Ingber, 2006;Stamenovic et al., 2004;Fabry et al., 2003), and modeling cells as soft glasses (Fabry et al., 2003).

The soft glass rheology model proposed by Sollich (Sollich, 1998) for materials like foams (shaving cream), pastes, colloids, emulsions, slurries etc was adopted by Fabry *et al.* to describe mechanical behavior of live cells. According to this theory, the complex

viscoelastic shear modulus $G^*(\omega)$ exhibits a weak power dependence on the frequency i.e. $G^*(\omega) \propto \omega^x$ where x is the rheology exponent that describes the "effective temperature" of the cell arising from the non-thermal fluctuations. This theory suggests that the extent of disorder in the cytoskeletal matrix as well as the metastability of its structural elements, play a central role in modulation of cell mechanics. Gunst *et al.*, have proposed that non-thermal fluctuations in cells are ATP driven and arise from the activity of motor proteins including myosin (Gunst and Fredberg, 2003). While soft glassy theory has been used to model smooth muscle cell rheology, recent studies by Van Critters *et al.* in epithelial cells suggest that ATP depletion and myosin motor inhibition did not affect the rheology exponent (Van Citters et al., 2006) . Their argument states that power-law rheology finds its origins in thermally activated stress relaxation processes.

The tensegrity model treats cells as a macroscopic system of tension-generating springs and compression-bearing struts, and the prestress in such a structure to be the primary determinant of the mechanical properties. The actin-myosin cytoskeleton network is thought to be the source of cell prestress and a primary component of tensegrity models (Wang et al., 2001).

Taken together, the current models of cell mechanics have remarkable disparity largely due to the relevant scales and biomechanical issues of interest. There remain many open questions in mechanotransduction despite the advances in measurement techniques and models of cell mechanics. To understand mechanobiology of cells, there is a need for multiscale integrative models to understand how externally applied mechanical forces are transmitted and distributed throughout the cell.

1.5 Significance of Research

The motivation for this dissertation stems from the hypothesis that endothelial cells adapt to a shear environment at very early time points by modulating their intracellular rheology and that these adaptations are driven by the actin cytoskeleton and myosin motor interactions. One goal of this project was to develop an automated, *in vitro* assay to generate spatial and temporal gradients in fluid shear stress in order to mimic *in vivo* conditions within recirculation zones. A custom-written, image-correlation-based algorithm was developed to quantify changes in intracellular rheology due to rapid changes in fluid shear stress. Furthermore, actomyosin interactions were selectively inhibited through using a panel of drug interventions and corresponding effects of rapid changes in shear stress on endothelial cells were studied. Finally, a phenomenological model of a viscoelasticity was used to predict mechanical constants. Taken together, these studies provide an insight into the early shear-mediated response of endothelial cells and the role of the actomyosin network in modulating this response. Since EC mechanotransduction has direct implications in vascular diseases such as atherosclerosis, cellular components associated with these early mechanotransduction events may be specific targets for therapeutic interventions (Ingber, 2003).

1.6 References

Alcaraz, J., L. Buscemi, M. Grabulosa, X. Trepat, B. Fabry, R. Farre, and D. Navajas. 2003. Microrheology of Human Lung Epithelial Cells Measured by Atomic Force Microscopy. *Biophys. J.* 84:2071-2079.

Bausch, A. R., F. Ziemann, A. A. Boulbitch, K. Jacobson, and E. Sackmann. 1998. Local measurements of viscoelastic parameters of adherent cell surfaces by magnetic bead microrheometry. *Biophys. J* 75:2038-2049.

Boal D. 2002. Mechanics of the cell. Cambridge University Press, Cambridge.

Bray D. 2001. Cell movements: from molecules to motility. Garland Publishing, New York.

Butler, P. J., G. Norwich, S. Weinbaum, and S. Chien. 2001. Shear stress induces a time- and position-dependent increase in endothelial cell membrane fluidity. *Am. J. Physiol Cell Physiol* 280:C962-C969.

Butler, PJ., S. Weinbaum, S. Chien, and D. E. Lemons. 2000. Endothelium-Dependent, Shear-Induced Vasodilation Is Rate-Sensitive. *Microcirculation* 7:53-65.

Charras, G. T. and M. A. Horton. 2002. Determination of cellular strains by combined atomic force microscopy and finite element modeling. *Biophys. J* 83:858-879.

Chiu, J. J., L. J. Chen, S. F. Chang, P. L. Lee, C. I. Lee, M. C. Tsai, D. Y. Lee, H. P. Hsieh, S. Usami, and S. Chien. 2005. Shear Stress Inhibits Smooth Muscle Cell-Induced Inflammatory Gene Expression in Endothelial Cells: Role of NF-{kappa}B. *Arterioscler Thromb Vasc Biol* 25:963-969.

Davies, P. F. 1995. Flow-mediated endothelial mechanotransduction. *Physiol Rev.* 75:519-560.

Desai, A. and T. J. Mitchison. 1997. MICROTUBULE POLYMERIZATION DYNAMICS. *Annual Review of Cell and Developmental Biology* 13:83-117.

Fabry, B., G. N. Maksym, J. P. Butler, M. Glogauer, D. Navajas, N. A. Taback, E. J. Millet, and J. J. Fredberg. 2003. Time scale and other invariants of integrative mechanical behavior in living cells. *Physical Review E (Statistical, Nonlinear, and Soft Matter Physics)* 68:041914-041918.

Ferko, M. C., A. Bhatnagar, M. B. Garcia, and P. J. Butler. 2007. Finite-element stress analysis of a multicomponent model of sheared and focally-adhered endothelial cells. *Ann Biomed. Eng* 35:208-223.

Florian, J. A., J. R. Kosky, K. Ainslie, Z. Pang, R. O. Dull, and J. M. Tarbell. 2003. Heparan sulfate proteoglycan is a mechanosensor on endothelial cells. *Circ Res.* 93:e136-e142.

Fujiwara, K., M. Masuda, M. Osawa, Y. Kano, and K. Katoh. 2001. Is PECAM-1 a mechanoresponsive molecule? *Cell Struct. Funct.* 26:11-17.

Furukawa, R. and M. Fechheimer. 1997. The structure, function, and assembly of actin filament bundles. *Int. Rev. Cytol.* 175:29-90.

Galbraith, C. G., R. Skalak, and S. Chien. 1998. Shear stress induces spatial reorganization of the endothelial cell cytoskeleton. *Cell Motil. Cytoskeleton* 40:317-330.

Galbusera, M., C. Zoja, R. Donadelli, S. Paris, M. Morigi, A. Benigni, M. Figliuzzi, G. Remuzzi, and A. Remuzzi. 1997. Fluid Shear Stress Modulates von Willebrand Factor Release From Human Vascular Endothelium. *Blood* 90:1558-1564.

Gardel, M. L., M. T. Valentine, J. C. Crocker, A. R. Bausch, and D. A. Weitz. 2003. Microrheology of Entangled F-Actin Solutions. *Physical Review Letters* 91:158302-158304.

Gojova, A. and A. I. Barakat. 2005. Vascular endothelial wound closure under shear stress: role of membrane fluidity and flow-sensitive ion channels. *J Appl Physiol* 98:2355-2362.

Grill, S. W., J. Howard, E. Schaffer, E. H. Stelzer, and A. A. Hyman. 2003. The distribution of active force generators controls mitotic spindle position. *Science* 301:518-521.

Gudi, S., J. P. Nolan, and J. A. Frangos. 1998. Modulation of GTPase activity of G proteins by fluid shear stress and phospholipid composition. *Proc. Natl. Acad Sci U. S. A* 95:2515-2519.

Gunst, S. J. and J. J. Fredberg. 2003. The first three minutes: smooth muscle contraction, cytoskeletal events, and soft glasses. *J Appl Physiol* 95:413-425.

Gusic, R. J., R. Myung, M. Petko, J. W. Gaynor, and K. J. Gooch. 2005. Shear stress and pressure modulate saphenous vein remodeling ex vivo. *Journal of Biomechanics* 38:1760-1769.

Haidekker, M. A., N. L'Heureux, and J. A. Frangos. 2000. Fluid shear stress increases membrane fluidity in endothelial cells: a study with DCVJ fluorescence. *Am J Physiol Heart Circ Physiol* 278:H1401-H1406.

Helmke, B. P. and P. F. Davies. 2002. The Cytoskeleton Under External Fluid Mechanical Forces: Hemodynamic Forces Acting on the Endothelium. *Annals of Biomedical Engineering* 30:284-296.

Herrmann, H. and U. Aebi. 2004. INTERMEDIATE FILAMENTS: Molecular Structure, Assembly Mechanism, and Integration Into Functionally Distinct Intracellular Scaffolds. *Annual Review of Biochemistry* 73:749-789.

Ingber, D. E. 2003. Mechanobiology and diseases of mechanotransduction. *Ann Med.* 35:564-577.

Ingber, D. E. 2006. Cellular mechanotransduction: putting all the pieces together again. *FASEB J* 20:811-827.

Ishida, T., M. Takahashi, M. A. Corson, and B. C. Berk. 1997. Fluid shear stress-mediated signal transduction: how do endothelial cells transduce mechanical force into biological responses? *Ann N. Y. Acad Sci* 811:12-23.

Janmey, P. A. and D. A. Weitz. 2004. Dealing with mechanics: mechanisms of force transduction in cells. *Trends in Biochemical Sciences* 29:364-370.

Kaazempur Mofrad, M. R., N. A. bdul-Rahim, H. Karcher, P. J. Mack, B. Yap, and R. D. Kamm. 2005. Exploring the molecular basis for mechanosensation, signal transduction, and cytoskeletal remodeling. *Acta Biomaterialia* 1:281-293.

Karcher, H., J. Lammerding, H. Huang, R. T. Lee, R. D. Kamm, and M. R. Kaazempur-Mofrad. 2003. A Three-Dimensional Viscoelastic Model for Cell Deformation with Experimental Verification. *Biophys. J.* 85:3336-3349.

Ku, D. N., D. P. Giddens, C. K. Zarins, and S. Glagov. 1985. Pulsatile flow and atherosclerosis in the human carotid bifurcation. Positive correlation between plaque location and low oscillating shear stress. *Arterioscler Thromb Vasc Biol* 5:293-302.

Laurent, V. M., S. Henon, E. Planus, R. Fodil, M. Balland, D. Isabey, and F. Gallet. 2002. Assessment of mechanical properties of adherent living cells by bead micromanipulation: comparison of magnetic twisting cytometry vs optical tweezers. *J Biomech. Eng* 124:408-421.

Lee, J. S. H., P. Panorchan, C. M. Hale, S. B. Khatau, T. P. Kole, Y. Tseng, and D. Wirtz. 2006. Ballistic intracellular nanorheology reveals ROCK-hard cytoplasmic stiffening response to fluid flow. *J Cell Sci* 119:1760-1768.

Li, S., M. Kim, Y. L. Hu, S. Jalali, D. D. Schlaepfer, T. Hunter, S. Chien, and J. Y. Shyy. 1997. Fluid shear stress activation of focal adhesion kinase. Linking to mitogen-activated protein kinases. *J Biol Chem.* 272:30455-30462.

Mason, T. G. 2000. Estimating the viscoelastic moduli of complex fluids using the generalized Stokes-Einstein equation. *Rheologica Acta* 39:371-378.

McGrath, J. L., J. H. Hartwig, and S. C. Kuo. 2000. The mechanics of F-actin microenvironments depend on the chemistry of probing surfaces. *Biophys. J* 79:3258-3266.

Naruse, K. and M. Sokabe. 1993. Involvement of stretch-activated ion channels in Ca2+ mobilization to mechanical stretch in endothelial cells. *Am. J. Physiol* 264:C1037-C1044.

Pahakis, M. Y., J. R. Kosky, R. O. Dull, and J. M. Tarbell. 2007. The role of endothelial glycocalyx components in mechanotransduction of fluid shear stress. *Biochem. Biophys. Res. Commun.* 355:228-233.

Sackmann, E. and R. F. Bruinsma. 2002. Cell adhesion as wetting transition? *Chemphyschem.* 3:262-269.

Sato, M., N. Ohshima, and R. M. Nerem. 1996. Viscoelastic properties of cultured porcine aortic endothelial cells exposed to shear stress. *Journal of Biomechanics* 29:461-467.

Schmid-Schonbein, G. W., K. L. Sung, H. Tozeren, R. Skalak, and S. Chien. 1981. Passive mechanical properties of human leukocytes. *Biophys. J.* 36:243-256.

Shyy, Y. J., H. J. Hsieh, S. Usami, and S. Chien. 1994. Fluid shear stress induces a biphasic response of human monocyte chemotactic protein 1 gene expression in vascular endothelium. *Proc. Natl. Acad Sci U. S. A* 91:4678-4682.

Sigurdson, W. J., F. Sachs, and S. L. Diamond. 1993. Mechanical perturbation of cultured human endothelial cells causes rapid increases of intracellular calcium. *Am. J. Physiol. Heart Circ. Physiol.* 264:H1745-H1752.

Sollich, P. 1998. Rheological constitutive equation for a model of soft glassy materials. *Phys. Rev. E* 58:738.

Stamenovic, D., B. Suki, B. Fabry, N. Wang, and J. J. Fredberg. 2004. Rheology of airway smooth muscle cells is associated with cytoskeletal contractile stress. *J Appl Physiol* 96:1600-1605.

Tseng, Y., T. P. Kole, and D. Wirtz. 2002. Micromechanical Mapping of Live Cells by Multiple-Particle-Tracking Microrheology. *Biophys. J.* 83:3162-3176.

Valentine, M. T., Z. E. Perlman, M. L. Gardel, J. H. Shin, P. Matsudaira, T. J. Mitchison, and D. A. Weitz. 2004. Colloid Surface Chemistry Critically Affects Multiple Particle Tracking Measurements of Biomaterials. *Biophys. J.* 86:4004-4014.

Van Citters, K. M., B. D. Hoffman, G. Massiera, and J. C. Crocker. 2006. The role of F-actin and myosin in epithelial cell rheology. *Biophys. J* 91:3946-3956.

Wang, N., J. P. Butler, and D. E. Ingber. 1993. Mechanotransduction across the cell surface and through the cytoskeleton. *Science* 260:1124-1127.

Wang, N., K. Naruse, D. Stamenovic, J. J. Fredberg, S. M. Mijailovich, I. M. Tolic-Norrelykke, T. Polte, R. Mannix, and D. E. Ingber. 2001. Mechanical behavior in living cells consistent with the tensegrity model. *Proc. Natl. Acad Sci U. S. A* 98:7765-7770.

Yamada, S., D. Wirtz, and S. C. Kuo. 2000. Mechanics of Living Cells Measured by Laser Tracking Microrheology. *Biophys. J.* 78:1736-1747.

Chapter 2

PARTICLE TRACKING, SYSTEM NOISE CHARACTERIZATION AND OPTICAL TRAP SETUP

Foreword

The following chapter is taken from the manuscripts: "Improved nanometer-scale particle tracking in optical microscopy using microfabricated fiduciary posts", Dangaria JH, Yang S, and Butler PJ. BioTechniques, 42: 437-8, 440, 2007 and "Integrated multimodal microscopy, time-resolved fluorescence, and optical-trap rheometry: toward single molecule mechanobiology", Gullapalli RR, Tabouillot T, Mathura R, Dangaria JH, and Butler PJ, Journal of Biomedical Optics, 12: 014012, 2007.

2.1 Introduction

Image-based particle tracking methods find numerous applications in biological studies at the cellular and molecular level. For example, tracking thermal motions of micron-sized spherical particles embedded in the cell cytoplasm reveal micro-heterogeneity of cellular rheology (Tseng et al., 2002). Fluorescent microspheres conjugated with protein analogs as well as colloidal gold beads have been used to study mobility of lipids and proteins in the cell membranes (Saxton and Jacobson, 1997) and to track motions of kinesin molecules on microtubules (Schnapp et al., 1988). Improved instrumentation and multiple particle tracking algorithms now permit high-throughput

nanometer scale positional resolution using time-lapse DIC and fluorescence imaging (Breedveld and Pine, 2003;Hung-Wing et al., 2007).

However, there remain impediments to accurate tracking at the nanometer scale. Despite advances in motorized stage design, stages still exhibit low frequency drift due to thermal cooling of stepper motors and high frequency vibrations arising from relative motion of sample and imaging instrumentation (e.g. ccd camera). Although immobilized beads adhered to glass coverslips have been used as stationary markers (Gelles et al., 1988), it is difficult to control their precise location and stability during cell culture. Also, for z-axis scanning of cells, the beads attached to glass surfaces are out-of focus at more than a micron away from the glass. Other avenues to mitigate mechanical instability are expensive piezo stages, high performance vibration isolation tables, and remote cooling of camera ccd chips. Even with these improvements, there will always remain some uncertainty as to whether particle trajectories represent true motion or coverglass motion artifacts.

To overcome uncertainty at both high and low frequency ranges and to enable tracking of coverslip motion relative to cell organelle motion, even at microns away from the coverslip, we microfabricated 10 μm high and 3 μm diameter, cylindrical SU 8 posts on glass coverslips to serve as fiduciary markers during tracking.

2.2 Material and Methods

Microposts were fabricated using SU-8 2010, a negative, epoxy-type photoresist (MicroChem Corp., Newton, MA, USA) on 40 mm circular, no.1 glass coverslips (Bioptechs Inc, Butler, PA, USA.) using standard photolithography techniques (Lorenz et al., 1998). Glass coverslips were initially cleaned using acetone (10 min), isopropanol (10 min), and DI water (10 min). An adhesion layer (OmiCoat, MicroChem Corp., Newton, MA, USA) was spun down on the glass surface using a spin coater (PWM32, Headway Research Inc., Garland, TX, USA) followed by a baking process on a hot plate at 200 ^{o}C for 1 min. SU-8 2010 was spun down on top of the adhesion layer at 5000 rpm for 30 sec to obtain a 10 μm-thick uniform photoresist layer. The resulting layer was baked at 65 ^{o}C for 10 min. and at 95 ^{o}C for 20 min.

A chromium mask was designed in AutoCad and fabricated commercially (MEMS and Nanotechnology Exchange, Reston, Virginia) to the desired specifications. The mask and glass samples were exposed under UV light for 30 sec to selectively activate SU-8 2010 layer and baked at 50 ^{o}C for 15 min and 95 ^{o}C for 20 min. Samples were then developed using SU-8 Developer (MicroChem Corp., Newton, MA, USA) to remove inactivated SU-8 2010 and adhesion layers and washed in isopropanol solution. Finally, the coverslips were baked at 150 ^{o}C for 3 min (Figure **2-1** A). Dimensions of posts were verified using sequential z-axis optical sectioning using DIC microscopy and a piezo-controlled stage Nanoview™/M (Madcity Labs, Madison, WI, USA). Additional verification was performed using a stylus (Alpha-step 200, TENCOR Instruments, San Jose, CA, USA).

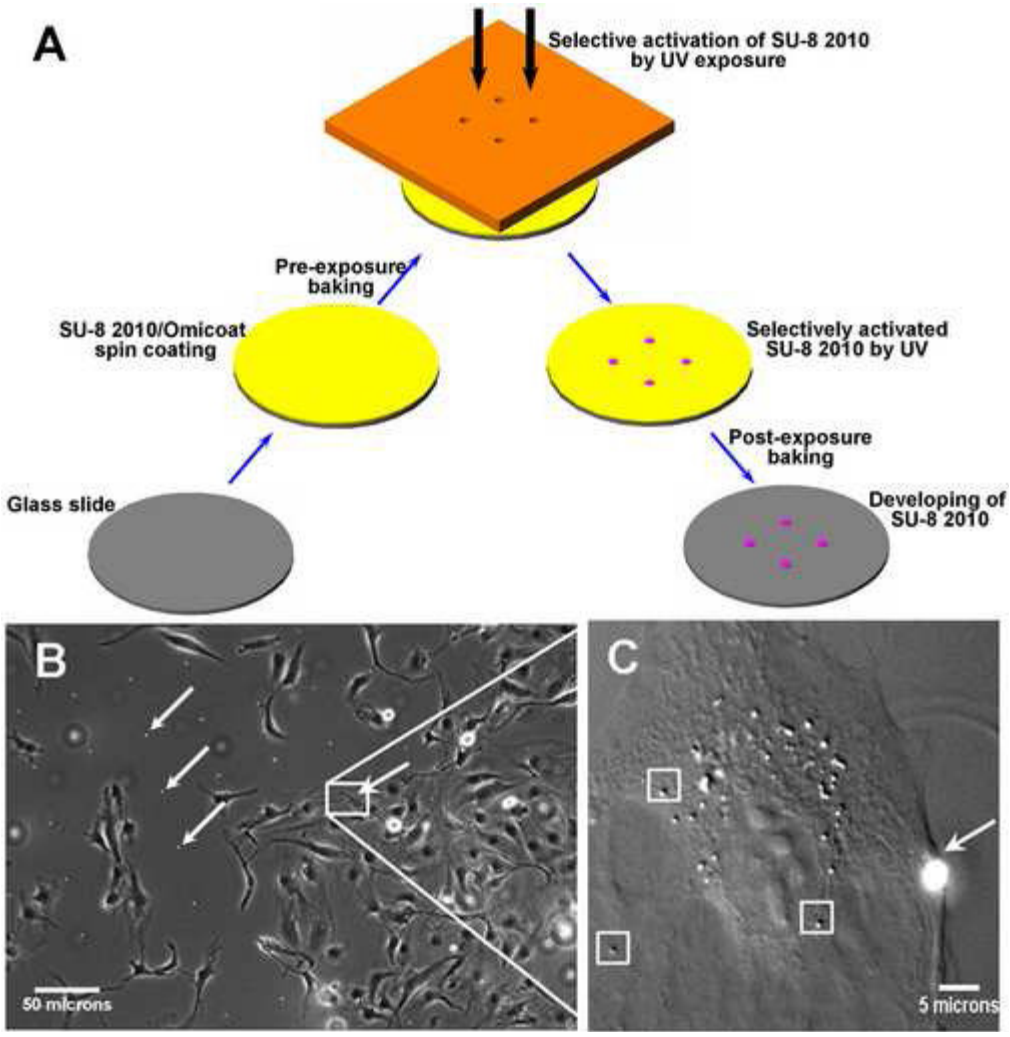

Figure **2-1**: (A) Photolithography-based fabrication process. (B) Endothelial cell monolayer growing around the microfabricated grid pattern of 3μm wide and 10μm high posts spaced 50 μm apart imaged under 20X phase contrast. (C) 60X DIC microscopy image of a bovine aortic endothelial cell. Tracked endogenous vesicles in the cell are highlighted by rectangles. Arrows indicate the microfabricated post.

Bovine Aortic Endothelial cells (BAECs, VEC technologies, Rennsaelear, NY) were sub-cultured between passages 3-10 on the processed coverslips (Figure **2-1** B and C). MCDB-131 complete medium supplemented with 11% fetal bovine serum (FBS), 10ng/ml EGF, 1µg/ml hydrocortisone, 100mg/500ml ENO-GRO (VEC Technologies, Inc), 45mg/500ml heparin and 5ml/500ml of 100X antibiotic/antimycotic solution was used as the culture medium. Cells were incubated at 37° C with 5% CO2, 90% humidity. In order to maintain the physiological environment while imaging, a closed system flow-chamber, (Focht Chamber System (FCS2), (Bioptechs Inc, Butler, PA)) was used. The FCS2 flow-chamber was mounted on a computer controlled, motorized microscope stage (Nano-View™, Madcity Labs, Madison, WI, USA).

Cells were imaged under DIC microscopy using an Olympus IX71 inverted research microscope with a 60X PlanApo oil immersion objective, NA= 1.45. To further improve the resolution in the DIC mode, a 60X LUMPlanFL water immersion objective (0.90NA) was used in place of the condenser. An immersion oil with refractive index = 1.33 (Series AAA, Cargille Laboratories Inc., NJ) was used in place of water to prevent evaporation of immersion medium. Images were acquired in real-time with a high resolution, 12bit CCD camera, Sensicam QE (Cooke Corp, Romulus, MI, USA). Camware 2.12 software (Cooke Corp, Romulus, MI, USA) was used to acquire time-lapse, 8-bit Tiff images at 15-30 frames per second with exposure times of 1-3ms with an image resolution of 0.1µm/pixel. Multiple particle tracking of microposts and endogenous cell organelles was performed using a custom algorithm written in LabVIEW (National Instruments, Austin, TX, USA). Briefly, the centroid of the maximum

correlation of a template image of the feature being tracked and its subsequent images in a time series was plotted.

2.3 Results and Discussion

Tracking of post and vesicle images verified readily distinguishable low and high frequency coverglass motion artifacts. When the motorized microscope stage was on, it exhibited a preferential drift in the Y direction with an average velocity of 0.3μm/sec (Figure **2-2** A). The presence of microposts as fiduciary markers in the time-lapse images enabled subtraction of the low frequency directional drift of the microscope stage from the cell organelles motion to reveal their natural trajectories (Figure **2-2** B).

Particle tracking measurements are subject to fluctuations in light source intensity, camera electronics, and shot noise of the CCD chip. Since the microposts and vesicles were tracked simultaneously, subtraction of micropost position corrected for errors due to system vibration and shot noise. To quantify such indeterminate errors (Cheezum et al., 2001), precision of our tracking algorithm was calculated as the standard deviation of the square root of the MSD and was found to be 2.4 nm.

Time-dependent position autocorrelation function or mean squared displacement (MSD) of endogenous vesicles was computed before and after subtracting stage drift to evaluate how well the procedure reduced high frequency system noise (Figure **2-2** C). This technique facilitated the segregation of vesicle trajectories into diffusive, sub-diffusive, and directed motion components and thus provided the ability to measure the Brownian dynamics as well as motor-driven active transport of molecules in cells.

Importantly, tracking analysis was carried out on vesicles which were about 2-5 μm away from the coverslip. Markers confined to the coverlip would not be useful for subtracting out the global stage and coverslip motion.

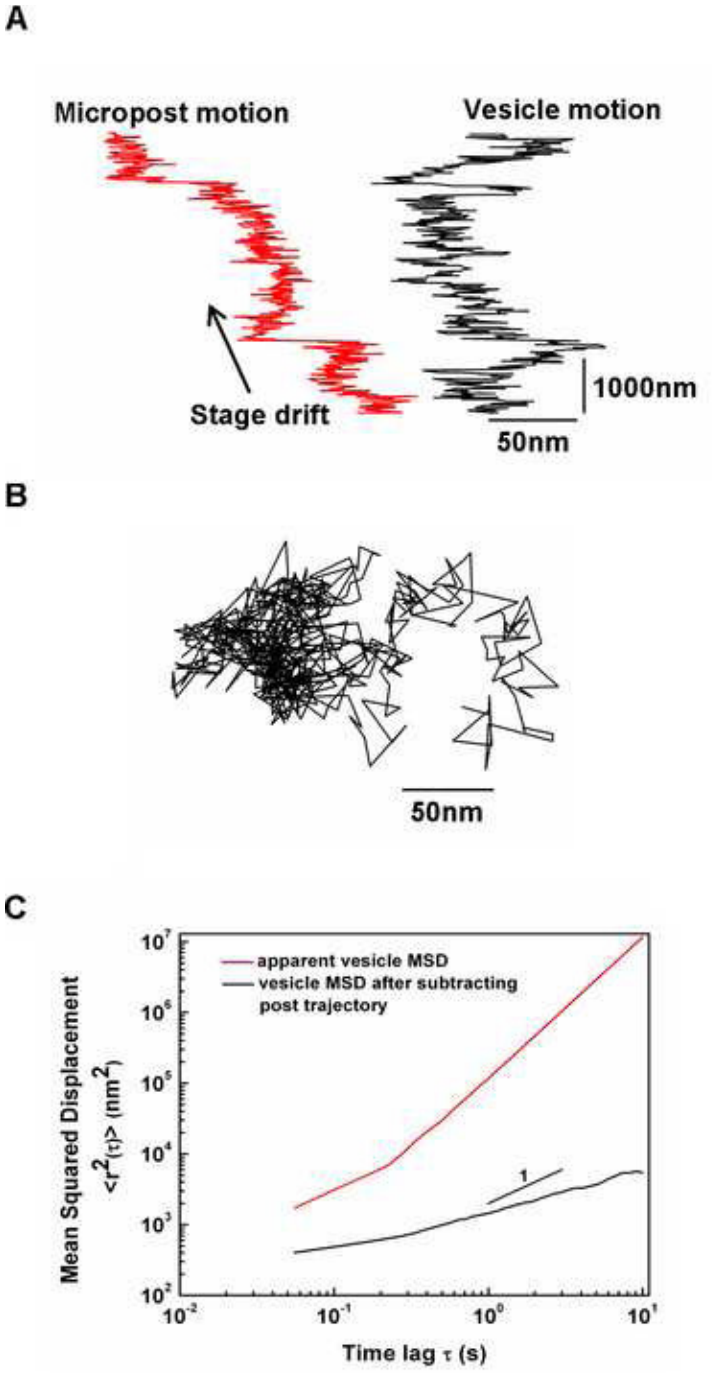

Figure **2-2**: (A) Apparent vesicle and post motion when the motors of microscope stage were on. A preferential drift in the Y direction with an average velocity of 0.3μm/sec, is observed. Time-lapse images captured for a total duration of 30 sec. (B) Vesicle trajectory after subtracting post motion. Scale applies to both x (horizontal) and y (vertical) scales. (C) Time-dependent position autocorrelation function (or Mean squared displacement (MSD)) of a vesicle before and after subtraction of post trajectory averaged at all starting times. High frequency ($\tau < 1$ sec) noise is a decade lower and low frequency ($\tau > 1$ sec) noise is ~ 4 decades lower. Slope < 1 indicates sub-diffusive motion of the vesicle.

Conventional analog as well as motorized, piezo and galvanometer driven microscope stages exhibit temperature-related drifts over long time periods (min-hours) (Adler and Pagakis, 2003) even when motors are turned off. This low frequency noise can be quantified by tracking the stationary microposts and can be easily subtracted out from the particle trajectories during post processing. It is anticipated that 3-D fiduciary markers could also serve to correct for long term changes in focus. In the z-direction the microposts have characteristic 3-D refraction patterns which could be exploited using correlation methods in the z-direction to quantify changes in focus. To acquire images in 3D, z axis calibrations may be required to compensate for any image distortions due to z axis stage drift. Rapid 3-D sectioning of microposts can be performed to calibrate the z noise level and thus time-dependent changes in focus can be quantified. A computer controlled feedback loop could be set-up to correct for the z axis stage drift over time. Similarly, long range scanning where it is important to return to precisely the same location after scanning could be facilitated through image processing and fiduciary markers. Such methods could improve high throughput screening in scanning cytometry experiments (Bajaj et al., 2000).

In conclusion, the technique of microfabricating fiduciary markers on glass coverslips along with multiple particle tracking algorithm provides a cost-effective solution to eliminate low and high frequency microscope stage and coverglass motion from time-lapse images of adherent cells. Potentially, micro-contact printing can be utilized to add fluorescent tracer molecules to the microposts for corrections in coverglass motion under confocal and fluorescence imaging (Quist et al., 2005;Xia and Whitesides, 1998).

2.4 Optical trap

2.4.1 Theory

An optical trap was designed with the motive of applying small-scale forces on adherent cells and assessing local changes in cellular mechanical properties using particle tracking microrheology.

Optical tweezers or optical traps employ highly-focused light beams to capture and manipulate small dielectric particles (Ashkin, 1998;Block, 1992). Such photonic forces are limited in the range of 0.1 – 200 pN. Using a high NA objective to focus the laser beam onto the sample, small beads or endogenous vesicles in a cell can be trapped. Using a beam-focusing objective allows simultaneous observation of the trapped particles. The force on a particle as it moves from the center of the trap is given by:

$$F = -\alpha \frac{n_1 V}{cR^2}\left(\frac{n_2^2 - n_1^2}{n_2^2 - 2n_1^2}\right) I_0 \exp\left(-r^2 \big/ R^2\right) r\hat{r} \qquad (\mathbf{2.1})$$

where α is a geometrical factor of order one, n_1 and n_2 are the refractive indices of the surrounding medium and the particle, respectively, V is the volume of the particle, c is the speed of light in a vacuum, I_0 is the intensity of the incident light, r is the distance between the centers of the bead and laser beam, $\hat{r}$ is a unit vector, and R is the 1/e width of the Gaussian laser beam at the trap. The requirement for trapping to occur is $n_1 > n_2$. For small displacements, this force can be approximated using Hooke's law with a spring constant k_{ot} (Hough L.A. and H.D.Ou-Yang, 1999).

$$F = -k_{ot}\, r \exp\left(-r^2 \big/ R^2\right) \qquad (\mathbf{2.2})$$

Rheology of a medium can be measured by applying local stress by moving the trap with respect to the position of the particle and measuring the resulting displacement as strain. For small displacements, spring constant k_{ot} calibrations can be performed by measuring thermal fluctuations in the position of the trapped particle and using the equipartition theorem:

$$\frac{1}{2} k_{ot} \left\langle (x - x_0)^2 \right\rangle = \frac{1}{2} k_B T \qquad (\mathbf{2.3})$$

where k_B is the Boltzmann constant (1.38×10^{-23} J/K), T is absolute temperature and x is the particle position, x_0 is the mean value of x and $\langle\ \rangle$ denotes the time average of 1-D displacements.

2.4.2 Design

The optical trap was first modeled using ray-tracing software Optics-Lab (Carlsbad, California) to assist in lens placement (Figure **2-3**). The trap was constructed using C-mount components and is introduced into the expanded infinity space under the microscope objective as seen in Figure **2-4**. Coherent 830-nm laser light can be continuous or transistor-transistor logic TTL-modulated using a 5-V square wave with 50% duty cycle from an analog to digital A/D board National Instruments, Austin, Texas. A water-immersion 60/ 1.2-NA objective is used to focus the collimated and expanded laser beam down to a diffraction limited spot. The coordinates of the laser focal point corresponding to the image is determined by imaging the focused beam reflecting off the back of a glass coverslip. Dielectric polystyrene beads in a solution of 1% albumin and

DPBS were then successfully trapped and tracked with a spatial sensitivity of 10 nm using time-lapse digital imaging and particle tracking algorithms based on the methods of (Gelles et al., 1988). TTL-modulation of the laser power enabled precise modulation of trap strength for rapid mechanical testing of 3% gelatin/water solution, which has elastic properties similar to endothelial cell cytoplasm (35). Recently a quadrant photodiode was integrated above the condenser, which will enable 3-D tracking of trapped microbeads and photonic force microscopy.

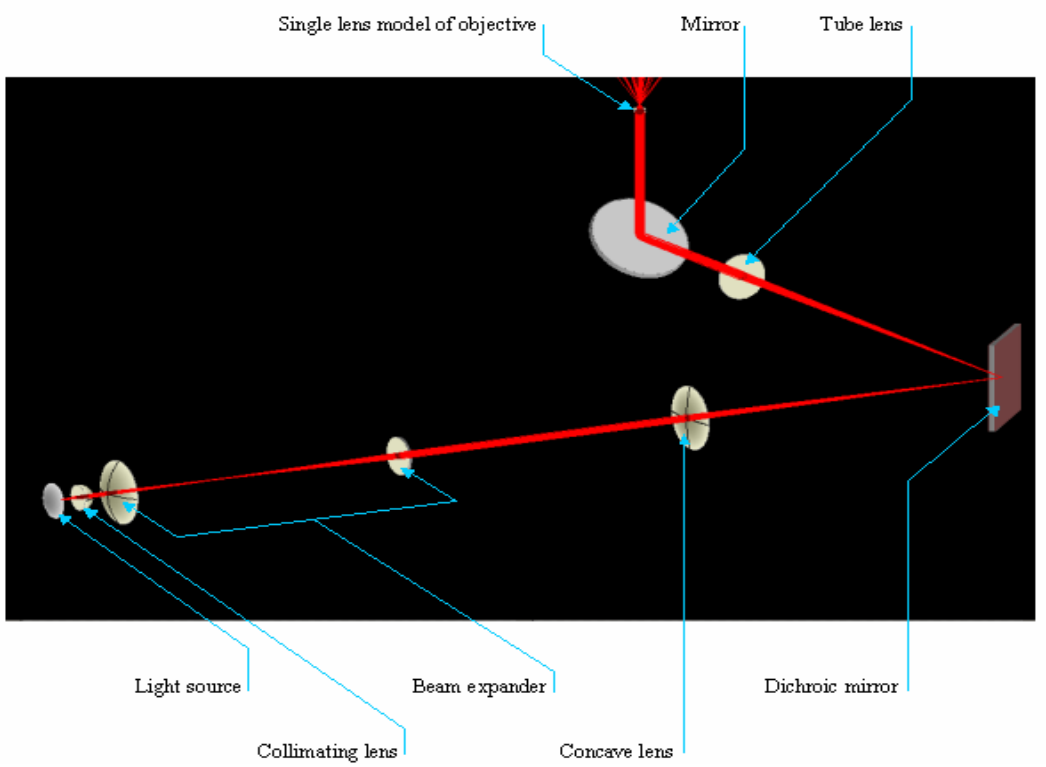

Figure **2-3**: Simulated optical trap layout using ray-tracing software Optics-Lab. Courtesy Rishi Mathura.

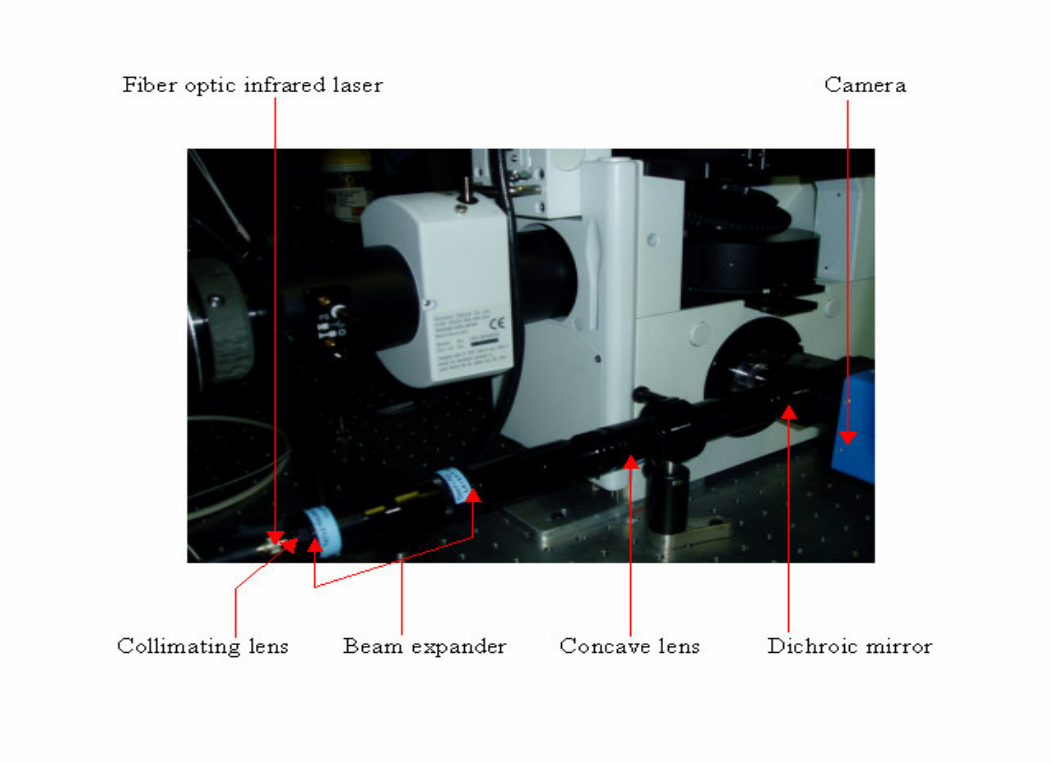

Figure **2-4**: Optical trap setup. Courtesy Rishi Mathura.

2.4.3 Optical trap rheometry

The value of the optical trap's spring constant 11 pN/nm was determined from particle trajectories in water and the equipartition theorem using Hooke's law. The spring constant of an optical trap was modulated by a TTL pulse delivered to the laser controller. The result was a trap stiffness exerted on polystyrene beads that varied as a square wave. Bead displacement as a function of time depended on this time-varying trap stiffness and the mechanical properties of the matrix surrounding the bead. To demonstrate the interaction of beads and a viscoelastic environment, a mixture of 3%

gelatin and filtered water—intended to mimic the cell cytoplasm—was combined with beads in a solution of 1% albumin and DPBS.

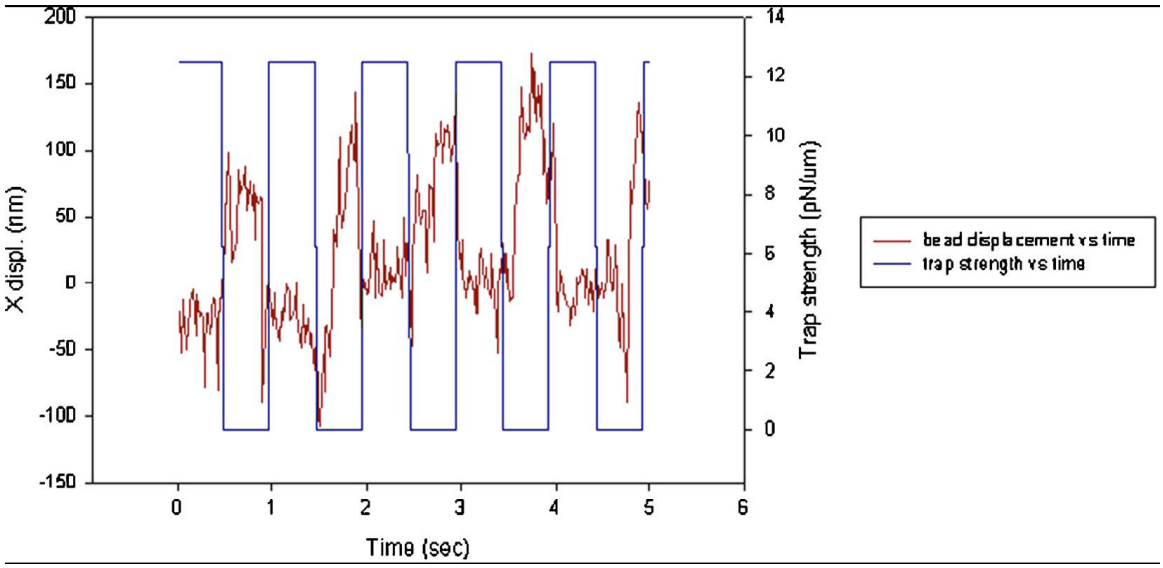

Figure **2-5**: TTL trap induced displacement of a 0.5-m bead embedded in a 3% gelatin solution. The TTL trap can also operate in continuous mode. Trap stiffness was determined to be 11 pN/m by tracking thermally induced displacements of trapped 0.5-m polystyrene beads in DPBS and 1% albumin. The statistical variance of x coordinates for trapped beads was computed and compared to the potential energy and trap spring constant using Hooke's law and the equipartition theorem. TTL modulation enables analysis of time-dependent responses of the surrounding environment of the bead in response to step changes in trap strength.

Trapped-bead locations were imaged and tracked using a custom written particle tracking software. When the trap was turned on, a large time-dependent displacement of the bead toward the center of the trap was observed (Figure **2-5**). The time lag of displacement relative to the laser power indicated that the bead was in a viscoelastic environment. Thus, modulating optical trap forces and measuring the time-dependent displacements of beads provides a convenient means to measure the viscoelastic properties of endothelial cells without moving the cells or the trap location.

2.5 References

Adler, J. and S. N. Pagakis. 2003. Reducing image distortions due to temperature-related microscope stage drift. *Journal of Microscopy* 210:131-137.

Ashkin, A. 1998. Forces of a single-beam gradient laser trap on a dielectric sphere in the ray optics regime. *Methods Cell Biol.* 55:1-27.

Bajaj, S., J. B. Welsh, R. C. Leif, and J. H. Price. 2000. Ultra-rare-event detection performance of a custom scanning cytometer on a model preparation of fetal nRBCs. *Cytometry* 39:285-294.

Block, S. M. 1992. Making light work with optical tweezers. *Nature* 360:493-495.

Breedveld, V. and D. J. Pine. 2003. Microrheology as a tool for high-throughput screening. *Journal of Materials Science* V38:4461-4470.

Cheezum, M. K., W. F. Walker, and W. H. Guilford. 2001. Quantitative comparison of algorithms for tracking single fluorescent particles. *Biophys. J* 81:2378-2388.

Gelles, J., B. J. Schnapp, and M. P. Sheetz. 1988. Tracking kinesin-driven movements with nanometre-scale precision. *Nature* 331:450-453.

Hough L.A. and H.D.Ou-Yang. 1999. A New Probe for Mechanical Testing of Nanostructures in Soft Materials. *Journal of Nanoparticle Research* Volume 1,495-499.

Hung-Wing, L., M. Michael, H. Yan, and Edward S.Yeung. 2007. Real-time dynamics of label-free single mast cell granules revealed by differential interference contrast microscopy. *Analytical and Bioanalytical Chemistry* V387:63-69.

Lorenz, H., M. Despont, N. Fahrni, J. Brugger, P. Vettiger, and P. Renaud. 1998. High-aspect-ratio, ultrathick, negative-tone near-UV photoresist and its applications for MEMS. *Sensors and Actuators A: Physical* 64:33-39.

Quist, A. P., E. Pavlovic, and S. Oscarsson. 2005. Recent advances in microcontact printing. *Analytical and Bioanalytical Chemistry* V381:591-600.

Saxton, M. J. and K. Jacobson. 1997. Single-particle tracking: Applications to membrane dynamics. *Annual Review of Biophysics and Biomolecular Structure* 26:373-399.

Schnapp, B. J., J. Gelles, and M. P. Sheetz. 1988. Nanometer-scale measurements using video light microscopy. *Cell Motil. Cytoskeleton* 10:47-53.

Tseng, Y., T. P. Kole, and D. Wirtz. 2002. Micromechanical Mapping of Live Cells by Multiple-Particle-Tracking Microrheology. *Biophys. J.* 83:3162-3176.

Xia, Y. and G. M. Whitesides. 1998. Soft Lithography. *Angew. Chem. Int. Ed. ,* 37: 550-575.

Chapter 3

MACRORHEOLOGY AND ADAPTIVE MICRORHEOLOGY OF ENDOTHELIAL CELLS SUBJECTED TO FLUID SHEAR STRESS

Foreword

The following chapter is taken from the manuscript "Macrorheology and adaptive microrheology of endothelial cells subjected to fluid shear stress", Dangaria JH and Butler PJ. American Journal of Physiology Cell Physiology, 293(5):C1568-75, 2007.

3.1 Introduction

The endothelium plays a primary role in vascular health and disease. As an interface between the blood and the vessel wall it is exposed to hemodynamic forces which, in turn, influence endothelial cell-regulated vascular function. In particular, shear stress, the tangential component of hemodynamic forces, induces endothelial cells (ECs) to modulate inflammation (Chiu et al., 2005), wound healing (Gojova and Barakat, 2005), hemostasis (Galbusera et al., 1997), vascular tone (Butler et al., 2000), and remodeling (Gusic et al., 2005). Temporal and spatial characteristics of hemodynamic shear stress determine whether these responses lead to vascular health or pathologies such as atherosclerosis (Butler et al., 2002;Davies et al., 1995). For example, rapidly-changing shear with low magnitude and high spatial gradients is thought to be atherogenic (Ku et al., 1985) because it leads to increased EC permeability to low density lipoprotein (Chien, 2003), increased adhesivity to monocytes (Tsao et al., 1996) and

increased expression of genes thought to be associated with vascular inflammation (Dai et al., 2004;Chen et al., 2001)

Although the precise molecular mechanisms of mechanotransduction remain the focus of many studies, there is an increasing effort to characterize mechanical properties of endothelial cells and to incorporate these properties into predictive mechanical models to characterize cellular responses to external forces (Charras and Horton, 2002;Ferko et al., 2007;Karcher et al., 2003;Mazzag et al., 2003). While these models tend to use static mechanical properties, adaptive changes in mechanical properties are particularly relevant because it is possible that mechanical adaptation is related to whether endothelial cells exhibit a physiological or pathophysiological phenotype. For example, using micropipette aspiration technique, Sato *et al.* reported that porcine aortic endothelial cells exposed to 24 hrs of fluid shear exhibited a two-fold increase in elasticity and three-fold increase in viscosity (Sato et al., 1996) compared to non-sheared counterparts. In a similar study on endothelial cells (ECs) using atomic force microscopy (AFM), a significant increase in Young's modulus was reported after 6 hours of exposure to shear stress as compared to pre-shear values (Ohashi et al., 2002). Using particle tracking microrheology, Lee *et al.* demonstrated a Rho-kinase-dependent stiffening of the fibroblast cytoplasm, 40 minutes after the onset of shear stress (Lee et al., 2006). Together, these studies suggest that endothelial cells undergo adaptations in their rheological properties in response to fluid shear stress on the time scale of hours. It is not yet clear, however, whether there exist shear-mediated changes in endothelial cell mechanics on the time scale of seconds to minutes. These time scales are important

because they are equivalent to the time scales of temporal changes in shear stress during the cardiac cycle and during rapid changes in vascular load resulting from exercise.

Although cells change their mechanical properties in response to extracellular chemical and mechanical stimuli, there exists a need for mathematical models by which cell deformations in response to force are predicted through the use of time-independent mechanical constants. Provided these models are used for time scales shorter than those governing adaptive changes, these models can be invaluable in computational methods in mechanobiology (Charras and Horton, 2002;Ferko et al., 2007;Karcher et al., 2003). AFM and micropipette aspiration can characterize mechanical properties of cells; but these methods use forces that different than shear stress in magnitude and direction leading to bulk rheological constants which may be inappropriate for models which characterize the time-dependent EC deformation and intracellular stresses in response to fluid flow.

Thus, we designed experiments to test whether shear induces rapid changes in EC rheology and determined bulk rheological properties which characterize time-dependent deformation of ECs due to shear stress. Multiple particle tracking microrheology (Tseng et al., 2002) was used to determine the evolution of cytoplasmic microrheological parameters in response to a step change in shear stress and the bulk motion of embedded endogenous vesicles was converted to shear strain and fit with the analytical solution to the creep response of the cytoplasm using a phenomenological model of a linear viscoelastic liquid. Such studies establish the earliest measured time scale of EC mechano-adaptation, that is adaptation of EC mechanical properties, and provide the first

rheological constants for mechanical models of ECs measured using shear stress as the forcing function.

3.2 Materials and Methods

3.2.1 Cell Culture

Bovine aortic endothelial cells (VEC technologies, Rensselaer, NY) were cultured in MCDB-131 complete medium supplemented with 11% fetal bovine serum (FBS), 100 Units/ml penicillin, and 100 μg/ml streptomycin. Cells between passages 3-10 were initially sub-cultured in T-25 flasks, maintained at 37° C in a humidified environment with 5% CO_2 and were later grown to ~90% confluence on 40 mm circular, no.1 glass coverslips.

3.2.2 Flow chamber, vibration control, and imaging system

In order to maintain the physiological environment during imaging, coverslips with confluent cell monolayers were assembled in a closed-system, parallel plate flow chamber (Focht Chamber System (FCS2), Bioptechs Inc, Butler, PA). The flow-chamber was then mounted on a piezo-controlled microscope stage (Nano-View™/M, Mad City Labs, Madison, WI), with a manual 2-axis coarse positioning system and a locking feature to prevent long-term stage drift. These methods of ensuring mechanical stability were essential features in accurate nano-scale tracking measurements.

The flow loop system consisted of four media reservoirs connected through a computer-controlled, 6 port modular valve positioner (MVP), (Hamilton Company, Reno, NV) such that at a time only two reservoirs were connected to the flow chamber. Through this system, the MVP could switch between upstream and downstream reservoirs that had equal pressures or ones that induced a pressure gradient. This set-up resulted in a step change in shear stress from 0 to 10 dynes/cm^2 with negligible pressure changes inside the flow chamber (and negligible attendant coverslip deflection). In order to correlate cell deformations with time-dependent stresses, pressure changes across the flow chamber were continuously monitored using a differential pressure transducer (Model DP-15, Validyne Engineering, Northridge, CA). Dulbecco's Modified Eagle's Medium supplemented with 10% FBS (Gibco, Carlsbad, CA) was used as the perfusion medium. pH was maintained by using superfusion of 5% CO_2 over the media reservoirs.

Cells were imaged under DIC microscopy using an Olympus IX71 inverted research microscope with a 60X PlanApo oil immersion objective, NA= 1.45. To further improve the resolution in the DIC mode, a 60X LUMPlanFL water-immersion objective (0.90NA) was used in place of the condenser and an immersion oil with refractive index of 1.33 (Series AAA, Cargille Laboratories Inc., NJ) was used in place of water to prevent evaporation of immersion medium. Time-lapse images were acquired using a high-resolution 12 bit CCD camera, Sensicam QE (Cooke Corp, MI) at 20-30 frames per second with exposure times of 1-3 ms with an image resolution of 0.1 μm/pixel.

3.2.3 Experimental protocols

To study shear-induced variations in cell microrheology, ECs were exposed to a step change in fluid shear stress of 10 dynes/cm^2 which was held constant for a total duration of 5 minutes. Continuous imaging was employed over time spans of up to 90 seconds (limited by camera memory) to capture steady state vesicle motion before, during and after shear, and the temporal characteristics of the responses of the cell to a step-shear from 0 to 10 dynes/cm^2 or from 10 to 0 dynes/cm^2. The exact temporal characteristics of the step were evaluated by fitting the shear-versus-time waveform to a sigmoidal curve. The half maximal shear was obtained at 0.36 sec, which was an order of magnitude shorter than the time-constant governing cell deformation.

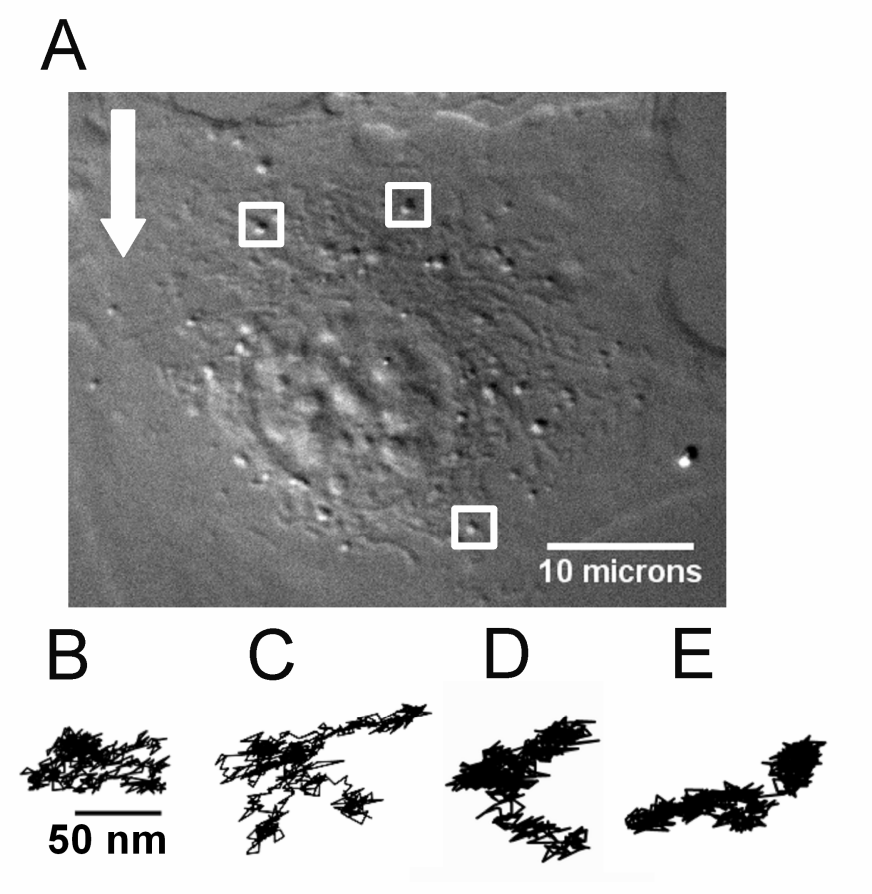

Figure **3-1**: High-resolution imaging and tracking of endogenous vesicles in endothelial cells. *A*: bovine aortic endothelial cell (EC) imaged under high resolution differential interference contrast microscopy. Endogenous vesicles (highlighted by white boxes) were tracked in a focal plane 2 – 4 μm from the base of the cell. Arrow indicates direction of fluid flow. Two-dimensional trajectories of endogenous vesicles calculated before step flow (preshear) was imposed (*B*), 30 s (*C*) and 4 min (*D*) after the onset of step flow (during shear), and 30 s after step flow was turned off (postshear; *E*).

Endogenous vesicles were tracked in a focal plane 2- 4 μm (average of 3 μm) from the base of each cell. 2D trajectories of endogenous vesicles were calculated before step flow was imposed (pre shear) (Figure **3-1** B), 30 sec and 4 min after onset of flow (during shear) (Figure **3-1** C,D) and 30 sec after returning flow to 0 dynes/cm^2 in a step-wise manner (post shear) (Figure **3-1** E). In each case, data were collected for a duration of 30 seconds during a period where cell deformation was minimal. Control experiments in which flow was delivered through the chamber without cells demonstrated that flow imposition did not induce system vibration. Use of fiduciary markers during shear stress application is an alternative way to address artifacts due to system vibration (Dangaria JH et al., 2007).

3.2.4 Particle tracking microrheology

2D trajectories of endogenous vesicles in ECs were measured using an intensity-weighted, centroid-based particle tracking algorithm custom-written in LabVIEW 7.0 (National Instruments, Austin, TX). To measure intracellular mechanics, particle tracking data of endogenous vesicles in each cell were pooled. Random displacements of vesicles over 30 seconds were then converted to time-averaged mean squared displacements (MSD), $\left\langle \Delta r^2(\tau) \right\rangle$ for various lag times τ,

$$\left\langle \Delta r^2(\tau) \right\rangle = \left\langle \left[x(t+\tau) - x(t) \right]^2 \right\rangle + \left\langle \left[y(t+\tau) - y(t) \right]^2 \right\rangle \qquad (\mathbf{3.1})$$

Creep compliance ($\Gamma(\tau)$) was related to the ensemble-averaged MSD by

$$\Gamma(\tau) = \frac{3\pi a}{2k_B T}\left\langle \Delta r^2(\tau)\right\rangle \qquad (\mathbf{3.2})$$

This equation describes the local deformation of the cytoplasm by the thermally-driven tracer motions (Xu et al., 1998). The factor $3/2$ accounts for tracking 2D projections of 3D displacements (Kole et al., 2005). Frequency-dependent viscoelastic moduli of the EC cytoplasm were also calculated from MSD using the generalized Stokes-Einstein relation (Mason T.G. et al., 1997;Mason, 2000)

$$G^*(\omega) = G'(\omega) + iG''(\omega) = \frac{k_B T}{\pi a i\omega \Im\left\{\left\langle \Delta r^2(\tau)\right\rangle\right\}} \qquad (\mathbf{3.3})$$

where $G^*(\omega)$ is the complex shear modulus, k_B is Boltzmann's constant, T is temperature (Kelvin), a is the vesicle radius, i is $\sqrt{(-1)}$, and $\Im\left\{\left\langle \Delta r^2(\tau)\right\rangle\right\}$ is the Fourier transform of the MSD. The elastic (storage) modulus, $G'(\omega)$ and viscous (loss) modulus $G''(\omega)$ are the real and imaginary components of the complex shear modulus. The phase angle $\delta(\omega)$, is an indication of the medium's solid-like ($\delta = 0°$) or liquid-like ($\delta = 90°$) behavior (Yamada et al., 2000).

$$\delta(\omega) = \tan^{-1}\left(\frac{G''(\omega)}{G'(\omega)}\right) \qquad (\mathbf{3.4})$$

Ensemble averaged MSDs of at least 8 vesicles in each cell were used to compute the rheological parameters. Bovine aortic endothelial cells have very limited endogenous vesicles thus precluding detection of regional variations of EC mechanical properties. Hence, $G'(\omega)$ and $G''(\omega)$ were calculated from average MSD of all vesicles in a given

cell. Compliance, elastic and shear moduli were averaged across multiple cells (n = 6) and reported as mean ± S.E.M.

3.2.5 Using shear stress and bulk deformation to determine macrorheology

In order to study the macro-scale viscoelasticity (or macrorheology) of ECs, the creep function $J(t)$ (equation **3.5**) for a phenomenological model consisting of springs and dashpots was fit to the average creep response. Creep response is the average time-dependent shear strain in response to step-shear of 10 dynes/cm^2. The shear strain is the average displacement of all vesicles divided by the height (3 μm) of the vesicles above the coverslip. All vesicle displacements were computed as relative to their location at the instant step-shear was initiated or removed. The creep compliance for the model shown in figure 4C relating shear strain to a step change in shear stress is given by:

$$J(t) = \frac{\gamma(t)}{\sigma_0} = \frac{1}{\mu_V}\left(1 - e^{-t/\tau_V}\right) + \frac{1}{\eta_S}t \qquad (\mathbf{3.5})$$

where $\gamma(t)$ is the shear strain, σ_0 is the shear stress, μ_V, η_V are the elastic and viscous moduli of the Voigt body, respectively, $\tau_V = \eta_V / \mu_V$ is the relaxation time, and η_S is the viscosity of the dashpot in series with the Voigt body.

3.2.6 Data Analysis and Statistics

Compliance and shear moduli were expressed as mean ± S.E.M. Significance of shear-induced changes in compliance and shear moduli with respect to pre-shear values

were assessed using repeated measures ANOVA applied at selected time lags and frequencies with $p< 0.05$ indicating significance. For macrorheology, time-dependent vesicle displacements (as indices of shear deformations) were plotted and displacements at selected time points were expressed as mean ± SD in order to illustrate cell-to-cell variation. 95% confidence intervals were computed and displacements were considered significant if confidence intervals did not include 0 (no displacement). The average displacement curve was converted to creep compliance as described in Methods and curve-fit with the model for a viscoelastic liquid (eq. 3.5). All curve fitting was performed using Origin 7.5 (OriginLab Corp., Northampton, MA) and statistical analysis was performed using SAS (SAS Institute Inc., Cary, NC).

3.3 Results

3.3.1 Shear stress induces an increase in MSD of endogenous vesicles

Vesicle trajectories were converted into ensemble-averaged MSD plotted against increasing lag times. Overall, the MSD curves exhibited power-law scaling $\left\langle \Delta r^2(\tau) \right\rangle \sim \tau^{\alpha}$ where $\alpha < 1$ indicates sub-diffusive behavior (Saxton and Jacobson, 1997). When step shear stress was applied, MSD evaluated at 30 seconds after step increased for all time lags (Figure **3-2**). MSD returned to control values at 4 minutes, despite the maintenance of shear stress and remained the same after cessation of shear stress. Furthermore, there was no change in the x,y distribution of vesicle trajectories, indicating that MSDs were not skewed by cell deformation. MSDs were converted to creep

compliance using equation 2. Creep compliance increased 2 fold over static conditions as early as 30 seconds after shear stimulation (Figure **3-3**). This increase was significant and consistent for all lag times greater than 1 second. A 1.5 fold increase in mean cellular compliance was observed after 4 minutes of shear although this increase was not found to be significant, suggesting that cell compliance returned to control values after 4 minutes of shearing. Stimulating cells with step-wise removal of shear stress did not influence EC mechanical properties. Thus, ECs respond rapidly and transiently to applied step change in shear stress by softening their cytoplasm.

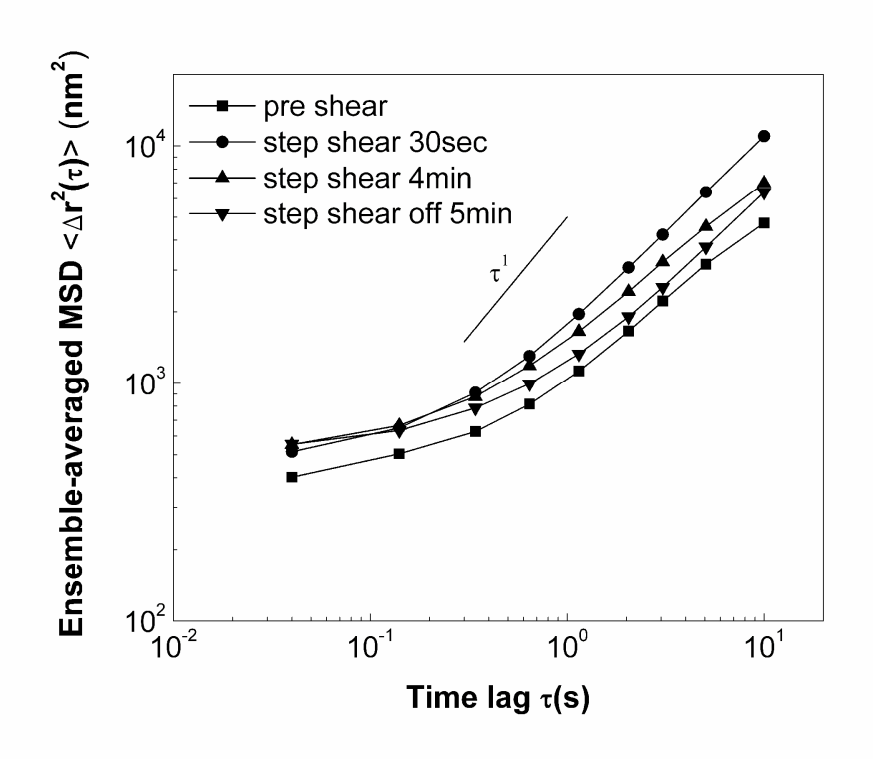

Figure **3-2**: EC mechanics in response to step change in shear stress from 0 to 10 dynes/cm^2. Ensemble-averaged mean square displacement (MSD) plotted against increasing time lags exhibits power-law scaling. $\alpha < 1$ indicates sub-diffusive behavior of tracked endogenous vesicles.

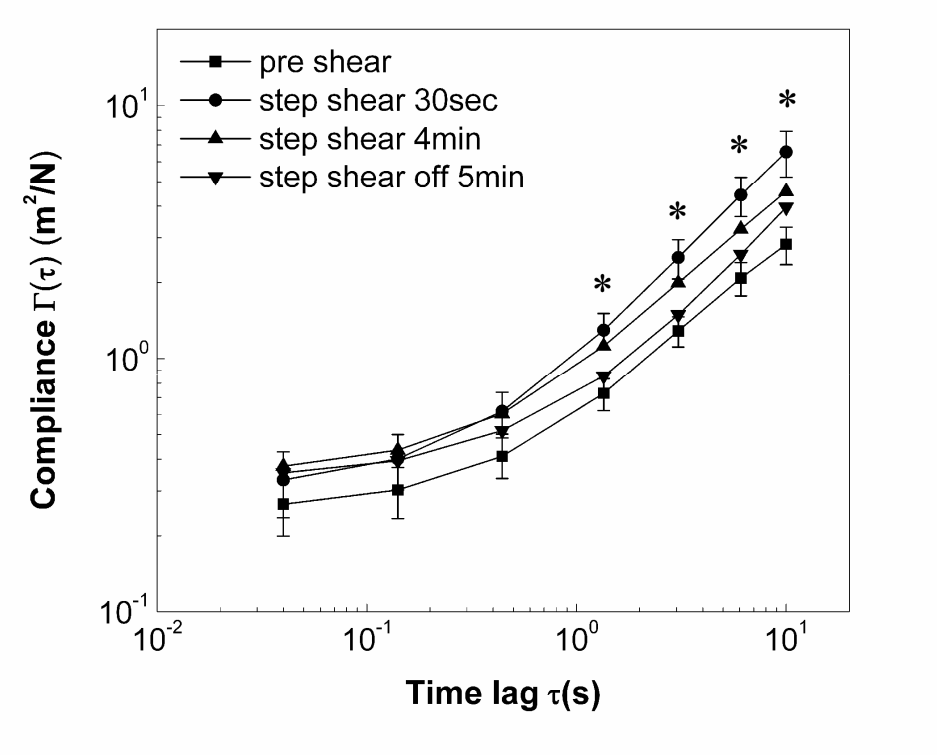

Figure **3-3**: Creep compliance curves of ECs for all experimental conditions. A twofold increase in creep compliance compared with preshear values was observed at very early time points (30 s) after onset of step shear stress. No change in creep compliance was observed when compared with initial static conditions, after shearing cells for 4 min, and after shear stress was removed in a stepwise manner. Data are means ± SE (n= 6). *P < 0.05 for 30 s step shear vs. static control preshear. Error bars for 4 min shear and 5 min postshear are not shown for clarity.

3.3.2 Shear induces changes in microrheology

To characterize the intracellular mechanics of ECs, frequency-dependent viscoelastic moduli, $G'(\omega)$ and $G''(\omega)$ were calculated from the ensemble-averaged MSD, where the frequency ω is the inverse of time lag τ. The entire frequency spectrum was plotted to highlight the frequency-dependent nature of shear effects on viscoelastic moduli. 30 sec after onset of step flow, a significant decrease ($p< 0.05$) in $G'(\omega)$ at all frequencies and $G''(\omega)$ at all frequencies less than 1 sec^{-1} compared with pre shear values was observed (Figure **3-4** and Figure **3-5**). After 4 minutes of exposure to shear stress, $G'(\omega)$ and $G''(\omega)$ returned to control values and no additional modulation of microrheology was observed in response to step change in shear stress from 10 to 0 $dynes/cm^2$. Thus, ECs exhibit time-varying, frequency-dependent changes in microrheological properties in response to step-changes in fluid shear stress.

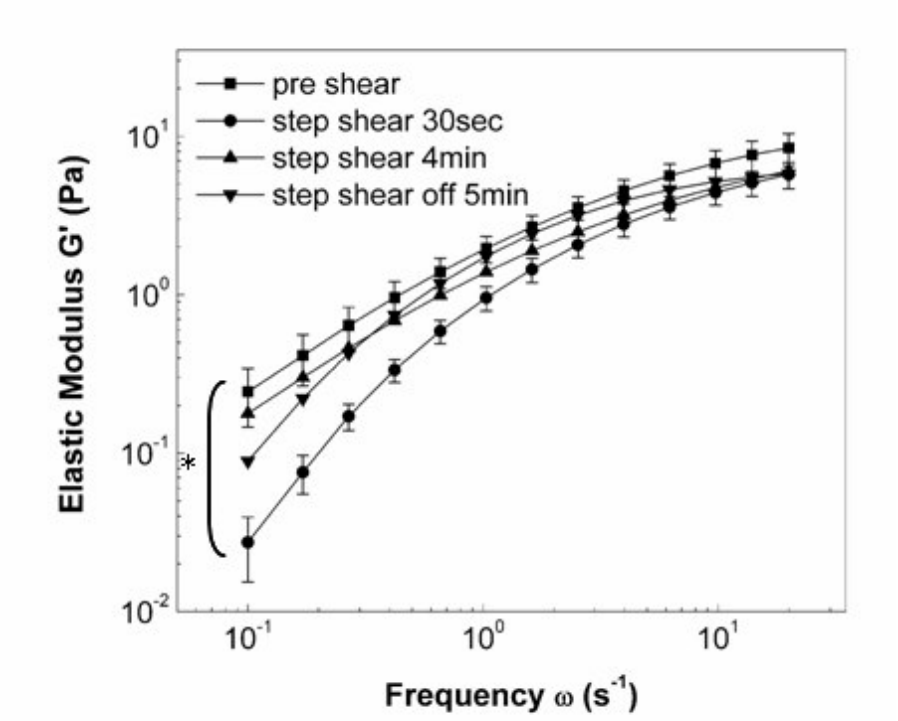

Figure **3-4**: Shear-induced adaptive microrheology. Frequency-dependent elastic moduli decreased rapidly after exposure to step shear of 0 to 10 dyn/cm^2. After 4 min of shearing was completed, values returned to preshear levels. No change in rheology was seen after shear stress was removed. 1Pa =10 dyn/cm2. Data are means ± SE; n = 6. *Significant differences between preshear and 30 s shear rheological moduli (P < 0.05) at all frequencies. Error bars for 4 min shear and 5 min postshear are not shown for clarity.

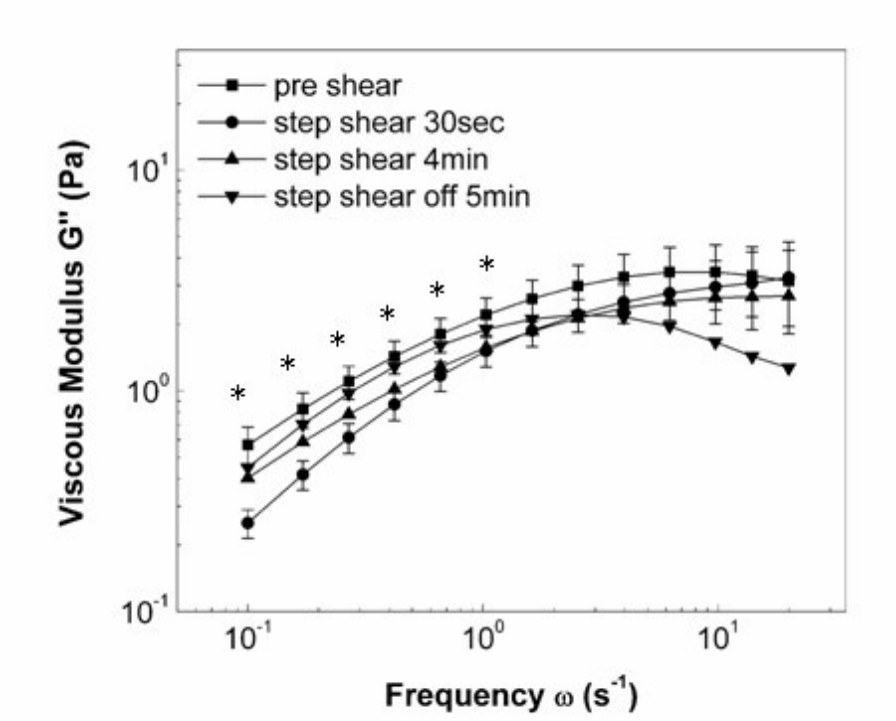

Figure **3-5**: Shear-induced adaptive microrheology. Frequency-dependent viscous moduli decreased rapidly after exposure to step shear of 0 to 10 dyn/cm^2. After 4 min of shearing was completed, values returned to preshear levels. No change in rheology was seen after shear stress was removed. 1Pa =10 dyn/cm2. Data are means ± SE; n = 6. *Significant differences between preshear and 30 s shear rheological moduli ($P < 0.05$) for indicated frequencies. Error bars for 4 min shear and 5 min postshear are not shown for clarity.

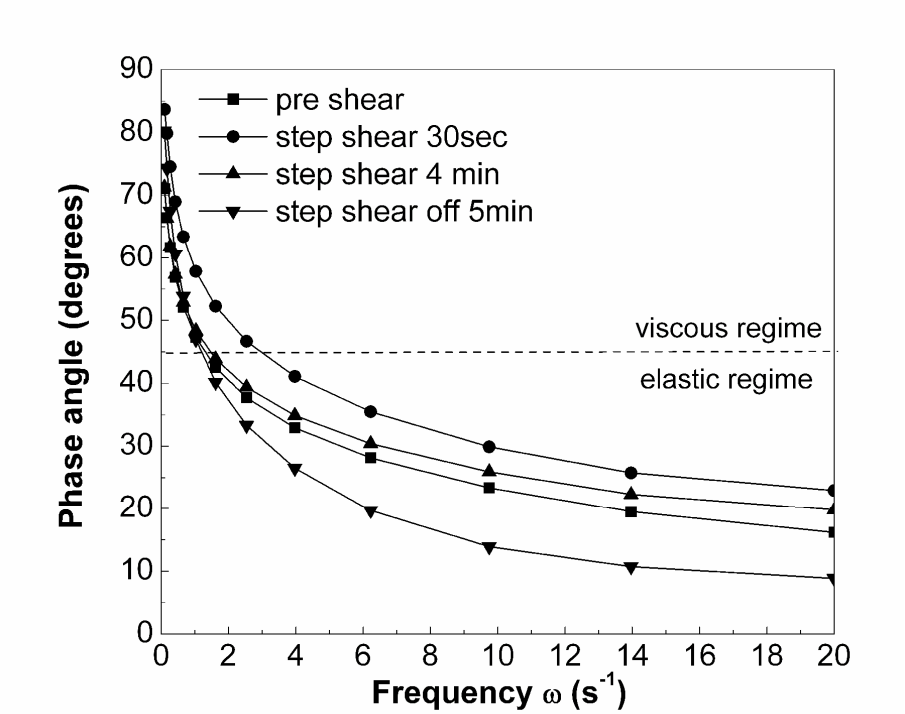

Figure **3-6**: Frequency-dependent viscoelastic phase angles indicate that ECs cross over from the viscous to the elastic regime at frequency of 1 s^{-1}. Imposition of step shear stress increases the crossover frequency to $3s^{-1}$.

Plots of phase angles suggest that at lower frequencies ($\omega < 1$ sec^{-1}), EC cytoplasm behaved like a viscoelastic liquid while a solid-like behavior was observed at higher frequencies, ($\omega > 1$ sec^{-1}) (Figure **3-6**). 30 seconds after onset of step shear stress, the cross-over frequency (i.e. frequency at which $\delta = 45°$) increased from the control value $\omega = 1$ sec^{-1} to $\omega = 3$ sec^{-1} ; i.e. the EC cytoplasm behaved more liquid-like as compared to pre-shear conditions. After shear was turned off, even though cross-over frequency was comparable to pre-shear, ECs exhibited lower phase angles and thus a dominant elastic nature.

3.3.3 Shear induces viscoelastic fluid-like deformation

Global cell deformation was determined from average vesicle displacements at the moment of shear onset and is shown in figs. 4 A and B. When analyzing individual cell responses, it was noted that the deformation was highly heterogeneous (indicated by large standard deviations) with some cells deforming rapidly and dramatically and others exhibiting little or no deformation. On average, ECs exhibited a rapid deformation on the order of 50 nm in the direction of shear stress. The initial phase of rapid deformation is seen within seconds while a slow gradual rise is observed soon after shear stress peaked (Figure **3-7**). Deformation in the orthogonal (x) direction was negligible for all instances. After shearing cells for 5 min, shear was returned to 0 dynes/cm^2 in a step-wise fashion. Cells showed negligible average deformation in response to the removal of shear stress, although standard deviations of deformations were reduced upon shear removal (Figure **3-8**).

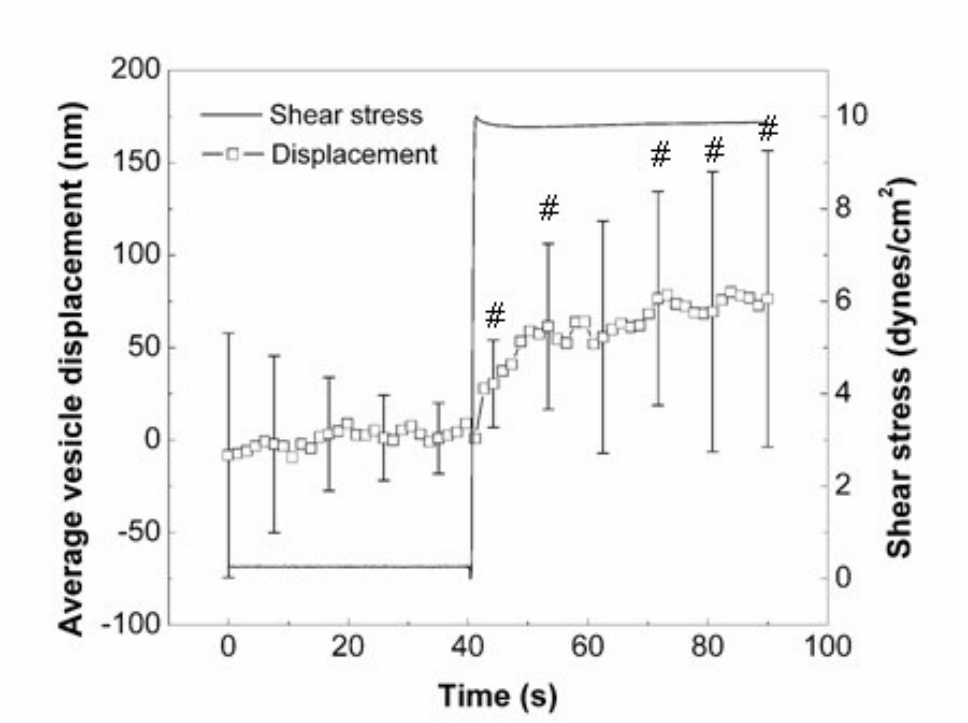

Figure **3-7**: Macrorheology of endothelial cells. Heterogeneous global cell deformation measured from average vesicle displacements due to step change in shear stress. ECs exhibited time-dependent deformation when step shear stress was turned on (0 to 10 dynes/cm^2). #Significant displacements compared with 0 displacement using 95% confidence intervals. Data are means ± SD (n = 6).

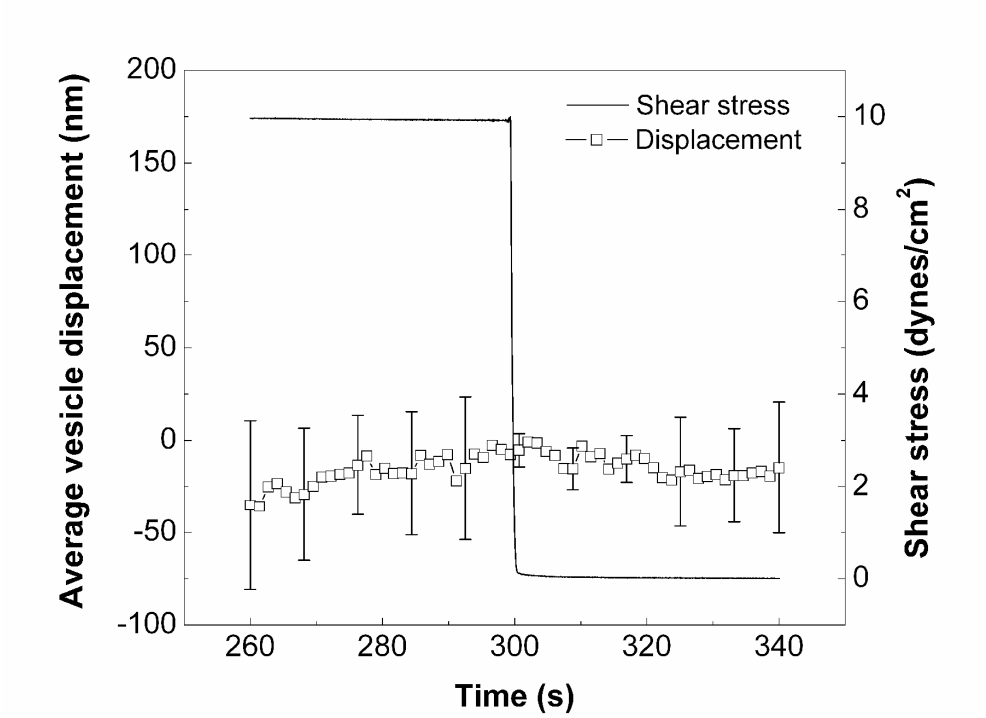

Figure **3-8**: Macrorheology of endothelial cells. Negligible cell deformation was seen upon removal of shear stress in a stepwise manner (10 to 0 dynes/cm^2). Data are means ± SD (n = 6).

To examine the macro-scale EC mechanical properties, average creep response was plotted as a function of time after the onset of step change in shear stress (Figure **3-10**). Global cell mechanics was characterized by fitting the average creep response relating shear stress to shear strain using a phenomenological Voigt-Maxwell model of springs and dashpots (Figure **3-9**) (Feneberg et al., 2001). The initial rapid response correlated with the onset of step shear was the solid-like behavior described by the Voigt body while the liquid-like behavior at long times was accounted for by the series dashpot.

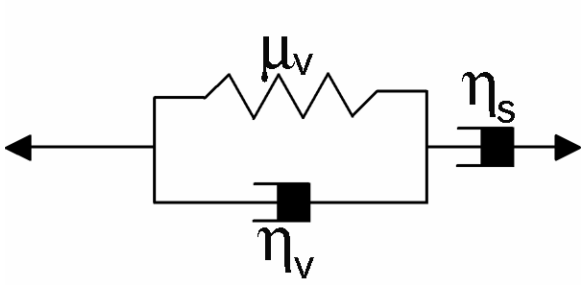

Figure **3-9**: Voigt-Maxwell model used to describe the creep response of ECs.

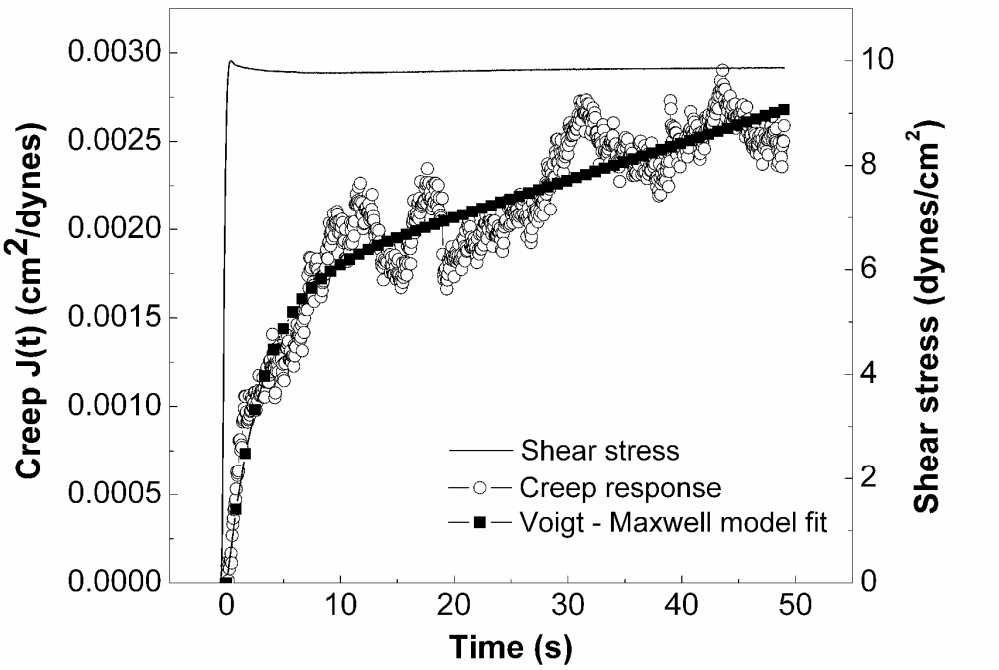

Figure **3-10**: Curve-fitting average creep response to a phenomenological model shows that ECs behave like viscoelastic liquids with a relaxation time of 3 s.

Average macrorheological properties were calculated to be: shear modulus, μ_V = 60.6 Pa and viscosities η_V = 183.65 Pa-sec, η_S = 5000 Pa-sec, relaxation time τ_V = 3.03 sec. $\tau_V = \eta_V / \mu_V$ is the effective relaxation time of the Voigt body which reflects the time required to establish initial elastic stresses and flow; $\tau_S = \eta_S / \mu_V$ describes the effective relaxation time of the Voigt-Maxwell model describing long term viscous flow and was calculated to be τ_S = 83 sec.

3.4 Discussion

The main findings of this study are as follows. First, shear stress was found to induce an increase in cellular compliance and corresponding changes in microrheological moduli as early as 30 seconds after shear onset as measured by particle tracking microrheology. Second, shear stress elicited heterogeneous viscoelastic deformations which could be well described using linear viscoelasticity theory with a length scale of 50 nm and two time scales: a viscoelastic solid-like deformation with a time scale of 3 sec and a long term viscoelastic fluid-like deformation with a time scale of 83 sec. Such results provide insight into adaptive rheology of endothelial cells and provide the first quantitative measurements of macrorheology relevant to shear-induced deformation.

3.4.1 Shear-induced adaptive microrheology

We report for the first time that ECs respond to shear stress at very early time points (on the order of seconds) by softening, *i.e.* reducing their elasticity and viscosity. Mechanical properties recovered during 4 minutes of exposure to shear stress and no additional change was observed after shear was turned off indicating that cells actively remodeled during exposure to shear to reach a new mechanical state. Consistent with this observation, in a study on neutrophils, Yap *et al*. reported a drop in shear moduli within seconds after mechanical stimulation suggesting a sudden cytoskeleton disruption (Yap and Kamm, 2005). In contrast, Lee *et al.* demonstrated a Rho-kinase-dependent stiffening of the fibroblast cytoplasm, 40 minutes after the onset of shear stress (Lee et al., 2006). It is possible that these apparent contradictions can be reconciled by noting that cells may soften at early time points followed by stiffening at later time points. In other words, adaptation of cells may be sensitive to the duration of exposure to shear stress. Although the exact mechanisms of adaptive rheology were beyond the scope of our study, it is possible that these early shear-mediated effects were due to rapid deformation or turnover in the cytoskeleton. With respect to deformation, Helmke *et al*., reported intermediate filament displacements, minutes after the onset of fluid flow (Helmke et al., 2001). An increase in actin filament turnover and net depolymerization of the actin cytoskeleton due to fluid shear stress within 5 minutes of shear exposure was observed by *Osborn et al*.,(Osborn et al., 2006). Rho GTPases have been implicated in shear-mediated cytoskeletal remodeling in which shear stress triggers a decrease in Rho activity after 5 min of exposure (Tzima et al., 2001). Reductions in Rho activity have been implicated in

depolymerization of actin. Furthermore, shear stress elicits an increase in G-actin content in EC due to actin depolymerization through Ca^{2+} and PKC-dependent pathways (Morita et al., 1994). Taken together, these studies and ours support the idea that the time scales of deformation and remodeling of the cytoskeleton in response to shear stress may be complementary.

While the use of particle tracking to determine microrheolgy is widespread, there exists controversy regarding the molecular underpinnings of constrained motion of endogenous particles. In our study we tracked the same vesicles before and after shear stress and determined changes in rheological parameters by average mean squared displacements of multiple vesicles on a cell-by-cell basis. Thus, although the magnitudes of microrheological parameters should be considered effective values, the changes in MSD and resulting microrheology due to shear stress are substantial and significant. Nevertheless, microrheological evidence of elastic behavior at high frequencies and viscous behavior at low frequencies agrees well with macrorheological model of a viscolelastic liquid. Quantitative differences between internal microrheological measurements (obtained from particle tracking) and surface rheological measurements (e.g. atomic force microscopy (Alcaraz et al., 2003), magnetic twisting cytometry (Wang et al., 1993) and laser tracking rheology (Yamada et al., 2000)) have recently been reported and support a mechanical model for ECs of a stiff cortical shell surrounding a softer cytoplasm (Hoffman et al., 2006). Consistent with this model, our cytoplasmic measurements of $G'(\omega)$ and $G''(\omega)$ ranged from 0.1 to 10 Pa. These values are lower than surface measurements obtained using AFM for alveolar and

bronchial lung epithelial cells in which $G'(\omega)$ ranged from 400 to 2000 Pa and $G''(\omega)$ ranged from 100 to 3000 Pa over frequencies of 0.1 to 100 Hz (Alcaraz et al., 2003). Using laser tracking microrheology of endogenous granules, Yamada *et al*., reported differences in shear moduli around the nucleus and in the lamella with the lamella being stiffer (thin lamella are sensitive to cortical actin rheology). Values ranged from 10 to 1000 Pa (Yamada et al., 2000). Yanai *et al*., optically trapped intracellular granules in neutrophils and computed viscoelastic parameters from measured granular displacements after step changes in trap position. Similar to our results, stiffness values were reported on the order of 0.7 to 7 Pa (Yanai et al., 2004). Taken together, these results suggest that the cytoplasm is softer than the cortical actin-membrane shell. Thus, our detection of shear-induced increased in compliance from particle tracking of intracellular endogenous organelles should be interpreted as shear-induced softening of the EC cytoplasm. Shear-induced changes in the cortical cytoskeleton remain a topic of further investigations.

3.4.2 Measurements of microrheology using shear-induced organelles displacement

Various techniques have been used to determine cell macrorheology including micropipette aspiration (Schmid-Schonbein et al., 1981;Sato et al., 1996), AFM (Ohashi et al., 2002) and magnetic bead microrheometry (Bausch et al., 1998). Using micropipette aspiration technique, Sato *et al*., reported values of elastic constants on the order of 100 - 300 Pa while viscosity and relaxation time were on the order of 10 kPa-sec and 100-200 sec, respectively (Sato et al., 1996). Elastic moduli for static and sheared cells obtained by AFM were 0.87 and 1.75 kPa, respectively (Ohashi et al., 2002). Similarly, using

magnetic bead microrheometry on fibroblasts, Bausch *et al*., reported average shear modulus and viscosity to be 20 to 40 kPa and 2000 Pa-sec, respectively. Compared with magnitude of shear forces on the order of 300 Pa in magnetic bead microrheometry technique, our values are on the order of 1 Pa (Bausch et al., 1998) . While the shear modulus is orders of magnitude higher than our reported value of 60 Pa, the effective viscosity is comparable with our value of 5000 Pa-sec.

Although the elastic moduli obtained by micropipette aspiration were similar to those obtained in our study on macrorheology, the effective macrorheological elastic constants, viscosities, and relaxation times obtained in our study by tracking average motion of endogenous organelles in response to step shear, are an order of magnitude lower than those obtained by the above mentioned techniques. Discrepancies in macrorheological constants may arise from factors including differences in the nature and magnitude of applied force, (e.g. shear stress versus twisting force), region where the cell is probed, (e.g. surface or in the interior of cell), and cell type. In our study, macrorheological parameters were measured from small-scale deformations on the order of 50 nm in response to step changes in shear stress. It is likely that the large deformations used in AFM and micropipette aspiration result in different measured viscoelastic moduli than those resulting from small displacements induced by physiological shear stress. Second, AFM indents the cell normal to the surface while shear stress is tangential. Mechanical anisotropy of the cell would result in force-direction-dependent moduli. Third, micropipette aspiration measures mechanical constants of cells detached from their substrate. Detachment may affect the effective mechanical properties of cells. Fourth, discrepancies in moduli may arise from the fact

that both AFM and micropipette aspiration techniques probe the cell externally whereas deformation of endogenous probes yields trajectories which arise from surface deformation transmitted to the interior. In conclusion, the use of shear stress as a forcing function and interior organelle tracking to assess deformation yields viscoelastic moduli which have direct application to models of sheared endothelium while avoiding inherent assumptions used in other mechanical techniques.

In this study, we characterized the EC viscoelasticity in terms of a simple mechanical equivalent circuit consisting of elementary springs and dashpots. The response of ECs to a step change in shear stress were described by a Voigt - Maxwell model. The Voigt element consisted of a parallel arrangement of a spring and dashpot, and accounted for the solid-like behavior at short times, while a dashpot in series was responsible for the liquid-like behavior at long times. The relaxation time τ_V governed the initial viscous flow regime. After time τ_V, the EC cytoplasm behaved like a viscoelastic liquid with viscosity η_S. The rapid short time-scale response could be due to softer and moderately elastic cortical cytoskeleton while the longer and more viscous response could be due to the deep cytoskeleton component (Laurent et al., 2003) . This conclusion is consistent with the elastic behavior of the cell during rapidly-changing shear stress and microrheological determination of solid like behavior at high frequencies, while at low frequencies, (e.g. steady shear) the cell behaved as a viscoelastic liquid (see fig 3C).

Modeling ECs as viscoelastic liquids has an inherent limitation in that it cannot account adaptive changes in rheological constants. In our study, at the 5 minute time

point, ECs did not exhibit any elastic recoil when shear stress was turned off in a step-wise manner, thus indicating cell adaptation to shear stress on the time scale of few minutes. Even though the macrorheology model does not explain this long term adaptation, it nonetheless represents an important advancement in EC mechanics by providing mechanical constants for models of early (sec) time-dependent cell deformation in response to shear stress.

Ferko *et al*., recently developed a multi-component continuum elastic model for sheared and focally-adhered endothelial cells, which, despite its simplicity in ascribing all mechanics to organelle-dependent elastic constants, was capable of predicting experimentally-observed deformation in response to physiologically- (e.g. shear stress) and experimentally- (magnetic bead) relevant mechanical stimuli (Ferko et al., 2007). The magnitude of overall EC deformation in the direction of shear stress was on the order of 50 nm which is consistent with the results reported in this study. The Ferko model could be improved through the use of elastic and viscous moduli determined from physiological forcing functions and measured time-dependent cell deformations. Together, assessment of macrorheological constants along with adaptive microrheology would elucidate the transient nature of cell mechanics while providing inputs into a viscoelastic model with predictive value.

Heterogeneity in individual cell deformations was observed which may indicate heterogeneous responses to mechanical stimuli. If the time dependence of deformation in response to shear stress is different from cell to cell, this could setup stresses between cells leading to mechanotransduction events (DePaola et al., 1999;Tzima et al., 2005;Miao et al., 2005). In a similar argument, variations in shear stress from cell to cell

may induce gradations in cell deformation resulting in intercellular junctional stresses (M.H. Friedman, personal communication). Also, the time- varying mechanical properties may be related to increased lipid diffusion as studied previously by Butler *et al.* (Butler et al., 2001). Shear-mediated softening response may lead to increased deformation and membrane stresses leading to increases in lipid diffusion (Gov, 2006).

3.4.3 Endothelial cell cytoskeleton and cell mechanics

Although molecular mechanisms of mechanotransduction remain at the center of controversy, growing evidence points towards a greater role of the endothelial cell actin cytoskeleton in transmission and intracellular distribution of shear forces from the apical cell surface. *In vivo*, actin filaments are associated into complex, prestressed network of bundles cross-linked by proteins such as α-actinin and filamin, which, together, provide a mechanical framework to sustain cell shape, motility and mechanosensitivity. To better understand the role of the cytoskeleton in modulating cell mechanics and shear-mediated responses, it may be necessary to study the underlying origin of the viscoelasticity of the cytoskeleton network and its associated components as a whole. The current results showing a softening of the cell cytoplasm in response to shear stress suggest that shear stress may initiate signaling pathways leading to rapid changes in actin prestress, bundling, crosslinking, or polymerization state.

3.4.4 Shear-induced microrheology and adaptive microrheology in endothelial cells

In this study, shear-induced deformations and adaptive rheology have been demonstrated to occur on time scales close to those governing rate-sensitive responses of ECs, suggesting that EC rate sensitivity (Butler et al., 2002;Butler et al., 2000) to shear stress may find its origins in cell viscoelasticity. Furthermore, the phenomenological model for macrorheology does not distinguish between passive and active mechanisms of time-dependent deformation. Therefore, viscous dissipation in the macrorheological model may, in part, be due to adaptive microrheology. While our microrheological and macrorheological data support the concept that cells are solid at high rates of force application and liquid at lower rates, further research is necessary to precisely determine the molecular origins of microrheology, macrorheology, and their connections. Macrorheological parameters measured here will also be helpful in the development of cell-specific mechanical models which predict time-dependent stress distributions in subcellular locations (Ferko et al., 2007). Together, the present studies on adaptive microrheology and macrorheology support an emerging paradigm in cell mechanics in which mechanical parameters adapt to the prevailing force. Thus, adaptive rheology may be an important parameter in cellular mechanotransduction and vascular mechanobiology.

3.5 References

Alcaraz, J., L. Buscemi, M. Grabulosa, X. Trepat, B. Fabry, R. Farre, and D. Navajas. 2003. Microrheology of Human Lung Epithelial Cells Measured by Atomic Force Microscopy. *Biophys. J.* 84:2071-2079.

Bausch, A. R., F. Ziemann, A. A. Boulbitch, K. Jacobson, and E. Sackmann. 1998. Local measurements of viscoelastic parameters of adherent cell surfaces by magnetic bead microrheometry. *Biophys. J* 75:2038-2049.

Butler, P. J., G. Norwich, S. Weinbaum, and S. Chien. 2001. Shear stress induces a time- and position-dependent increase in endothelial cell membrane fluidity. *Am. J. Physiol Cell Physiol* 280:C962-C969.

Butler, P. J., Tsou TC, Li JY-S, Usami S, and Chien S. 2002. Rate sensitivity of shear-induced changes in the lateral diffusion of endothelial cell membrane lipids: a role for membrane perturbation in shear-induced MAPK activation. *FASEB J.* 16:216-218.

Butler, P. J., S. Weinbaum, S. Chien, and D. E. Lemons. 2000. Endothelium-Dependent, Shear-Induced Vasodilation Is Rate-Sensitive. *Microcirculation* 7:53-65.

Charras, G. T. and M. A. Horton. 2002. Determination of cellular strains by combined atomic force microscopy and finite element modeling. *Biophys. J* 83:858-879.

Chen, B. P. C., Y. S. Li, Y. Zhao, K. D. Chen, S. Li, J. Lao, S. Yuan, J. Y. J. Shyy, and S. Chien. 2001. DNA microarray analysis of gene expression in endothelial cells in response to 24-h shear stress. *Physiol. Genomics* 7:55-63.

Chien, S. 2003. Molecular and mechanical bases of focal lipid accumulation in arterial wall. *Progress in Biophysics and Molecular Biology* 83:131-151.

Chiu, J. J., L. J. Chen, S. F. Chang, P. L. Lee, C. I. Lee, M. C. Tsai, D. Y. Lee, H. P. Hsieh, S. Usami, and S. Chien. 2005. Shear Stress Inhibits Smooth Muscle Cell-Induced Inflammatory Gene Expression in Endothelial Cells: Role of NF-{kappa}B. *Arterioscler Thromb Vasc Biol* 25:963-969.

Dai, G., M. R. Kaazempur-Mofrad, S. Natarajan, Y. Zhang, S. Vaughn, B. R. Blackman, R. D. Kamm, G. Garcia-Cardena, and M. A. GIMBRONE, Jr. 2004. Distinct endothelial phenotypes evoked by arterial waveforms derived from atherosclerosis-susceptible and -resistant regions of human vasculature. *PNAS* 101:14871-14876.

Dangaria JH, Yang S, and Butler PJ. 2007. Improved nanometer-scale particle tracking in optical microscopyusing microfabricated fiduciary posts. *Biotechniques* 42:437-440.

Davies, P. F., K. A. Barbee, R. Lal, A. Robotewskyj, and M. L. Griem. 1995. Hemodynamics and atherogenesis. Endothelial surface dynamics in flow signal transduction. *Ann N. Y. Acad Sci* 748:86-102.

DePaola, N., P. F. Davies, W. F. Pritchard, Jr., L. Florez, N. Harbeck, and D. C. Polacek. 1999. Spatial and temporal regulation of gap junction connexin43 in vascular endothelial cells exposed to controlled disturbed flows in vitro. *PNAS* 96:3154-3159.

Feneberg, W., M. Westphal, and E. Sackmann. 2001. Dictyostelium cells' cytoplasm as an active viscoplastic body. *Eur. Biophys. J* 30:284-294.

Ferko, M. C., A. Bhatnagar, M. B. Garcia, and P. J. Butler. 2007. Finite-element stress analysis of a multicomponent model of sheared and focally-adhered endothelial cells. *Ann Biomed. Eng* 35:208-223.

Galbusera, M., C. Zoja, R. Donadelli, S. Paris, M. Morigi, A. Benigni, M. Figliuzzi, G. Remuzzi, and A. Remuzzi. 1997. Fluid Shear Stress Modulates von Willebrand Factor Release From Human Vascular Endothelium. *Blood* 90:1558-1564.

Gojova, A. and A. I. Barakat. 2005. Vascular endothelial wound closure under shear stress: role of membrane fluidity and flow-sensitive ion channels. *J Appl Physiol* 98:2355-2362.

Gov, N. S. 2006. Diffusion in curved fluid membranes. *Physical Review E (Statistical, Nonlinear, and Soft Matter Physics)* 73:041918-6.

Gusic, R. J., R. Myung, M. Petko, J. W. Gaynor, and K. J. Gooch. 2005. Shear stress and pressure modulate saphenous vein remodeling ex vivo. *Journal of Biomechanics* 38:1760-1769.

Helmke, B. P., D. B. Thakker, R. D. Goldman, and P. F. Davies. 2001. Spatiotemporal Analysis of Flow-Induced Intermediate Filament Displacement in Living Endothelial Cells. *Biophys. J.* 80:184-194.

Hoffman, B. D., G. Massiera, K. M. Van Citters, and J. C. Crocker. 2006. The consensus mechanics of cultured mammalian cells. *Proc. Natl. Acad Sci U. S. A* 103:10259-10264.

Karcher, H., J. Lammerding, H. Huang, R. T. Lee, R. D. Kamm, and M. R. Kaazempur-Mofrad. 2003. A Three-Dimensional Viscoelastic Model for Cell Deformation with Experimental Verification. *Biophys. J.* 85:3336-3349.

Kole, T. P., Y. Tseng, I. Jiang, J. L. Katz, and D. Wirtz. 2005. Intracellular Mechanics of Migrating Fibroblasts. *Mol. Biol. Cell* 16:328-338.

Ku, D. N., D. P. Giddens, C. K. Zarins, and S. Glagov. 1985. Pulsatile flow and atherosclerosis in the human carotid bifurcation. Positive correlation between plaque location and low oscillating shear stress. *Arterioscler Thromb Vasc Biol* 5:293-302.

Laurent, V. M., R. Fodil, P. Canadas, S. Fereol, B. Louis, E. Planus, and D. Isabey. 2003. Partitioning of cortical and deep cytoskeleton responses from transient magnetic bead twisting. *Ann Biomed. Eng* 31:1263-1278.

Lee, J. S. H., P. Panorchan, C. M. Hale, S. B. Khatau, T. P. Kole, Y. Tseng, and D. Wirtz. 2006. Ballistic intracellular nanorheology reveals ROCK-hard cytoplasmic stiffening response to fluid flow. *J Cell Sci* 119:1760-1768.

Mason T.G., Ganesan K, van Zanten JH, Wirtz D, and Kuo SC. 1997. Particle Tracking Microrheology of Complex Fluids. *Physical Review Letters* 79:3282-3285.

Mason, T. G. 2000. Estimating the viscoelastic moduli of complex fluids using the generalized Stokes-Einstein equation. *Rheologica Acta* 39:371-378.

Mazzag, B. M., J. S. Tamaresis, and A. I. Barakat. 2003. A Model for Shear Stress Sensing and Transmission in Vascular Endothelial Cells. *Biophys. J.* 84:4087-4101.

Miao, H., Y. L. Hu, Y. T. Shiu, S. Yuan, Y. Zhao, R. Kaunas, Y. Wang, G. Jin, S. Usami, and S. Chien. 2005. Effects of Flow Patterns on the Localization and Expression of VE-Cadherin at Vascular Endothelial Cell Junctions: In vivo and in vitro Investigations. *Journal of Vascular Research* 42:77-89.

Morita, T., H. Kurihara, K. Maemura, M. Yoshizumi, R. Nagai, and Y. Yazaki. 1994. Role of Ca2+ and protein kinase C in shear stress-induced actin depolymerization and endothelin 1 gene expression. *Circ Res.* 75:630-636.

Ohashi, T., Y. Ishii, Y. Ishikawa, T. Matsumoto, and M. Sato. 2002. Experimental and numerical analyses of local mechanical properties measured by atomic force microscopy for sheared endothelial cells. *Biomed. Mater. Eng* 12:319-327.

Osborn, E. A., A. Rabodzey, C. F. Dewey, Jr., and J. H. Hartwig. 2006. Endothelial actin cytoskeleton remodeling during mechanostimulation with fluid shear stress. *Am J Physiol Cell Physiol* 290:C444-C452.

Sato, M., N. Ohshima, and R. M. Nerem. 1996. Viscoelastic properties of cultured porcine aortic endothelial cells exposed to shear stress. *Journal of Biomechanics* 29:461-467.

Saxton, M. J. and K. Jacobson. 1997. Single-particle tracking: Applications to membrane dynamics. *Annual Review of Biophysics and Biomolecular Structure* 26:373-399.

Schmid-Schonbein, G. W., K. L. Sung, H. Tozeren, R. Skalak, and S. Chien. 1981. Passive mechanical properties of human leukocytes. *Biophys. J.* 36:243-256.

Tsao, P. S., R. Buitrago, J. R. Chan, and J. P. Cooke. 1996. Fluid Flow Inhibits Endothelial Adhesiveness: Nitric Oxide and Transcriptional Regulation of VCAM-1. *Circulation* 94:1682-1689.

Tseng, Y., T. P. Kole, and D. Wirtz. 2002. Micromechanical Mapping of Live Cells by Multiple-Particle-Tracking Microrheology. *Biophys. J.* 83:3162-3176.

Tzima, E., M. A. del Pozo, S. J. Shattil, S. Chien, and M. A. Schwartz. 2001. Activation of integrins in endothelial cells by fluid shear stress mediates Rho-dependent cytoskeletal alignment. *EMBO J* 20:4639-4647.

Tzima, E., M. Irani-Tehrani, W. B. Kiosses, E. Dejana, D. A. Schultz, B. Engelhardt, G. Cao, H. DeLisser, and M. A. Schwartz. 2005. A mechanosensory complex that mediates the endothelial cell response to fluid shear stress. *Nature* 437:426-431.

Wang, N., J. P. Butler, and D. E. Ingber. 1993. Mechanotransduction across the cell surface and through the cytoskeleton. *Science* 260:1124-1127.

Xu, J., V. Viasnoff, and D. Wirtz. 1998. Compliance of actin filament networks measured by particle-tracking microrheology and diffusing wave spectroscopy. *Rheologica Acta* 37:387-398.

Yamada, S., D. Wirtz, and S. C. Kuo. 2000. Mechanics of Living Cells Measured by Laser Tracking Microrheology. *Biophys. J.* 78:1736-1747.

Yanai, M., J. P. Butler, T. Suzuki, H. Sasaki, and H. Higuchi. 2004. Regional rheological differences in locomoting neutrophils. *Am J Physiol Cell Physiol* 287:C603-C611.

Yap, B. and R. D. Kamm. 2005. Mechanical deformation of neutrophils into narrow channels induces pseudopod projection and changes in biomechanical properties. *J Appl Physiol* 98:1930-1939.

Chapter 4

MYOSIN II MOTORS MODULATE ENDOTHELIAL CELL RHEOLOGY AND ACTIVATION BY SHEAR STRESS

4.1 Introduction

The endothelial cell cytoskeleton constitutes the chemo-mechanical machinery that mediates a number of cellular functions important to vascular health and disease. For example, dynamic regulation of the cytoskeleton mediates cell shape, adhesion, migration, and cell division (Stossel, 1993) that, together, modulate endothelium permeability to solutes (Chien, 2003) and circulating blood cells (Tsao et al., 1996). To carry out these functions, cells orchestrate cytoskeleton structural rearrangements through a complex cascade of signaling molecules and through cytoskeleton-associated molecular motors. Of all the cytoskeletal components, actin filaments appear to be the most important for cell mechanics and are associated into complex, prestressed network of bundles cross-linked by proteins such as α-actinin, filamin and myosin II molecular motors which, together, provide a structural framework to sustain cell shape, permit motility and regulate mechanosensitivity (reviewed in (Clark et al., 2007)).

Myosins are a super-family of actin-associated molecular motor proteins that use chemical energy from ATP hydrolysis to generate force which permits movement along actin filaments towards the filament's barbed end. Out of the 24 classes of myosins based on phylogeny (Foth et al., 2006), myosin II is the major motor protein known to regulate actomyosin contractility in smooth muscle cells. Structurally myosin II consists of a pair

of heavy chains (MHCII) with a conserved motor domain at the N-terminus that binds to F-actin, a neck linker domain, and a non-conserved helical coiled-coil domain at the C-terminus (Figure **4-1**). Two pairs of light chains, essential and regulatory, bind to the neck domain. Essential light chains provide structural integrity to the motor head while regulatory light chains regulate the myosin II ATPase activity. Myosin II A, B, C, are three non-muscle myosin isoforms identified in mammalian cells.

Myosin motors govern cytokinesis, adhesion, migration, protein transport, phagocytosis, and contraction through their ability to generate tension in cells (Krendel and Mooseker, 2005). Myosin II is also present in non-muscle cells where it assembles into minifilaments that move actin filaments relative to each other thus generating intracellular tension or prestress (Ingber, 2003). Myosin II motors have been shown to facilitate diffusion through polymer networks and thus act as stress dissipaters (Humphrey et al., 2002). Finally, Myosin II motors behave as actin cross-linkers to assist in maintaining integrity of actin bundles (Wachsstock et al., 1994).

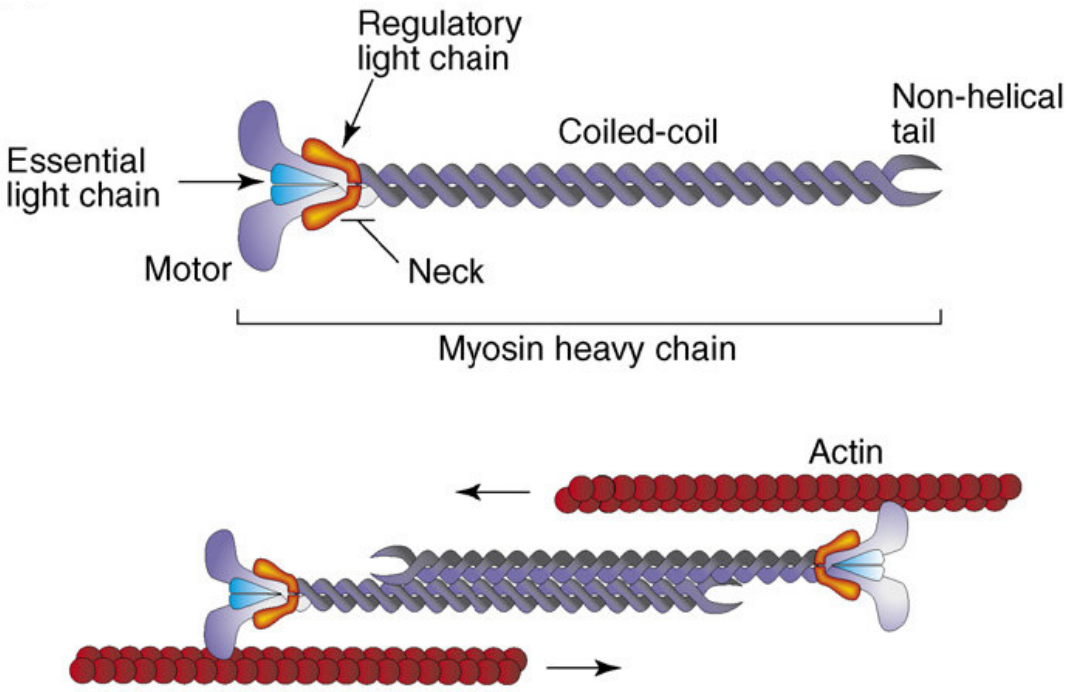

Figure **4-1**: Myosin II structure. Myosin II motors assemble into bipolar filaments, activation through phosphorylation leads to movement along F-actin and tension generation. Adapted from (Clark et al., 2007).

In a recent study, we reported rapid softening of EC cytoplasm as indicated by a reduction in magnitude of viscoelastic microrheological moduli, within seconds after the onset of shear stress (Dangaria and Butler, 2007). Because of the role of actomyosin interactions in governing cell prestress, contractility, and polymer diffusion, the present study aims at investigating the role of the actin cytoskeleton and myosin II motor interaction in this shear-mediated adaptive rheology of ECs. We used particle tracking microrheology (Mason T.G. et al., 1997) to quantify changes in EC microrheology and overall shear-induced cell deformation to quantify macrorheology under pharmacological interventions such as actin stabilizing and disrupting agents, or the myosin II-specific inhibitor, blebbistatin.

4.2 Materials and Methods

4.2.1 Cell culture and drug treatments

Bovine aortic endothelial cells (VEC technologies, Rensselaer, NY) were cultured in MCDB-131 complete medium supplemented with 11% fetal bovine serum (FBS), 100 Units/ml penicillin, and 100 μg/ml streptomycin. Cells between passages 3-10 were initially sub-cultured in T-25 flasks, maintained at 37° C in a humidified environment with 5% CO_2 and were later grown to ~90% confluence on 40 mm circular, no.1 glass coverslips. 0.5 μm polystyrene-carboxylated beads (Invitrogen, Carlsbad, CA) were added to the medium and incubated overnight. Before flow experiments, cells were incubated at 37° C with drugs including blebbistatin (50 μM) for 30 min, cytochalasin D (2 μM) for 30 min and jasplakinolide (1 μM) (Invitrogen, Carlsbad, CA) for 20 min.

4.2.2 Fluorescence labeling and confocal imaging

To stain F-actin, cells were washed with calcium and magnesium free DPBS and fixed with 3.7% formaldehyde in DPBS for 10 min at room temperature, permeablised for 3 mins using 0.1% Triton-X and stained with AlexaFluor phalloidin 488 (Invitrogen, CA) for 30 mins. Prior to adding the stain, cells were incubated in DPBS with 1% bovine serum albumin to reduce non-specific staining. Coverslips were then air-dried and mounted on slides using Cytoseal mounting media (n=1.54) (Richard Allen, Kalamazoo, MI).

Cells were imaged using an Olympus FV300 laser scanning confocal microscope (Melville, NY), an Olympus 60X Plan apochromatic oil objective (NA=1.4) and a 10mW 488 nm excitation argon laser. Z-stacks of images were obtained with 0.25 μm spacing using a stepper motor integrated on the focus knob of the confocal microscope.

4.2.3 High resolution DIC imaging

Cells were imaged under DIC microscopy using an Olympus IX71 inverted research microscope with a 60X PlanApo oil immersion objective, NA= 1.45. To further improve the resolution in the DIC mode, a 60X LUMPlanFL water-immersion objective (0.90NA) was used in place of the condenser and an immersion oil with refractive index of 1.33 (Series AAA, Cargille Laboratories Inc., NJ) was used in place of water to prevent evaporation of immersion medium. Time-lapse images were acquired using a high-resolution 14 bit CCD camera, PCO.1600 (Cooke Corp, MI), with 4GB on-board RAM, at 25-30 frames per second with exposure times of 1-3 ms with an image resolution of 0.123 μm/pixel.

4.2.4 Shear flow assay

The shear flow assay as seen in Figure **4-2** has been discussed in detail in section **3.2.2**.

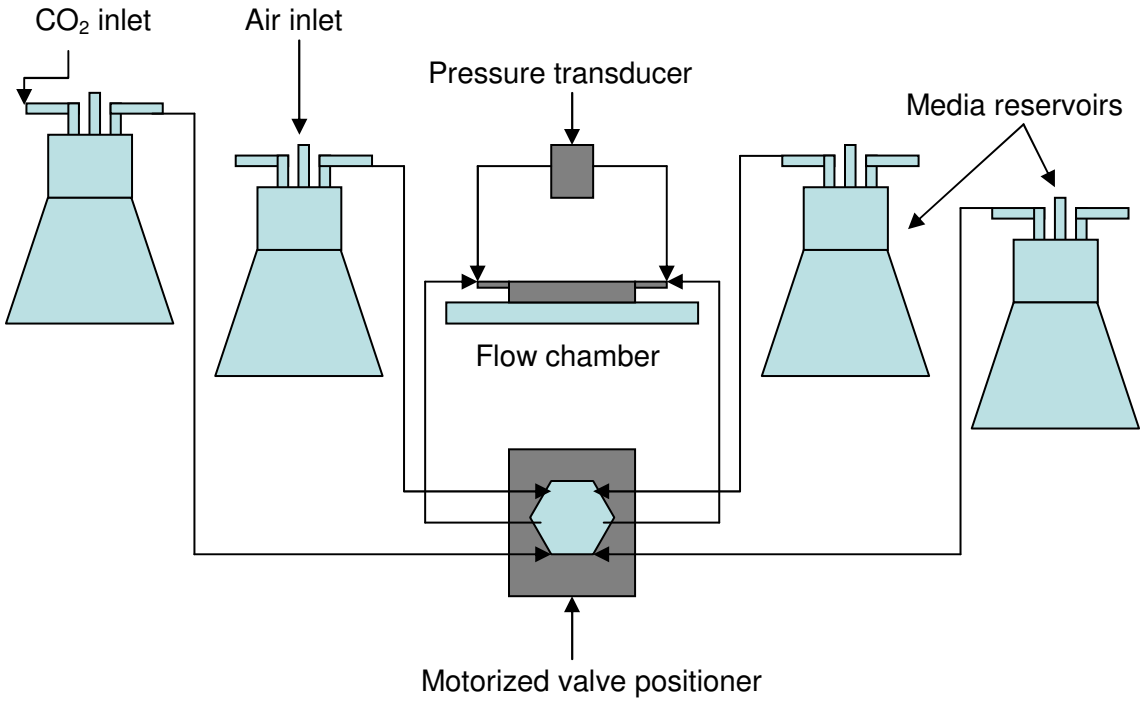

Figure **4-2**: Experimental set-up of shear flow assay. Four media reservoirs were connected to the flow chamber through a motorized valve positioner. At a time two reservoirs were connected to deliver either zero or 25ml/hr flow. Switching between reservoir pairs generated a step change in shear stress from 0 to 10 dynes/cm^2. At all times, 5% CO_2 was suffused over the media reservoirs to maintain pH.

4.2.5 Experimental protocols

ECs mounted in a flow chamber were exposed to a step change in shear stress from 0 to 10 dynes/cm^2 for 30 seconds, after which shear was returned to 0 dynes/cm^2 in a stepwise fashion. The exact temporal characteristics of step shear were evaluated as in section **3.2.3**. Time-lapse images were collected continuously for a total duration of 95 seconds. To study shear-induced changes in rheology, time-lapse images were divided

into three 30 second intervals: pre-shear, during-shear and post-shear. Endocytosed beads in each cell were imaged at 3 to 4 μm above the coverglass and were tracked off line using a custom written algorithm in LabVIEW 7.0 (National Instruments, Austin, TX). 2D trajectories of all beads in a cell were pooled to calculate frequency-dependent viscoelastic moduli on a cell-by-cell basis.

Section **3.2.4** describes the mathematical derivation of the elastic (storage) modulus $G'(\omega)$, and viscous (loss) modulus $G''(\omega)$ from 2D particle trajectories. In each case storage and loss moduli were average across multiple cells and reported as mean ± S.E.M. Section **3.2.5** describes the calculation of macrorheological moduli from phenomenological model of a viscoelastic liquid. The creep compliance for the model shown in Figure **4-15** relating shear strain to a step change in shear stress is given by

$$J(t) = \frac{\gamma(t)}{\sigma_0} = \frac{1}{\mu_V}\left(1 - e^{-t/\tau_V}\right) + \frac{1}{\eta_S}t \qquad (\mathbf{4.1})$$

where $\gamma(t)$ is the shear strain, σ_0 is the shear stress, μ_V, η_V are the elastic and viscous moduli of the Voigt body, respectively, $\tau_V = \eta_V / \mu_V$ is the relaxation time, and η_S is the viscosity of the dashpot in series with the Voigt body.

4.2.6 Statistical analysis and curve-fit

Repeated measure ANOVA at select frequencies was used to determine significance of change in viscoelastic moduli between control and drug treatments, and between pre-shear and during-shear values within each treatment group. $p < 0.05$

indicates significance. Statistical analysis was performed in SAS (SAS Institute Inc., Cary, NC). Significance ($p< 0.05$) between cross-over frequencies was computed using 2-tailed paired *t*-test. Curve fitting analyses for creep deformation was performed using Origin 7.5 (Origin Lab Corp., Northampton, MA).

4.3 Results

Frequency-dependent elastic $G'(\omega)$ and viscous $G''(\omega)$ moduli were evaluated from MSDs of endocytosed beads for cells under static conditions (untreated, n=15), shear stress, and ECs under pharmacological interventions including a myosin II-specific inhibitor, blebbistatin (n=9), an actin disrupting agent, cytochalasin D (n=9), and an actin stabilizing drug, jasplakinolide (n=7). Effects on cells of these stimuli are expressed as cell softening and fluidization. Cell softening is defined as a decrease in both viscous and elastic moduli for a majority of frequencies tested. A drug was said to abolish shear-induced cell softening if the significance of the shear response was abolished.

The inverse tangent of the ratio of $G''(\omega)$ and $G'(\omega)$: $\delta = \tan^{-1}\left(G''/G'\right)$ is the phase angle which has a cross over frequency where the phase angle equals 45º. Fluidization is defined as a significant increase in the crossover frequency.

Macrorheological constants were evaluated by fitting a creep function to the creep response which was determined from the net deformation of vesicles in response to step-shear. Macrorheology is quantified by noting the relaxation time and the creep

magnitude. Investigations of macrorheological creep uncovered a shear-induced contraction which was quantified by its onset time.

4.3.1 Myosin II interactions with actin cytoskeleton modulate endothelial cell microrheology.

We investigated the role of the actomyosin network in maintaining mechanical properties of quiescent ECs. Microrheological moduli calculated before application of step shear (pre-shear) for drug treated cells were compared with pre-shear values of untreated control cells. Particle tracking microrheology was used to assess the local mechanical properties of ECs under various pharmacological interventions. Inhibiting motor activity with the myosin II specific blocker blebbistatin, lead to three fold lower elastic and two fold lower viscous modulus compared with untreated control cells (Figure **4-3**). While stabilizing actin with jasplakinolide did not significantly alter microrheological moduli, cytochalasin D an actin depolymerizing drug, induced a dramatic 28-fold decrease in $G'(\omega)$ and a two fold decrease in $G''(\omega)$. Thus, maintenance of intracellular rheology of ECs depends on intact actin-myosin motor interactions.

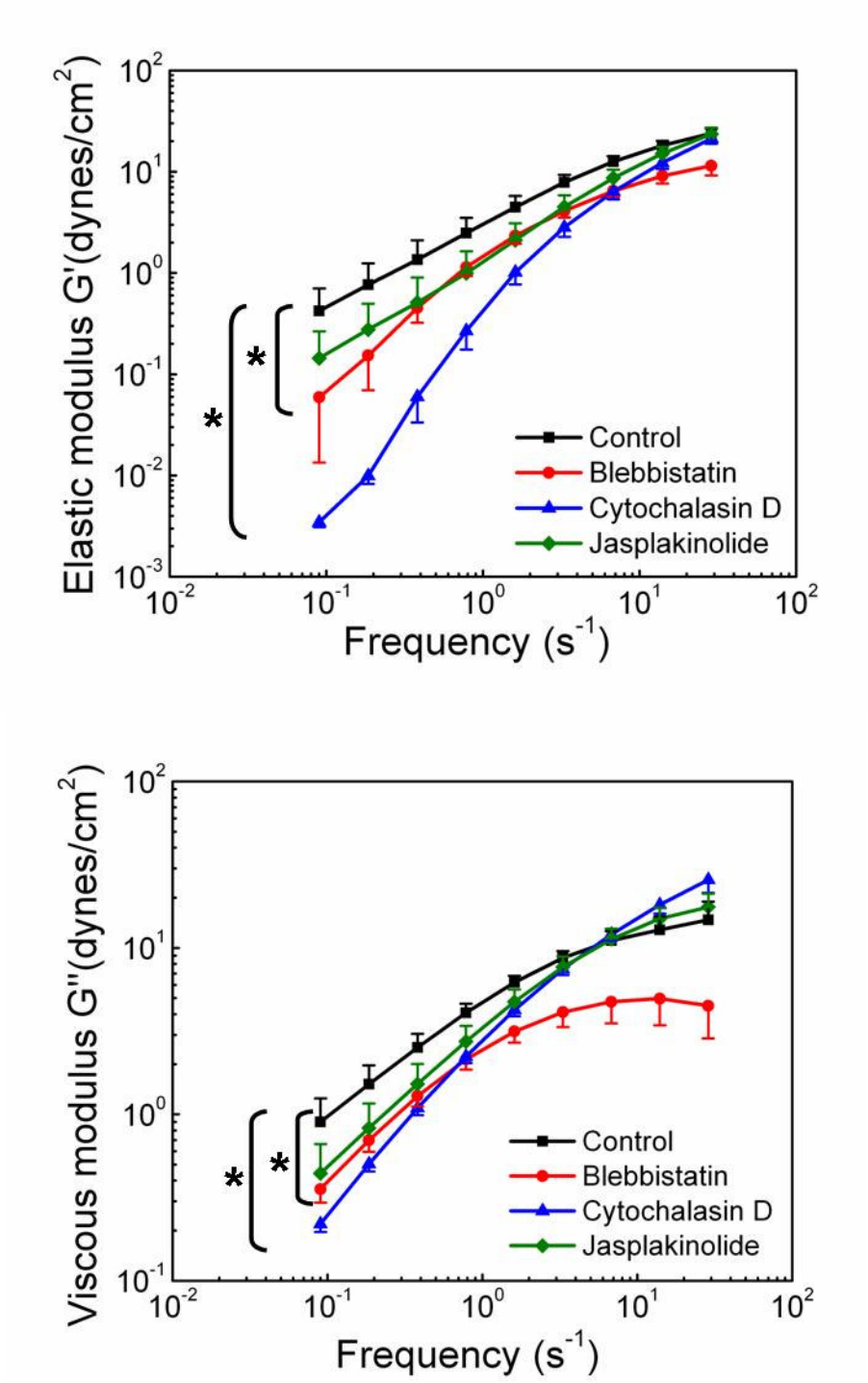

Figure **4-3**: Frequency-dependent storage (elastic) and loss (viscous) modulus of quiescent control and drug treated cells. Significant decrease in viscoelastic moduli in blebbistatin and cytochalasin D treated ECs is observed compared with untreated control cells. No effect on jasplakinolide treated cells. * indicates significance $p < 0.05$

Examination of phase angle δ (Figure **4-4**) revealed a biphasic mechanical nature of the EC cytoplasm. ECs behaved like viscoelastic liquids at low frequencies and like viscoelastic solids at high frequencies. Crossover frequency for untreated cells occurred at 4.75 ± 0.81 s^{-1} (Figure **4-9**). While crossover frequency of myosin II-inhibited cells was not significantly different compared with controls, both depolymerizing and stabilizing actin resulted in a dramatically higher crossover frequencies compared with untreated controls. Crossover frequency for jasplakinolide treated cells was 13.25 ± 2.5 s^{-1} (Figure **4-9**), which was significantly higher than controls. We did not observe a crossover from the viscous to the elastic regime within the range of measured frequencies (0.1 to 30 s^{-1}) for cells treated with cytochalasin D, suggesting that depolymerizing actin leads to a total loss of solid-like behavior. These results provide evidence that the biphasic mechanical nature of the EC cytoplasm is the result of the dynamic modulation of the actin polymerization state.

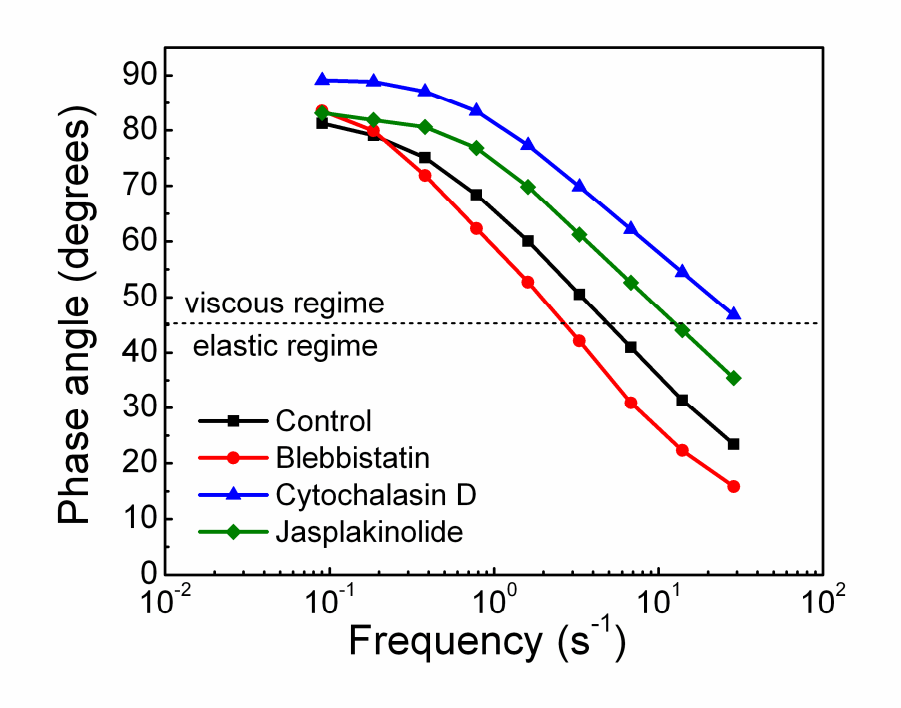

Figure **4-4**: Phase angle plots reveal biphasic nature of the EC cytoplasm. Cells exhibit viscoelastic liquid-like properties at low frequencies and solid-like properties at high frequencies. Crossover occurs at the frequency where $\delta = 45°$. For ECs treated with jasplakinolide and cytochalasin D, crossover occurs at a significantly higher frequency, indicating fluidization of the cell interior.

4.3.2 Inhibition of actomyosin interactions diminished shear-induced softening and fluidization of the cell interior in confluent endothelial cells.

Microrheological properties of control cells (untreated, n=15) and ECs under pharmacological interventions including a myosin II-specific inhibitor blebbistatin (n=9), an actin disrupting agent cytochalasin D (n=9), and an actin stabilizing drug jasplakinolide (n=7) were calculated from the nanometer-scale motions of endocytosed beads. As discussed in the section **3.2.4**, particle trajectories were transformed into ensemble-averaged time-dependent MSDs. Frequency-dependent elastic $G'(\omega)$ and viscous $G''(\omega)$ moduli were then calculated from MSDs, where frequency is the inverse of time lag $\left(\omega = 1/\tau\right)$. To investigate the role of the actin cytoskeleton and myosin II motors in the shear-mediated adaptive rheology of ECs, frequency-dependent viscoelastic moduli were computed pre-shear, during-shear stimulation (30 sec step shear), and post-shear for control (untreated) and drug-treated cells. For testing significance of change before and during shear, $G'(\omega)$ and $G''(\omega)$ during-shear were compared with pre-shear values of respective drug treatments. For each drug treatment, respective pre-shear values served as controls.

For untreated control cells, step change in shear stress induced a dramatic softening as indicated by a significant decrease (* $p < 0.05$) in elastic and viscous moduli at all frequencies (Figure **4-5**). We note that the less elastic or viscous the material is, the smaller is its resistance to deformation and the material is more compliant. Thus, softening in this case can be thought of as an increase in EC compliance. The units of $G'(\omega)$ and $G''(\omega)$ (dynes/cm^2) are inverse of the units of compliance (cm^2/dynes).

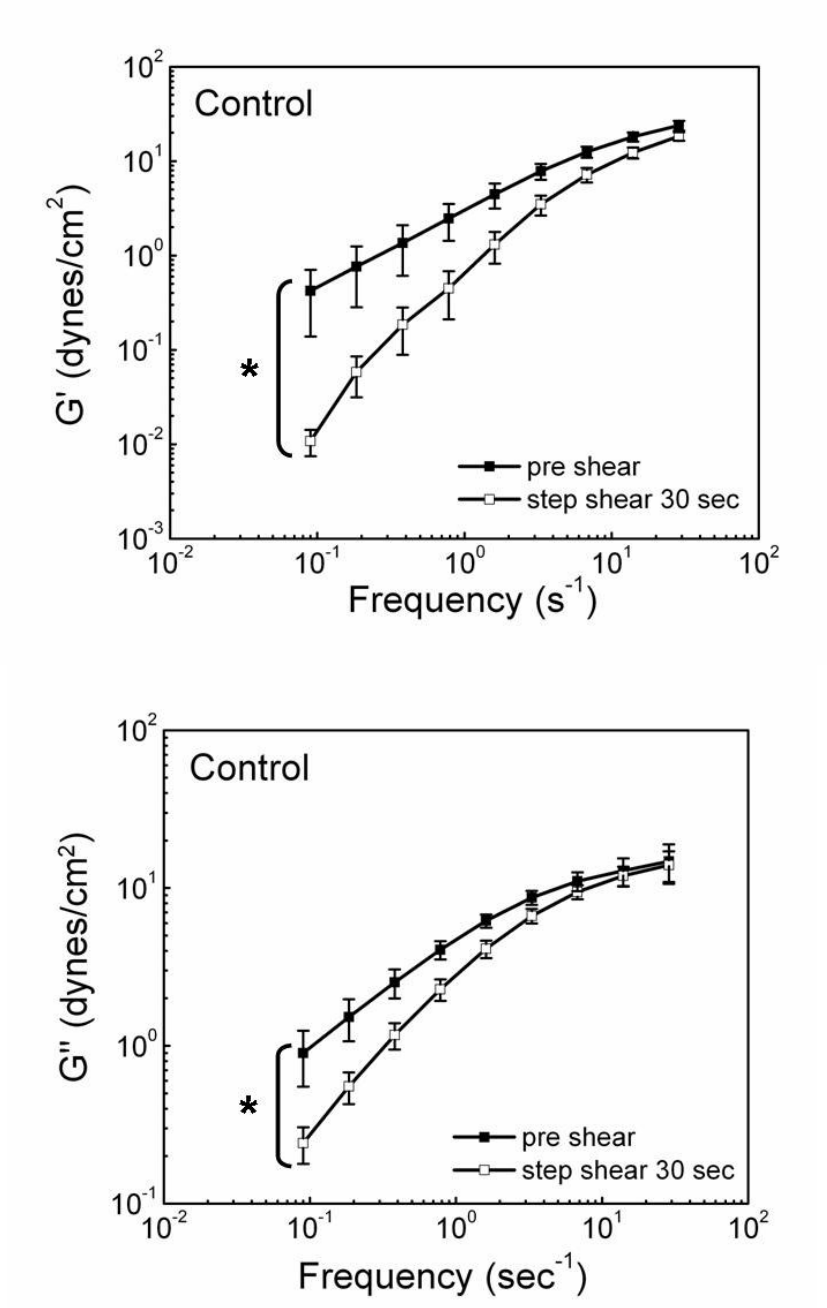

Figure **4-5**: Shear-induced EC softening. Significant decrease in elastic modulus is observed for 30 sec shear duration compared with pre-shear values (n=15). * indicates $p<0.05$.

Inhibition of myosin II motor activity by blebbistatin greatly attenuated shear-induced softening at all frequencies (Figure **4-6**). Depolymerizing the actin cytoskeleton with cytochalasin D led to moderate but significant shear-induced decrease in $G''(\omega)$ at all frequencies and in $G'(\omega)$ at all frequencies > 1 s^{-1}, compared with pre-shear values (Figure **4-7**). However, at small frequencies (< 0.5 s^{-1}), ECs without intact F-actin cytoskeleton exhibited shear-induced stiffening. Stabilizing F-actin (preventing depolymerization) with jasplakinolide had no effect on shear-induced cell softening (Figure **4-8**). This suggests that myosin II interactions with intact actin cytoskeleton rather than actin dynamics (e.g. depolymerization) are essential for the rapid shear-induced softening.

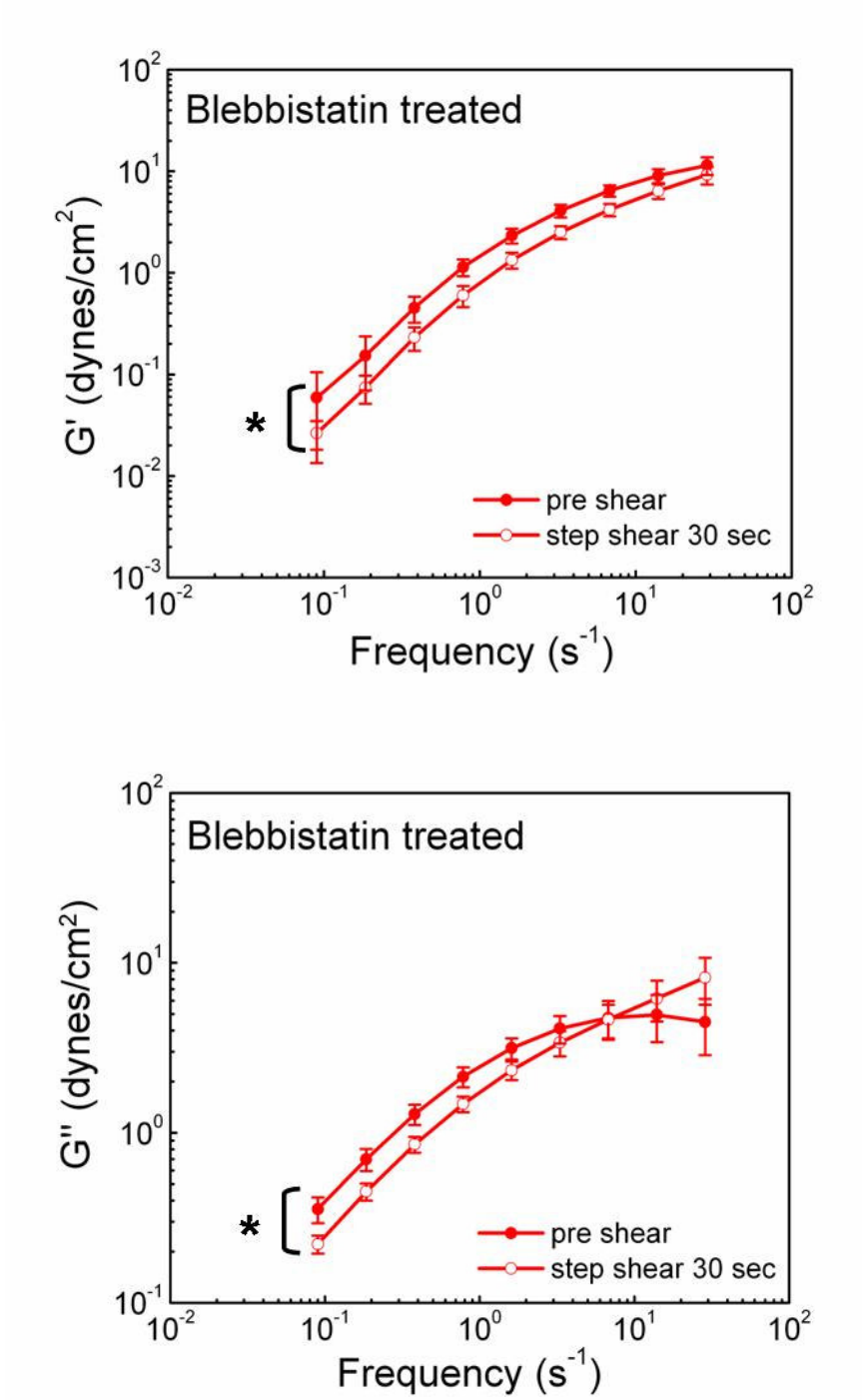

Figure **4-6**: Shear-induced softening response is diminished for EC treated with myosin II specific inhibitor blebbistatin (n=9). * $p<0.05$

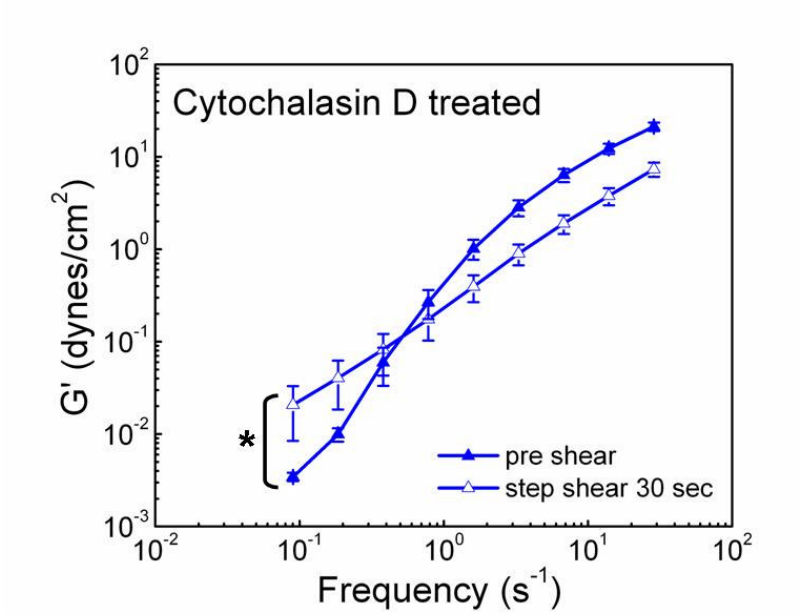

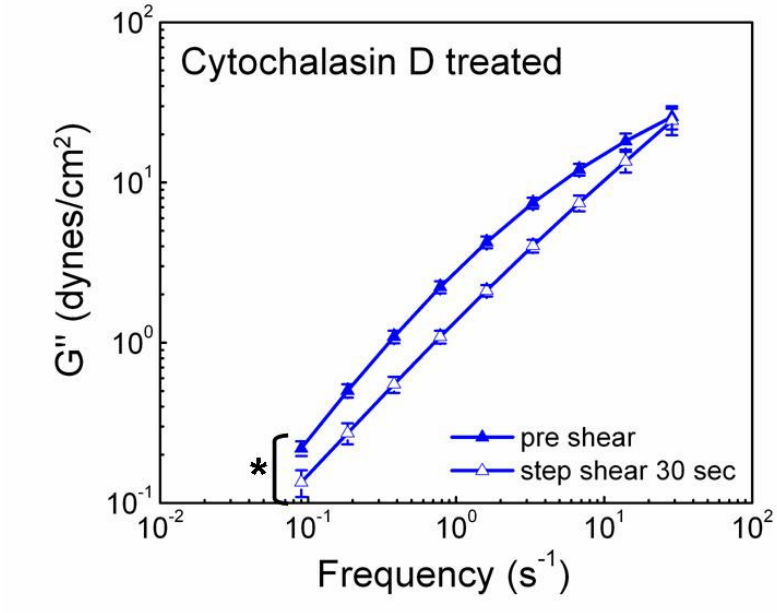

Figure **4-7**: At low frequencies f<0.5 s^{-1} dramatic stiffening response is observed in ECs treated with cytochalasin D. For f> 1 s^{-1}, shear-induced decrease in elastic modulus is observed (n=9). For all frequencies, shear-induced decrease in viscous modulus is observed for cytochalasin D treated cells (n=9).

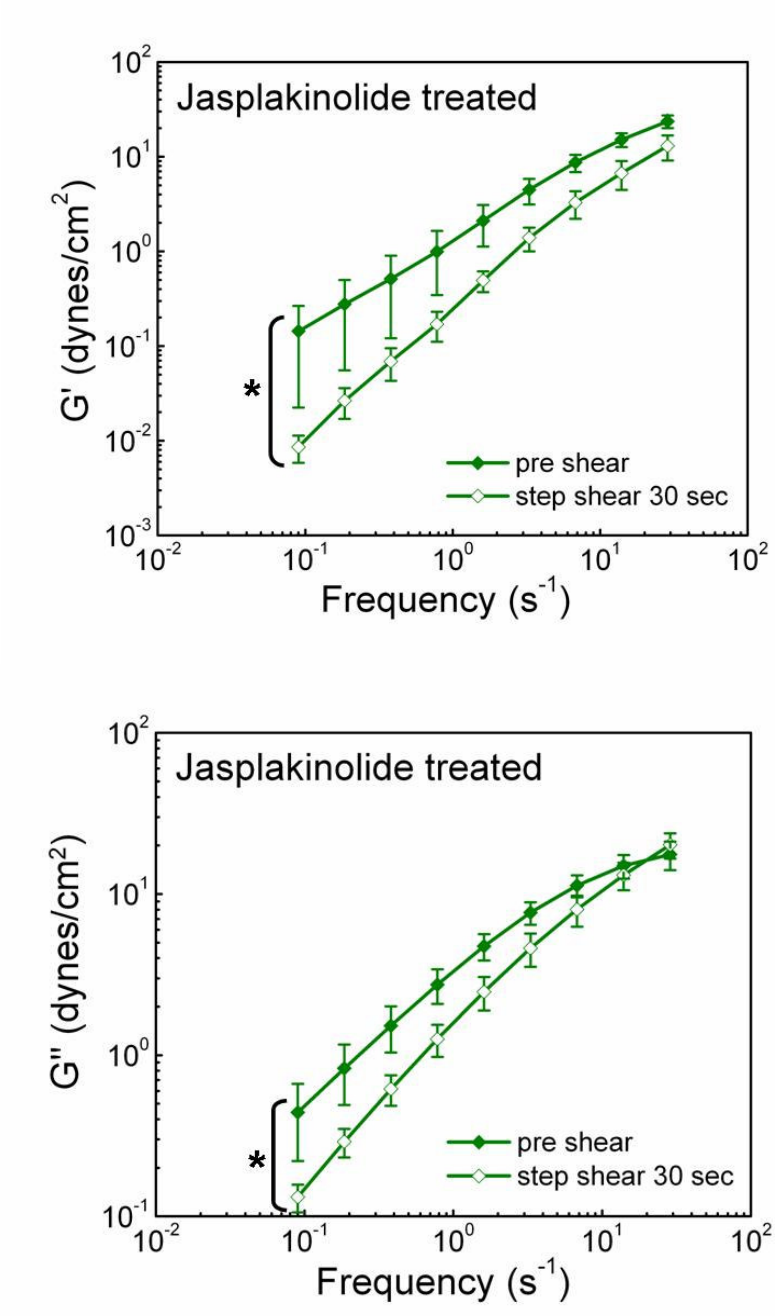

Figure **4-8**: Jasplakinolide has no effect on shear-induced EC softening (n=7). ECs treated with actin stabilizing agent jasplakinolide exhibit shear-induced softening response as indicated by significant decrease in elastic and viscous moduli. * indicates $p<0.05$.

The relationship between elastic and viscous moduli and their relative contribution to the overall mechanical response was evaluated by the phase angle, $\delta = \tan^{-1}\left(G''/G'\right)$. For $\delta = 0^{\circ}$ and $\delta = 90^{\circ}$, material behaves like a Hookean solid and a viscous liquid respectively. ECs demonstrate a viscoelastic behavior within the given frequency range (0.1 to 30 s^{-1}) such that $0^{\circ}<\delta<90^{\circ}$. Crossover frequency is defined as the frequency at which $\delta = 45^{\circ}$. It corresponds to the inverse of relaxation time at which transition from the solid-like to liquid-like behavior takes place, i.e. the material in which the particle is embedded begins to flow.

Plots of phase angle suggest that shear stress induced fluidization or enhanced viscoelastic liquid-like behavior in untreated ECs (Figure **4-10**). Crossover from the liquid –like to the solid-like regime occurred at a higher frequency compared with pre-shear conditions, indicating that relaxation time during shear stimulation was considerably shortened (Figure **4-9**). Shear-induced fluidization was completely eliminated in myosin II inhibited cells as indicated by the observation that no significant increase in crossover frequency during shear was observed in blebbistatin treated cells (Figures **4-11**, **4-9**). This result conforms to the idea that myosin II motor association with actin fluidizes the cytoskeleton and thus contributes to the force dissipative mechanisms in the cell.

In the absence of intact actin (ECs treated with cytochalasin D), cells exhibited liquid-like behavior at all frequencies pre-shear (Figure **4-12**). Exposure to step shear did not alter the already fluidized cell interior. In this case, we assume that cross-over occurs at very high frequencies or relaxation time is very small. ECs with stabilized actin

cytoskeleton demonstrated a dominant liquid-like behavior pre-shear and total fluidization was observed during shear (Figure **4-13**, Figure **4-9**). Crossover frequencies are summarized in Table **4-1**. Thus, stabilizing actin cytoskeleton did not block shear-induced fluidization of the EC interior. These results suggest that shear-induced fluidization does not depend on actin depolymerization rather actomyosin interactions are the dominant mechanism for shear-induced softening and fluidization.

Table **4-1**: Average crossover frequencies calculated from phase angle plots of untreated and drug-treated ECs.

	Crossover frequency pre-shear (s^{-1})	**Crossover frequency during-shear (s^{-1})**
Control	4.75 ± 0.8	16.14 ± 2.5
Blebbistatin	3.5 ± 1.4	7.7 ± 4.1
Cytochalasin D	viscoelastic liquid-like behavior	viscoelastic liquid-like behavior
Jasplakinolide	13.5 ± 2.5	viscoelastic liquid-like behavior

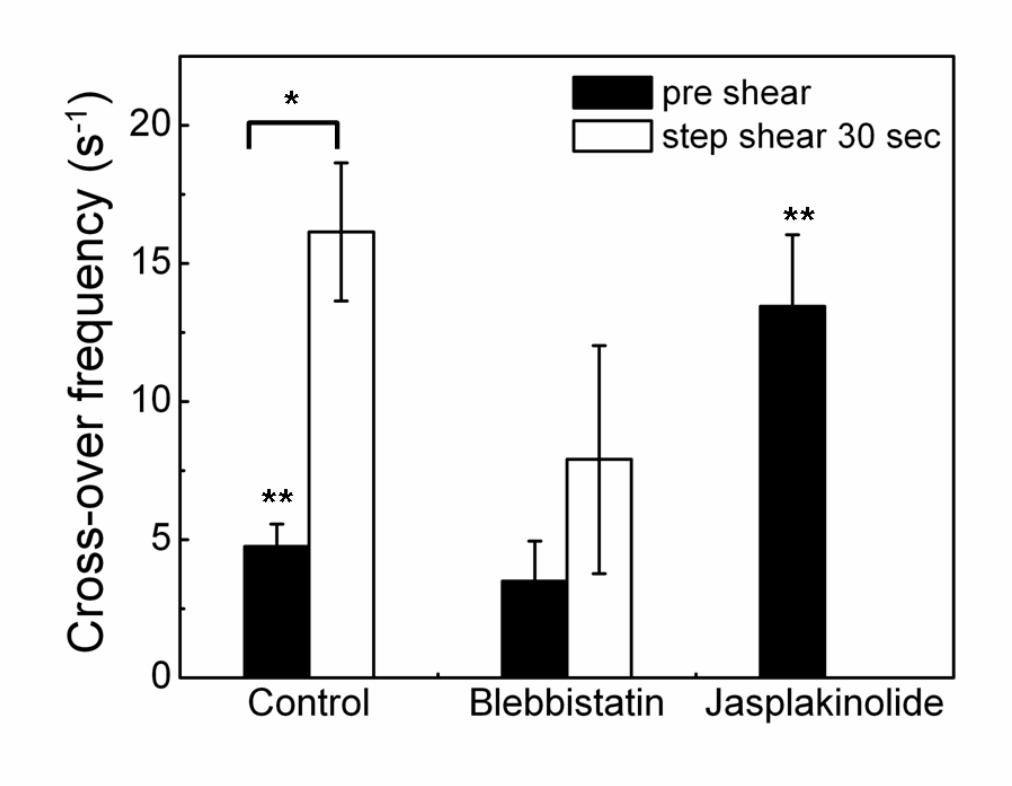

Figure **4-9**: Shear-induced fluidization is abrogated by myosin II motor inhibition. * indicates significance $p<0.05$ comparing pre-shear and during-shear control values, ** comparing with pre-shear control and pre-shear jasplakinolide treated cells. During shear ECs treated with jasplakinolide behaved like viscoelastic liquids at all frequencies and no crossover from liquid-like to solid-like regime is observed.

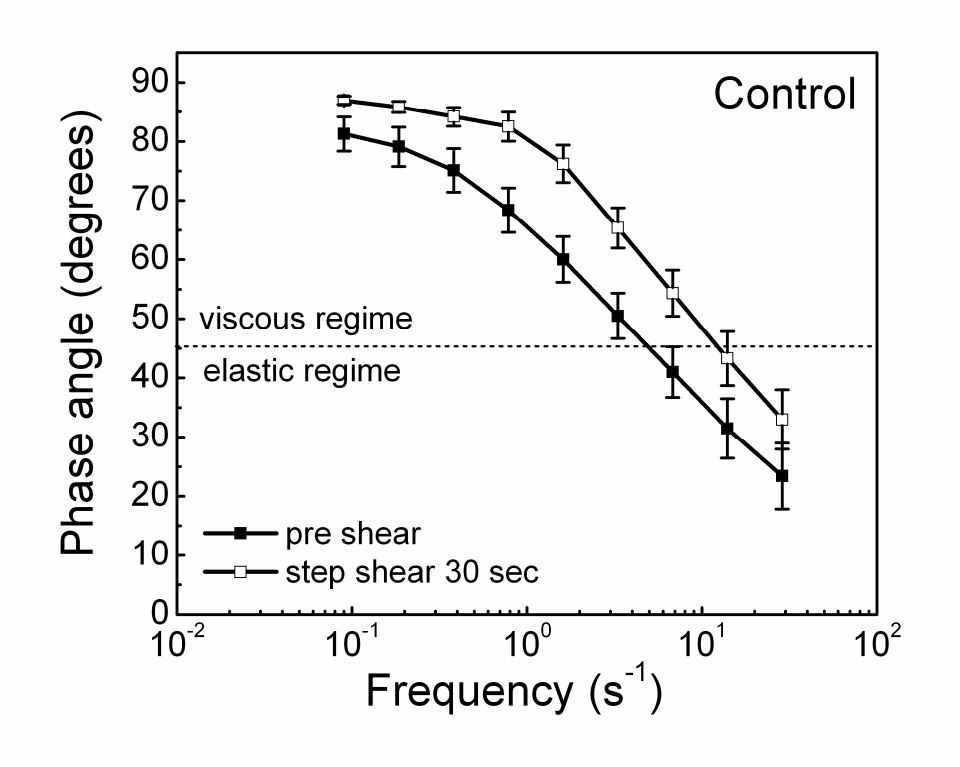

Figure **4-10**: Shear-induces a significant increase in crossover frequency indicative of fluidization in non-drug treated ECs (n=15).

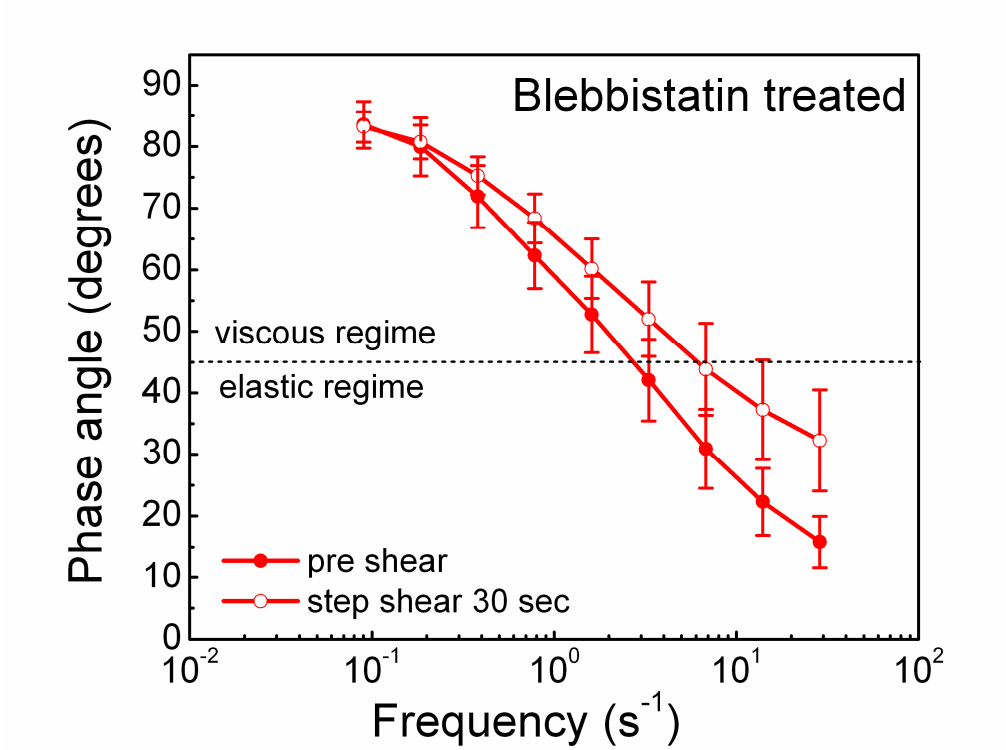

Figure **4-11**: Myosin II inhibition abolished shear-induced fluidization (n=9). No significant difference in the phase angles is observed.

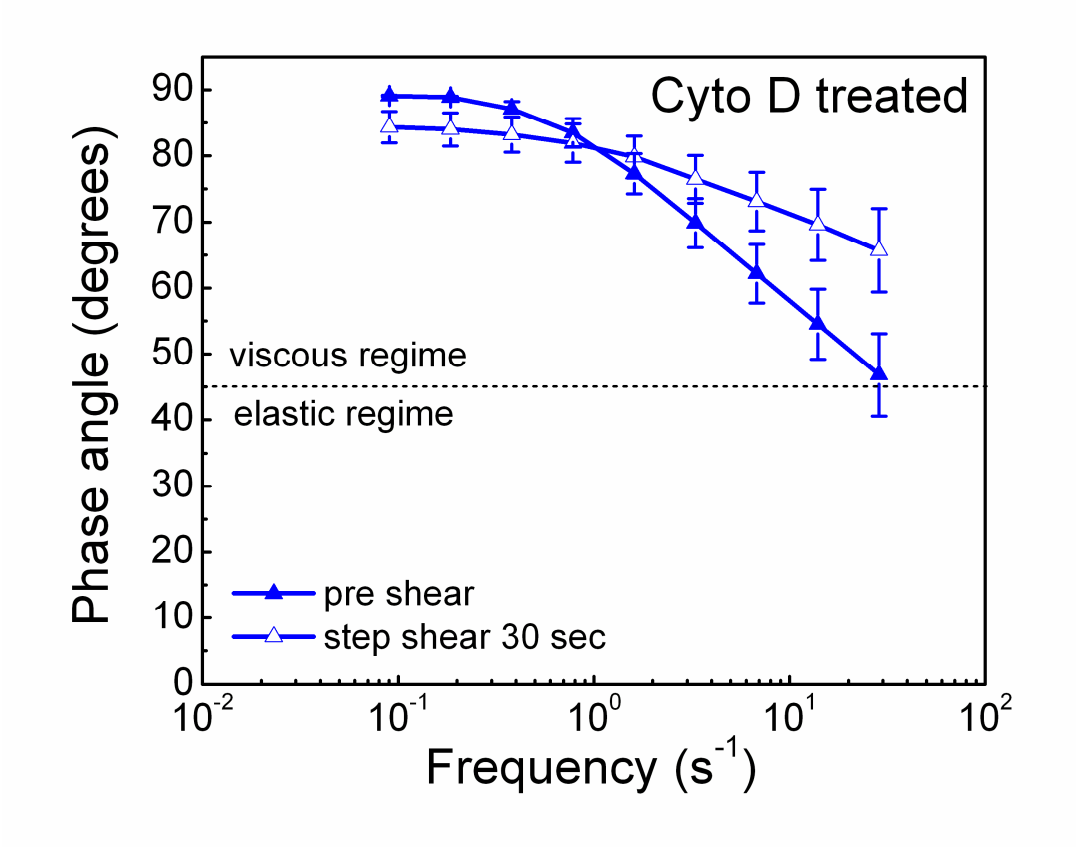

Figure **4-12**: Actin disruption causes a total loss of solid-like behavior (n=9). No crossover from liquid-like to solid-like regime before and during shear is observed.

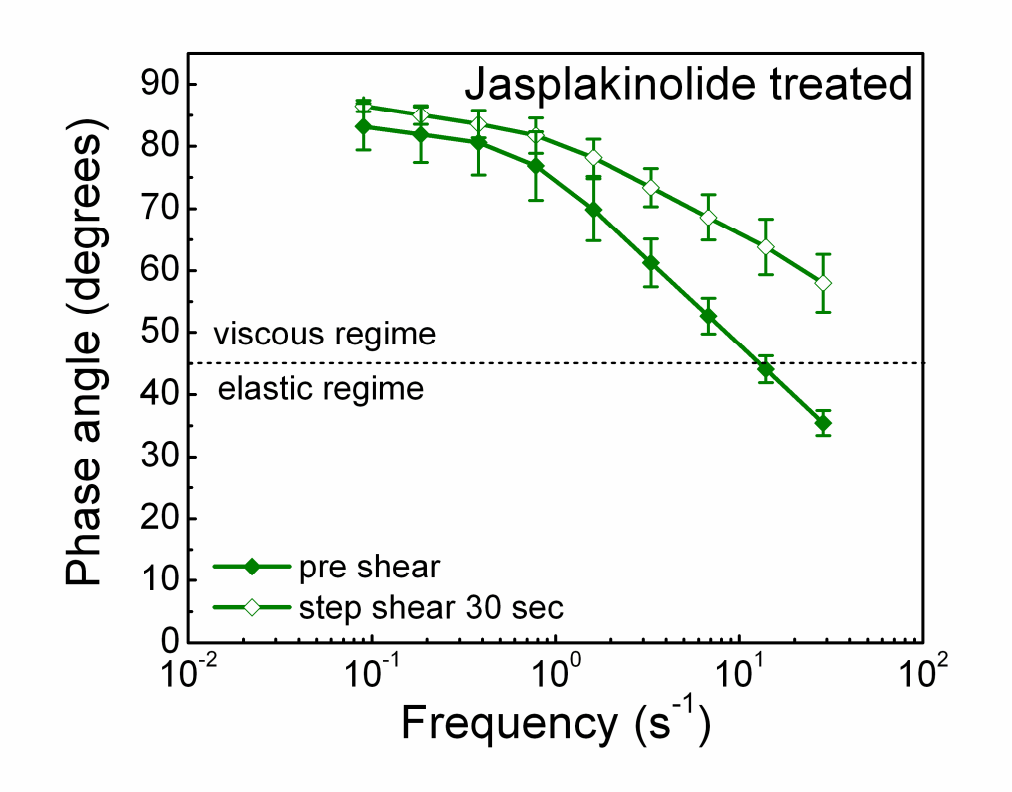

Figure **4-13**: Stabilizing actin cytoskeleton does not affect shear-induced fluidization (n=7). ECs demonstrate a dominant viscoelastic liquid-like behavior pre-shear. During-shear stimulation total fluidization of the EC interior is observed. Crossover from liquid-like to solid-like regime does not occur.

After returning shear stress to 0 dynes/cm^2 in a stepwise manner (post shear), only in the case of untreated cells, $G'(\omega)$ was significantly lower compared with pre-shear values (Figure **4-14**). ECs did not completely recover their viscoelastic properties after 30 sec of shear stimulation, in contrast to full recovery at 4 minutes observed in our previous study (Dangaria and Butler, 2007). For all drug treatments, rheology returned to baseline pre-shear values. It is interesting to note that after exposure to a 5 sec shear pulse, EC viscoelastic moduli recovered completely i.e. no significant change in $G'(\omega)$ and $G''(\omega)$

pre- and post-shear was observed (data not shown). ECs may thus be sensitive to the duration of shear stimulation. It is possible that shear-activation of endothelial cells occurs after a certain threshold value of exposure time. Thus, ECs respond rapidly to shear stress by softening and fluidizing their cytoplasm through the interaction of actin cytoskeleton and myosin motor activity.

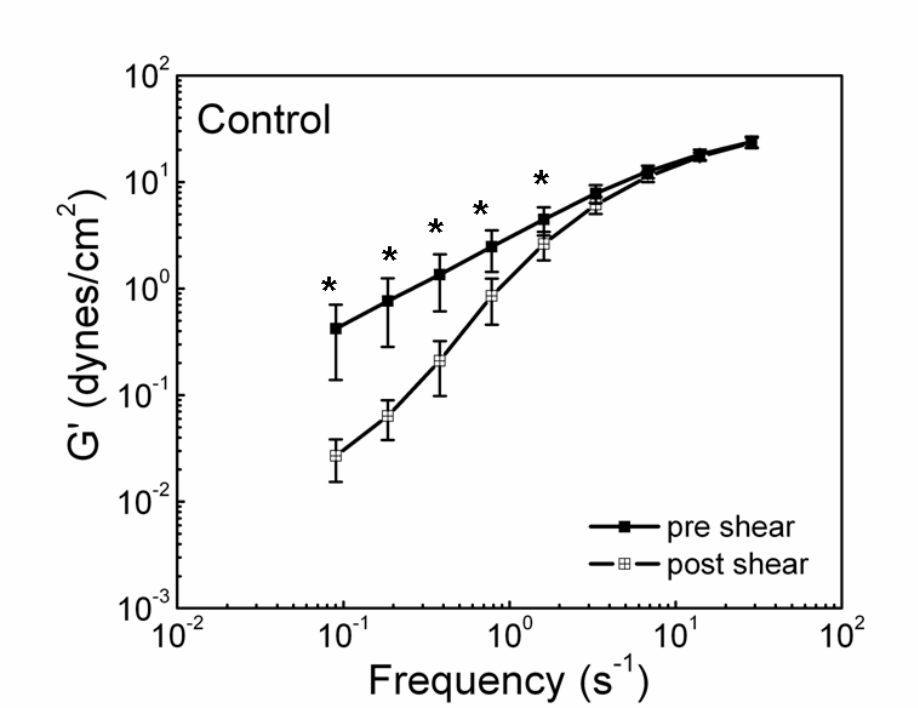

Figure **4-14**: Elastic modulus does not recover post shear in non-drug treated cells indicative of active remodeling of the EC interior in response to 30 second duration exposure to shear stress. * indicates $p < 0.05$

4.3.3 Myosin II modulates viscoelastic macrorheological moduli and actin-dependent shear stress-induced activation of EC.

To quantify the macroscale viscoelastic properties of ECs, average creep in response to a step change in shear was plotted. EC creep response exhibits two regimes: an early rapid elastic deformation followed by a longer-time viscous flow. This behavior is a characteristic of viscoelastic liquids. Creep response was fit to a phenomenological Voigt-Maxwell model of a spring and dashpot (Figure **4-15**) to quantify viscoelastic constants. Average macrorheological moduli were calculated to be: shear modulus μ_v = 66 Pa, viscosities η_v = 120 Pa-sec, η_s = 10,000 Pa-sec and relaxation time τ_v = 1.81 s.

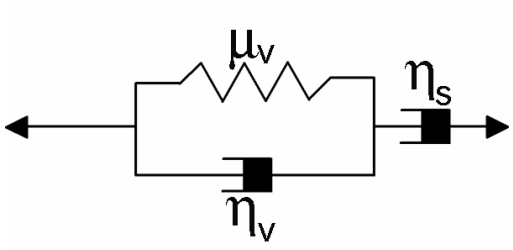

Figure **4-15**: Phenomenological model of a viscoelastic liquid: Voigt-Maxwell model used to curve-fit the creep response of endothelial cells.

Similar curve-fitting analyses were performed to obtain macrorheological moduli of ECs treated with a myosin inhibitor (blebbistatin), actin depolymerizing (cytochalasin D), and stabilizing (jasplakinolide) agents. We note that the elastic modulus μ_v was not affected dramatically by myosin II inhibition (μ_v = 50 Pa), and actin stabilization (μ_v = 60 Pa). Disrupting actin filaments with cytochalasin D, however, reduced the elastic modulus (μ_v = 34.5 Pa). These data demonstrate that intact actin filaments are the major

source of elasticity of the EC interior. Viscosity dropped in cells in which either actin was stabilized, disrupted or when myosin II activity was inhibited. Compared to a control value of η_v = 120 Pa-sec, myosin II inhibition resulted in η_v = 45 Pa-sec, actin stabilization resulted in η_v = 53.7 Pa-sec, and actin disruption resulted in η_v = 24.4 Pa-sec. This result suggests that the interaction of actin and myosin II governs the macrorheological viscosity of endothelial cells.

For a model describing mechanical behavior of viscoelastic liquids, the elastic modulus μ_v represents the high frequency deformation limit of the material. Relaxation time $\tau_v = \eta_v / \mu_v$ is a more effective parameter to describe the solid versus liquid-like behavior. For a rigid body, $\eta \to \infty$ and relaxation time is infinite, while for a purely viscous medium relaxation time is zero. Relaxation times of control and drug treatments are summarized in Table **4-2**. When actin filaments were depolymerized, stabilized, or myosin II motors were inhibited, relaxation time was considerably shorter as compared with untreated control cells, supporting the idea that actin-myosin interaction governs viscous stress dissipation in cells.

Table **4-2**: Characteristic time from curve fitting analyses of creep function and onset time of EC contraction.

	Characteristic time, τ_v (sec)	**Onset time of contraction (sec after step initiation)**
Control	1.81	22
Blebbistatin	0.9	2
Cytochalasin D	0.70	-
Jasplakinolide	0.86	13

Analysis of creep curves uncovered a previously undiscovered phenomenon, namely shear-induced endothelial cell contraction. For control cells, ECs began to contract after 22 seconds of exposure to shear stress, even while shear stress was held constant (Figure **4-16**). The onset of contraction for blebbistatin treated cells was ~2 seconds (Figure **4-17**) while that of jasplakinolide treated cells was ~13 seconds (Figure **4-19**). No active contraction during shear stimulation was seen in cells treated with cytochalasin D (Figure **4-18**) suggesting that intact F-actin is necessary for shear-induced active contraction of endothelial cells. These results also suggest that myosin II motors are not involved in contraction per se, but instead strongly modulate the onset time of contraction. Since inhibiting myosin II activity leads to an almost immediate contraction during shear, myosin motors may be responsible for viscous dissipation of forces generated due to suddenly applied stress thus, delaying active contraction.

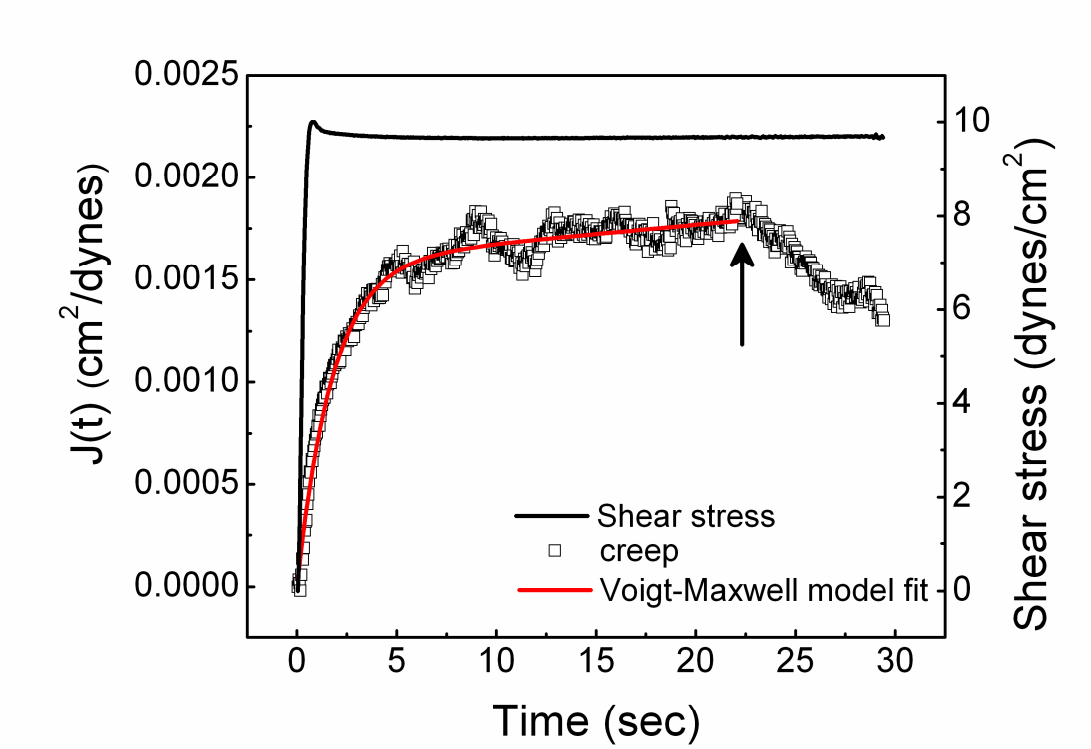

Figure **4-16**: Creep deformation due to step shear in untreated control ECs. Arrow indicates onset of contraction t= 22 seconds.

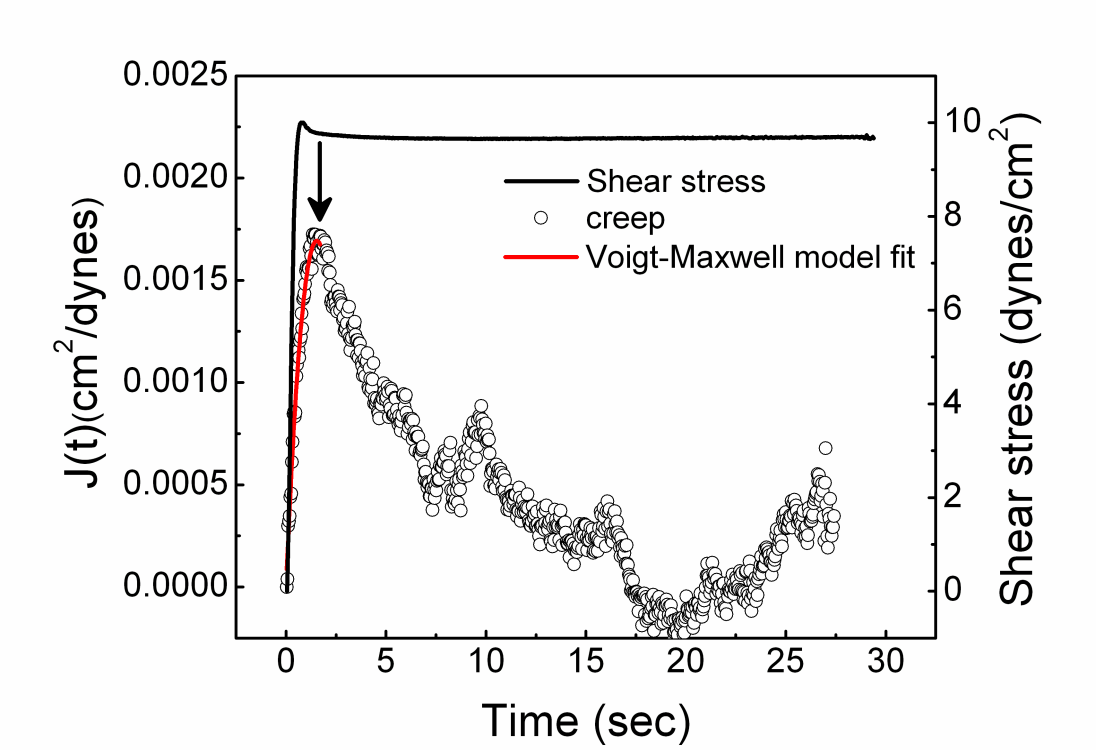

Figure **4-17**: Creep deformation due to step shear in myosin II motor inhibited ECs. Arrow indicates onset of contraction t= 2 seconds.

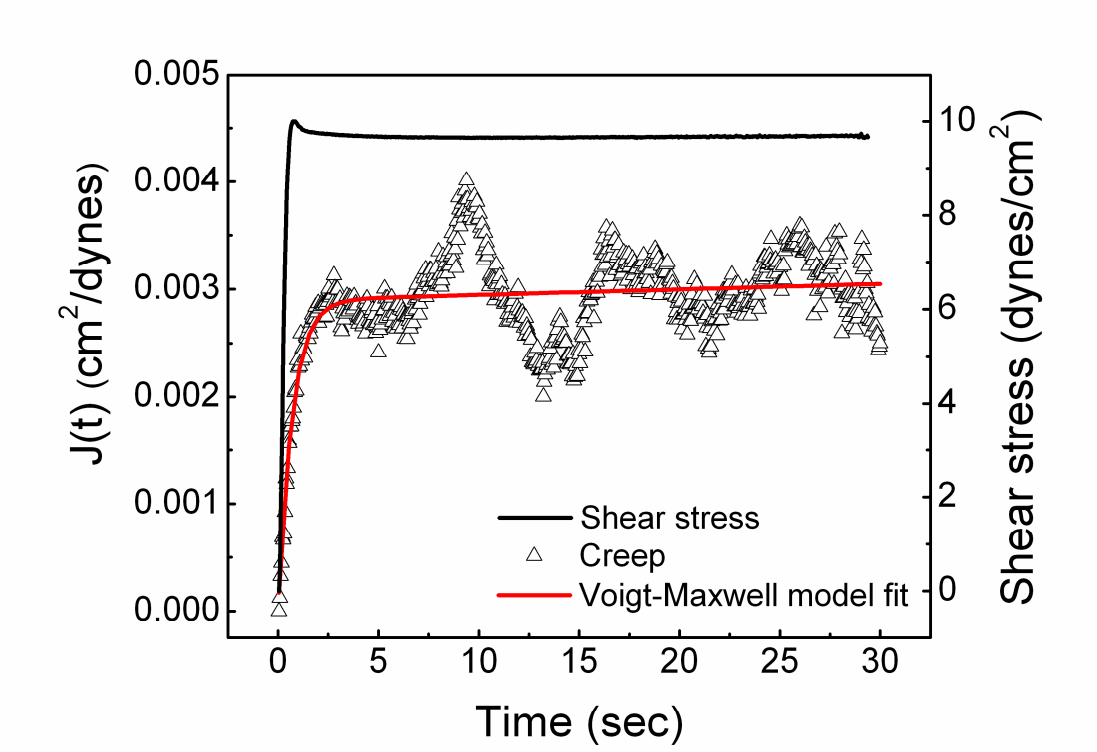

Figure **4-18**: Creep deformation due to step shear in cytochalasin D treated ECs. Shear-induced contraction is absent.

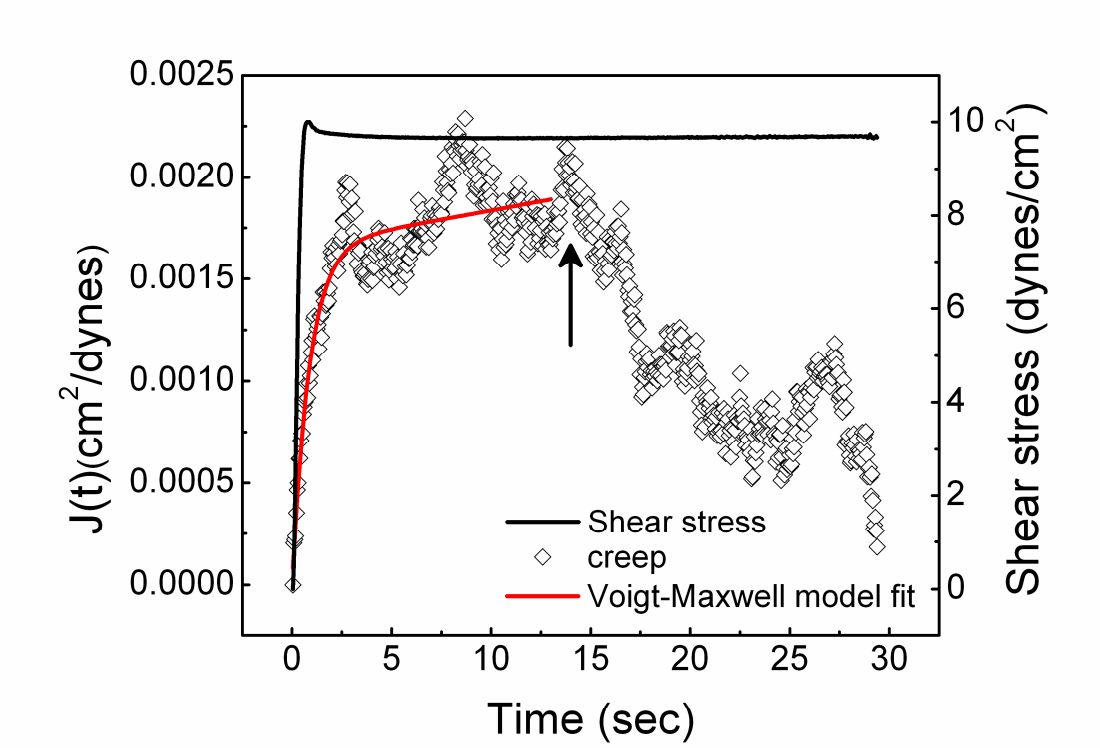

Figure **4-19**: Creep deformation due to step shear in jasplakinolide treated ECs. Arrow indicates onset of contraction t= 13 seconds.

4.4 Discussion

First, we investigated the role of actin cytoskeleton and myosin II motor activity in regulating the mechanical stability (micorheology) of endothelial cells. Our results indicate two important aspects: 1) actomyosin interactions provide rigidity to endothelial cells and 2) intact actin filaments are necessary for the biphasic mechanical behavior i.e. frequency-dependent viscoelastic solid- and liquid-like behavior of endothelial cells. We found that both actin and myosin II govern internal cellular rheology as indicated by the sensitivity of the storage and loss moduli to both the actin disrupting agent cytochalasin D, and the myosin II inhibiting drug blebbistatin. However, the fluidity of the cytoplasm, quantified by the crossover frequency of the phase angle, was weakly dependent on myosin II but strongly dependent on actin filament integrity.

Second, we investigated the role of actomyosin interactions in shear-induced cell softening and fluidization at very early time points. Shear stress also had a strong influence on cell rigidity and fluidity as indicated by the dramatic decrease in both moduli and increase in crossover frequency, respectively, in response to a step change in shear stress. Shear-induced softening was both myosin II and actin dependent as indicated by its sensitivity to blebbistatin and cytochalasin D, respectively. Results suggest that myosin motor interactions with actin rather than actin depolymerization are responsible for shear-induced rapid softening and fluidization of ECs.

Finally, we report that intact F-actin filaments along with myosin motor activity govern cellular macrorheology. We noted a strong contraction in response to shear stress that has not been reported until now, the onset time of which was strongly sensitive to

myosin II activity. Interestingly, myosin II is not necessary for contraction suggesting that there exist other actin-dependent mechanisms that are responsible for shear-induced EC contraction.

4.4.1 Actomyosin contribution in endothelial cell rheology

Myosins play a dual role in cells, by dynamically cross-linking F-actin and by force generation due to their motor activity. We used a panel of agents to modulate actin-myosin interactions to better understand their role in endothelial cell rheology and shear adaptation. Blebbistatin, a recently discovered molecule, is a potent selective inhibitor of skeletal muscle and non-muscle myosin II isoforms (Straight et al., 2003). It has little effect on smooth muscle myosin II and other classes of myosin (I, V, and X) (Limouze et al., 2004). Blebbistatin binds to the myosin –ADP-Pi complex with high affinity (Kovacs et al., 2004). This interferes with the phosphate release process and thus, the myosin head remains detached from actin. Blebbistatin prevents rigid actomyosin cross-linking thus hampering cytoskeletal tension generation. Inhibition of myosin motor activity by blebbistatin in endothelial cells as measured by internal particle tracking microrheology, lead to a softening of the cell as indicated by the reduced elastic and viscous moduli. It is interesting to note that even though we report a drop in macrorheological moduli, no change in crossover frequency or fluidization, as indicated by microrheological moduli, was observed compared with untreated controls. Confocal micrographs further provide supporting evidence to our quantitative microrheology results. Upon examination of confocal images of untreated and ECs treated with blebbistatin (Figure **4-20** A, B), it is

evident that blebbistatin treated cells exhibit altered morphology compared with untreated controls. Ruffles appear at the cell periphery and cells seem to retract. Actin filaments are still present in blebbistatin treated cells although they are more dispersed and virtually no stress fibers are observed.

Contrasting effects of myosin II inhibition on cell rheology have been reported in the literature. For example, Balland *et al.* in a study on myoblasts reported a five fold drop in $G'(\omega)$, and $G''(\omega)$ after myosin II inhibition with blebbistatin (Balland et al., 2005) while no change in intracellular rheology was observed in epithelial cells using the same myosin II specific inhibitor blebbistatin (Van Citters et al., 2006). These apparent differences in the above mentioned studies and ours can be reconciled by the explanation that first different cell types may respond differently to the same drug, blebbistatin in this case. Further, these results may be sensitive to the techniques used to measure rheological parameters as well as the region in which the cells were probed. For example, Balland *et al.* used optical tweezers to probe the cortical cytoskeleton of myoblasts using RGD-coated beads while Van Citters *et al.* probed intracellular rheology of epithelial cells using laser tracking microrheology. Finally, the force landscape induced by prestress may be affected by the presence of cell-cell junctions which are present in confluent cells in our study but absent when cells are cultured in isolation.

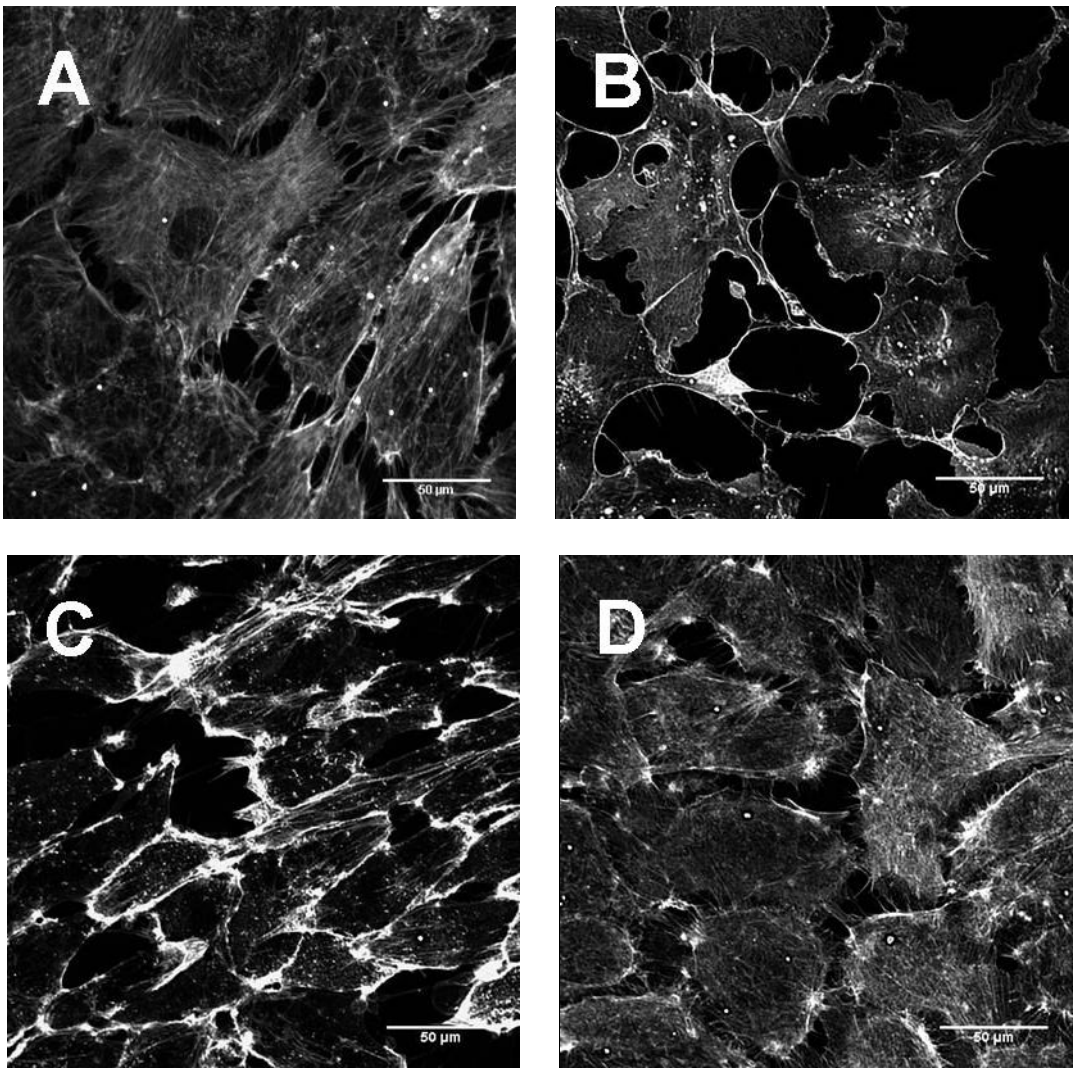

Figure **4-20**: Confocal micrographs of AlexaFluor 488 phalloidin labeled F-actin in (A) control; (B) sample treated with myosin II inhibitor, blebbistatin; few actin bundles and no stress fibers are seen. Membrane ruffles and cell retraction are observed. (C) sample treated with actin disruptor, cytochalasin D; total loss of stress fibers and punctate staining indicative of actin aggregates is observed, and (D) sample treated with actin stabilizing agent jasplakinolide; no distinct change in cell morphology is evident. Scale bar, 50 µm.

Cytochalasin D is another drug that modulates actomyosin interactions. Cytochalasin D depolymerizes F-actin filaments by binding to the growing plus (barbed) end of actin filaments, preventing actin polymerization (Bray, 1979;Cooper, 1987). Disrupting actin network leads to inhibition of myosin motor activity. A dramatic decrease in $G'(\omega)$, and $G''(\omega)$, and total loss of solid-like behavior compared with untreated control cells implies that intact F-actin cytoskeleton is the dominant source of elasticity and solid-like behavior in endothelial cells. Examination of confocal micrographs of cytochalasin D treated cells (Figure **4-20** C) reveal loss of stress fibers, rather punctuate staining consistent with actin aggregates is observed. Along the cell periphery, we observed F-actin enrichment. Qualitative analyses of confocal images further support our result that solid-like behavior of endothelial cells is primarily due to intact F-actin. In the absence of intact actin cytoskeleton, endocytosed beads experience a viscous environment and cell behave like viscoelastic liquids with very small relaxation time.

Actin stabilizing agent jasplakinolide is a naturally occurring peptide found in a marine sponge Jaspis johnstoni. Jasplakinolide is known to induce actin polymerization and/or stabilized pre-existing actin filaments in vivo (Bubb et al., 1994). In this study, no change in viscoelastic moduli was observed compared with controls. This is consistent with the confocal images (Figure **4-20**, D) where no distinct alterations in cell morphology or actin cytoskeleton structure are observed compared with untreated control cells (Figure **4-20**, A). However, the underlying cause of the dramatic increase in crossover frequency indicative of enhanced fluid-like behavior is unclear.

4.4.2 Contribution of actin-myosin cytoskeleton in shear-induced adaptive rheology

Previous studies have reported shear stress induced-dynamic realignment of focal adhesions in EC monolayers (Davies, 1995;Davies et al., 1994), spatial reorganization of cytoskeleton (Galbraith et al., 1998), and enhanced myosin light chain phosphorylation in ECs (Watanabe et al., 1998). A sudden drop in shear moduli within seconds after onset of mechanical stimulation has been reported in neutrophils (Yap and Kamm, 2005b) and it was suggested that rapid mechanical deformation leads to a sudden disruption of the cytoskeleton network (Yap and Kamm, 2005a). These studies taken together highlight actin dynamics along with myosin phosphorylation as important regulators of the effects of fluid shear stress on cells. Osborn *et al*. using the technique of fluorescence recovery after photobleaching reported that the earliest phase of actin cytoskeleton response to shear stress in endothelial cells was net cytoskeleton depolymerization (Osborn et al., 2006). The enhanced shear-mediated actin remodeling at 5 min observed in that study points towards an alternate mechanism involved in the very early (on the order of few seconds) shear-induced softening response of endothelial cells.

The observation that shear-induced cell softening was diminished and fluidization abrogated when myosin II motors were inhibited is consistent with the idea proposed by Humphrey *et al*., suggesting that myosin activity results in enhanced longitudinal motions of actin filaments (Humphrey et al., 2002). Normally, in entangled polymer solutions, diffusive transport of individual filaments is driven by Brownian motion. This concept is known as reptation (de Gennes, 1971;Doi and Edwards, 1986). If molecular motors enhance sliding motions of actin filaments, relaxation time for rapid stress imposition is

shortened. Rapid stress dissipation due to reptation-facilitated, shear-induced fluidization may thus be a mechanism by which endothelial cells rapidly adapt their mechanical properties in the face of external stress application. Interestingly, the theory of reptation in ECs may be relevant for sudden applications of shear stress because myosin II inhibition affected shear-induced fluidity dramatically while having no affect on fluidity of quiescent cells. Thus myosin II motor activity may be a dominant mechanism of internal stress regulation in ECs exposed to rapid shear stress changes, such as in areas of the vasculature exposed to oscillating fluid flow.

4.4.3 Macrorheology and shear-induced endothelial cell contraction

Viscoelastic creep deformation of cells is often characterized by simple mechanical models consisting of springs and dashpots. Various models have been proposed depending on the techniques used for deforming cells. For example, passive deformation of human leukocytes (Dong et al., 1988;Schmid-Schonbein et al., 1981) using micropipette aspiration has been modeled as an elastic cortical shell surrounding a Maxwell viscoelastic fluid. Sato *et al.* reported mechanical properties of porcine endothelial cells submitted to shear stress using a Kelvin model (Sato et al., 1996). In the present study, Voigt-Maxwell model of a viscoelastic liquid was used to describe the creep response of endothelial cells subjected to step change in shear stress. At short times (high frequency) the local dissipation accompanying the initial elastic deflection of endocytosed beads can be fully described by a Voigt model. During the characteristic

time τ_v, the matrix surrounding these beads behaves like a viscoelastic solid. After time τ_v, endothelial cell cytoplasm behaves like a viscoelastic liquid with viscosity η_s.

Creep curves also demonstrate a previously undiscovered phenomenon, namely shear-induced endothelial cell contraction. A possible explanation of this phenomenon follows. Let us think of myosin motors interacting with randomly-oriented actin filaments. For suddenly applied stress, actin filaments elastically resist deformations that occur faster than the stress relaxation time. Myosin motor activity enhances the longitudinal motion of actin filaments, pushing them through the crowed cell interior, rapidly dissipating locally generated stresses. If this stress dissipation mechanism is inhibited, internal stress build up may be enough to sever actin filaments, leading to filament retraction or rapid depolymerization. Thus, the remodeling response may manifest itself as shear-induced cell contraction.

Another possible explanation of shear-induced EC contraction could be attributed to Rho family of small (low molecular weight) GTPases. Rho GTPases regulate cytoskeletal changes involved in cell shape, motility, and contraction (van Nieuw Amerongen and van Hinsbergh, 2001). The dominant regulatory mechanism in non-muscle and smooth muscle contraction is Ca^{2+}/ calmodulin-dependent myosin light chain (MLC) phosphorylation (Adelstein and Sellers, 1987). However, the involvement of Rho in Ca^{2+} dependent smooth muscle cell contraction has been previously established (Hirata et al., 1992). Our observation that inhibiting myosin II motors does not alter shear-induced EC contraction indicates that there may be other molecular motors involved in shear-induced cell contraction.

It is interesting to note that the effective viscoelastic moduli measured using particle tracking microrheology and macrorheological moduli obtained from creep deformation both describe endothelial cells as viscoelastic liquids. Furthermore, shear-induced reduction in microrheological moduli occurs on the same time-scale as creep. Therefore it may be possible that softening and fluidization of the cell interior may contribute to the overall creep deformation. Together, these studies provide new insight into how early mechanotransduction events may depend on dynamic modulation of mechanical properties through actin-myosin dependent mechanisms.

4.5 References

Adelstein, R. S. and J. R. Sellers. 1987. Effects of calcium on vascular smooth muscle contraction. *Am J Cardiol.* 59:4B-10B.

Balland, M., A. Richert, and F. Gallet. 2005. The dissipative contribution of myosin II in the cytoskeleton dynamics of myoblasts. *Eur. Biophys. J* 34:255-261.

Bray, D. 1979. Cytochalasin action. *Nature* 282:671.

Bubb, M. R., A. M. Senderowicz, E. A. Sausville, K. L. Duncan, and E. D. Korn. 1994. Jasplakinolide, a cytotoxic natural product, induces actin polymerization and competitively inhibits the binding of phalloidin to F-actin. *J Biol. Chem.* 269:14869-14871.

Chien, S. 2003. Molecular and mechanical bases of focal lipid accumulation in arterial wall. *Prog. Biophys. Mol. Biol* 83:131-151.

Clark, K., M. Langeslag, C. G. Figdor, and F. N. van Leeuwen. 2007. Myosin II and mechanotransduction: a balancing act. *Trends Cell Biol* 17:178-186.

Cooper, J. A. 1987. Effects of cytochalasin and phalloidin on actin. *J Cell Biol* 105:1473-1478.

Dangaria, J. H. and P. J. Butler. 2007. Macrorheology and adaptive microrheology of endothelial cells subjected to fluid shear stress. *Am J Physiol Cell Physiol* 293:C1568-C1575.

Davies, P. F. 1995. Flow-mediated endothelial mechanotransduction. *Physiol Rev.* 75:519-560.

Davies, P. F., A. Robotewskyj, and M. L. Griem. 1994. Quantitative studies of endothelial cell adhesion. Directional remodeling of focal adhesion sites in response to flow forces. *J Clin. Invest* 93:2031-2038.

de Gennes, P. G. 1971. Reptation of a Polymer Chain in the Presence of Fixed Obstacles. *The Journal of Chemical Physics* 55:572-579.

Doi, M. and S. F. Edwards. 1986. The Theory of Polymer Dynamics. Clarendon Press, Oxford.

Dong, C., R. Skalak, K. L. Sung, G. W. Schmid-Schonbein, and S. Chien. 1988. Passive deformation analysis of human leukocytes. *J Biomech. Eng* 110:27-36.

Foth, B. J., M. C. Goedecke, and D. Soldati. 2006. New insights into myosin evolution and classification. *Proc. Natl. Acad Sci U. S. A* 103:3681-3686.

Galbraith, C. G., R. Skalak, and S. Chien. 1998. Shear stress induces spatial reorganization of the endothelial cell cytoskeleton. *Cell Motil. Cytoskeleton* 40:317-330.

Hirata, K., A. Kikuchi, T. Sasaki, S. Kuroda, K. Kaibuchi, Y. Matsuura, H. Seki, K. Saida, and Y. Takai. 1992. Involvement of rho p21 in the GTP-enhanced calcium ion sensitivity of smooth muscle contraction. *J Biol Chem.* 267:8719-8722.

Humphrey, D., C. Duggan, D. Saha, D. Smith, and J. Kas. 2002. Active fluidization of polymer networks through molecular motors. *Nature* 416:413-416.

Ingber, D. E. 2003. Tensegrity I. Cell structure and hierarchical systems biology. *J Cell Sci* 116:1157-1173.

Kovacs, M., J. Toth, C. Hetenyi, A. Malnasi-Csizmadia, and J. R. Sellers. 2004. Mechanism of blebbistatin inhibition of myosin II. *J Biol Chem.* 279:35557-35563.

Krendel, M. and M. S. Mooseker. 2005. Myosins: tails (and heads) of functional diversity. *Physiology (Bethesda.)* 20:239-251.

Limouze, J., A. F. Straight, T. Mitchison, and J. R. Sellers. 2004. Specificity of blebbistatin, an inhibitor of myosin II. *J Muscle Res. Cell Motil.* 25:337-341.

Mason T.G., K.Ganesan, J.H.van Zanten, D.Wirtz, and and S.C.Kuo. 1997. Particle Tracking Microrheology of Complex Fluids. *Physical Review Letters* 79:3282-3285.

Osborn, E. A., A. Rabodzey, C. F. Dewey, Jr., and J. H. Hartwig. 2006. Endothelial actin cytoskeleton remodeling during mechanostimulation with fluid shear stress. *Am J Physiol Cell Physiol* 290:C444-C452.

Sato, M., N. Ohshima, and R. M. Nerem. 1996. Viscoelastic properties of cultured porcine aortic endothelial cells exposed to shear stress. *Journal of Biomechanics* 29:461-467.

Schmid-Schonbein, G. W., K. L. Sung, H. Tozeren, R. Skalak, and S. Chien. 1981. Passive mechanical properties of human leukocytes. *Biophys. J.* 36:243-256.

Stossel, T. P. 1993. On the crawling of animal cells. *Science* 260:1086-1094.

Straight, A. F., A. Cheung, J. Limouze, I. Chen, N. J. Westwood, J. R. Sellers, and T. J. Mitchison. 2003. Dissecting temporal and spatial control of cytokinesis with a myosin II Inhibitor. *Science* 299:1743-1747.

Tsao, P. S., R. Buitrago, J. R. Chan, and J. P. Cooke. 1996. Fluid flow inhibits endothelial adhesiveness. Nitric oxide and transcriptional regulation of VCAM-1. *Circulation* 94:1682-1689.

Van Citters, K. M., B. D. Hoffman, G. Massiera, and J. C. Crocker. 2006. The role of F-actin and myosin in epithelial cell rheology. *Biophys. J* 91:3946-3956.

van Nieuw Amerongen, G. P. and V. W. M. van Hinsbergh. 2001. Cytoskeletal Effects of Rho-Like Small Guanine Nucleotide-Binding Proteins in the Vascular System. *Arterioscler Thromb Vasc Biol* 21:300-311.

Wachsstock, D. H., W. H. Schwarz, and T. D. Pollard. 1994. Cross-linker dynamics determine the mechanical properties of actin gels. *Biophys. J* 66:801-809.

Watanabe, H., R. Takahashi, X. x. Zhang, Y. Goto, H. Hayashi, J. Ando, M. Isshiki, M. Seto, H. Hidaka, I. Niki, and R. Ohno. 1998. An essential role of myosin light-chain kinase in the regulation of agonist- and fluid flow-stimulated Ca2+ influx in endothelial cells. *FASEB J.* 12:341-348.

Yap, B. and R. D. Kamm. 2005a. Cytoskeletal remodeling and cellular activation during deformation of neutrophils into narrow channels. *J Appl Physiol* 99:2323-2330.

Yap, B. and R. D. Kamm. 2005b. Mechanical deformation of neutrophils into narrow channels induces pseudopod projection and changes in biomechanical properties. *J Appl Physiol* 98:1930-1939.

Chapter 5

CONCLUSIONS AND FUTURE WORK

One of the major challenges in mechanobiology is the identification and characterization of the precise mechanism(s) by which cells sense and convert external mechanical forces to biological responses. The central feature of all cellular structures undergoing mechanical stimulation is force-dependent deformation. Cell mechanics then becomes the central unifying theme that relates the ability of cells to sustain and react to external forces. A major challenge is that cells cannot be treated as inert mechanical materials but are constantly changing and adapting to their environment. While mechanoadaptation of cells has been reported previously there are no studies reported to date which investigate adaptations that may occur on the same time scale of seconds, which is the time scale that forces are applied to endothelial cells in atherogenic areas of the vasculature.

Therefore, a central theme of this project was to study the rapid temporal effects of mechanical perturbation via step change in fluid shear stress on endothelial cell mechanical properties. A custom image processing algorithm was designed to quantify intracellular mechanics using high-resolution imaging and differential interference contrast microscopy. Cell mechanical properties were quantified using particle tracking microrheology. We report a novel observation that endothelial cells respond to rapid changes in shear stress by modulating their intracellular rheology. Furthermore, creep

response to step change in shear stress was fitted to the model of a viscoelastic liquid to obtain macrorheological parameters which could be useful for cell-specific computational modeling.

Next, we attempted to investigate the possible mechanisms underlying the rapid shear-induced adaptive rheology of endothelial cells. We examined two possible candidates namely, actin dynamics (i.e. depolymerization and polymerization), and actomyosin interactions. Our results suggest that myosin II motors regulate cytoplasmic rheology and intracellular tension in response to external mechanical perturbations through dynamic actin cross linking, and facilitated diffusion of F-actin filaments. A novel observation from these studies is that actomyosin regulates macrorheology (i.e. viscoelastic deformation in response to shear stress), microrheology (i.e. constrained thermal motion of small beads) and cell contraction. Taken together, these studies provide a novel avenue towards understanding endothelial cell mechanotransduction through the dynamic regulation of cell mechanics by myosin II and actin.

Given that we have laid tremendous emphasis on the ability of the vascular endothelium to dynamically regulate cell mechanics and rapidly adapt to external forces, it becomes important to study the molecular mechanisms involved in regulating intracellular rheology and internal tension generation to balance external mechanical forces. Since internal tensional homeostasis has been attributed to actomyosin contractility, an important aspect of future studies will be to investigate the molecular mechanisms involved in regulating cell mechanics through myosin II and other myosin motor dependent pathways.

Another interesting avenue will be to investigate the role of the extracellular matrix stiffness in shear-induced endothelial cell mechanics modulation. It is evident that cells grown on glass or polymer substrates experience a stiffer extracellular environment compared with physiological tissue in vivo. Understanding endothelial cell mechanoadaptation in a more physiological external mechanical environment may be relevant in the context of vascular biology and pathophysiology.

An important extension of this experimental study would be to develop integrated cell-specific computational models to account for matrix rigidity, temporal and spatial fluid shear gradients on the endothelial monolayer, and correlations between force gradients and corresponding adaptive changes in cell rheology. Such integrated modeling and measurement will help uncover mechanisms of adaptive rheology which may be important in understanding the role of force in cardiovascular health and disease.

VITA

Jhanvi Hirji Dangaria

Education

Doctor of Philosophy, Bioengineering May 2008
The Pennsylvania State University, University Park, PA

Master of Science, Bioengineering May 2006
The Pennsylvania State University, University Park, PA
Thesis: Particle tracking microrheology of the endothelial cell cytoplasm

Bachelor of Engineering, BioMedical Engineering August 2001
Dwarkadas J. Sanghvi College of Engineering, Mumbai University, India

Publications

Dangaria JH and Butler PJ, Myosin II motors modulate endothelial cell rheology and activation by shear stress. (In preparation)

Dangaria JH and Butler PJ, Macrorheology and adaptive microrheology of endothelial cells subjected to fluid shear stress. *American Journal of Physiology Cell Physiology*, Nov, 293(5):C1568-75, 2007

Dangaria JH, Yang S, and Butler PJ, Improved nanometer-scale particle tracking in optical microscopy using microfabricated fiduciary posts. *BioTechniques*, 42: 437-8, 440, 2007

Gullapalli RR, Tabouillot T, Mathura R, Dangaria JH, and Butler PJ, Integrated multimodal microscopy, time-resolved fluorescence and optical-trap rheometry: toward single molecule mechanobiology. *Journal of Biomedical Optics*, 12: 014012, 2007

Awards

The Pennsylvania State University, Bioengineering Graduate Student Forum Research Day, *Poster award*, February 2008.

Biomedical Engineering Society, *Outstanding Scientific and Engineering Innovation in a Poster Presentation*, October 2005.

The Pennsylvania State University, *Graduate School Exhibition Award in Engineering*, March 2003.